TECHNISCHE UNIVERSITÄT CHEMNITZ

Fakultät für Maschinenbau
Professur Sportgerätetechnik

spinfortec2022

Tagungsband zum 14. Symposium der Sektion Sportinformatik und Sporttechnologie der Deutschen Vereinigung für Sportwissenschaft

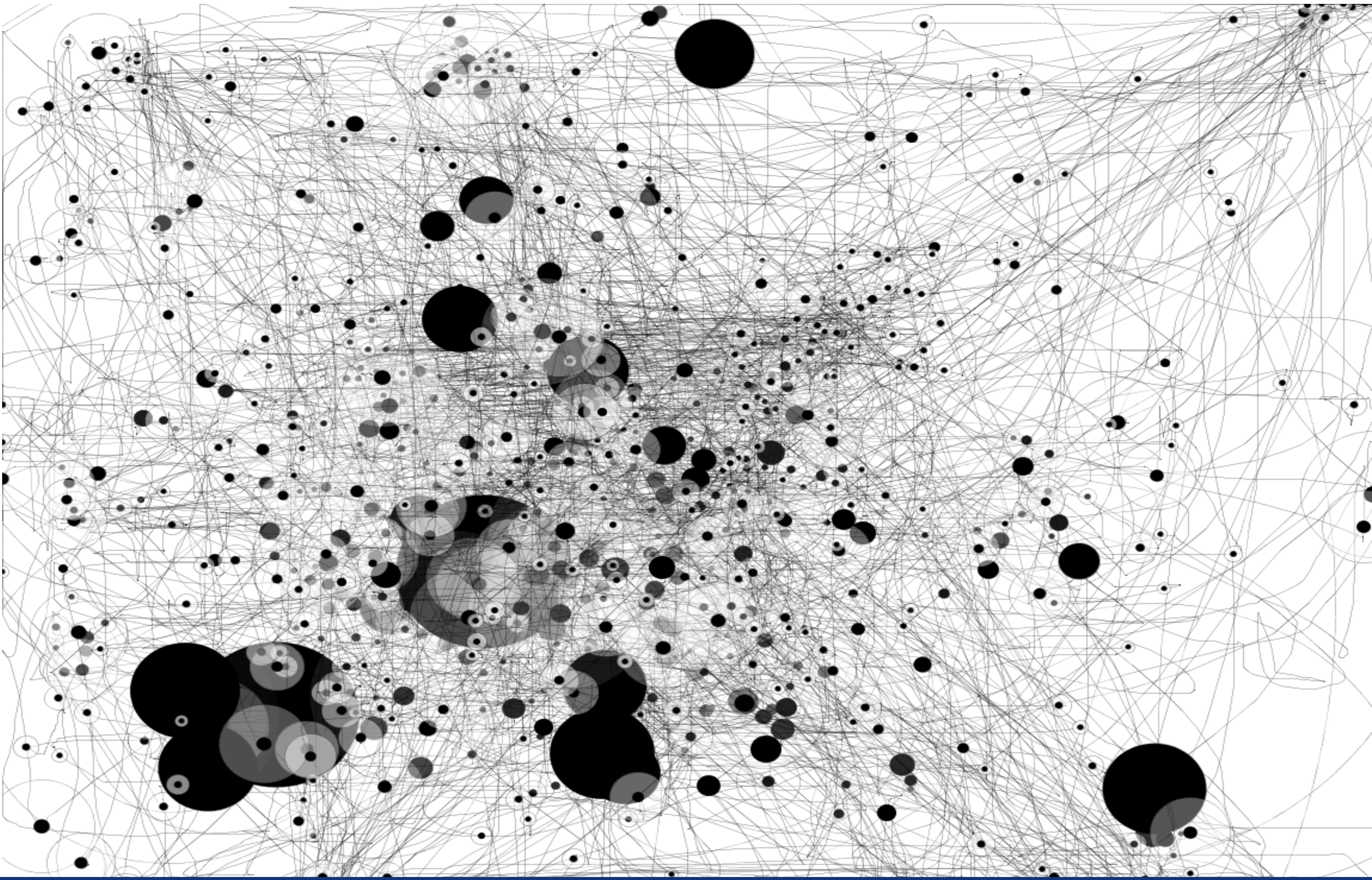

Dominik Krumm, Stefan Schwanitz & Stephan Odenwald (Hrsg.)

spinfortec[2022]

Tagungsband zum 14. Symposium
der Sektion Sportinformatik und Sporttechnologie
der Deutschen Vereinigung für Sportwissenschaft (dvs)

spinfortec^{2022}

Tagungsband zum 14. Symposium

der Sektion Sportinformatik und Sporttechnologie

der Deutschen Vereinigung für Sportwissenschaft (dvs)

Chemnitz 29. – 30. September 2022

TECHNISCHE UNIVERSITÄT
CHEMNITZ

Universitätsverlag Chemnitz

2022

Impressum

Bibliographische Informationen der Deutschen Nationalbibliothek

Die Deutsche Nationalbibliothek verzeichnet diese Publikation in der Deutschen Nationalbibliografie; detaillierte bibliografische Daten sind im Internet über http://www.dnb.de abrufbar.

Herausgeber

Dominik Krumm
Stefan Schwanitz
Stephan Odenwald

Technische Universität Chemnitz/ Universitätsbibliothek
Universitätsverlag
09107 Chemnitz
https://www.tu-chemnitz.de/ub/univerlag/index.html

ISBN 978-3-96100-176-7

https://nbn-resolving.org/urn:nbn:de:bsz:ch1-qucosa2-806704

Vorwort der Ausrichter

Liebe Teilnehmende der spinfortec^{2022},

wir freuen uns Sie in Chemnitz, der Kultuhauptstadt Europas 2025, zum 14. Symposium der Sektion Sportinformatik und Sporttechnologie der Deutschen Vereinigung für Sportwissenschaft (dvs) begrüßen zu dürfen. Die Technische Universität Chemnitz ist damit zwanzig Jahre nach Ausrichtung des zweiten divers* Workshops Sporttechnologie zwischen Theorie und Praxis (6.-7. Juni 2002) erneut Gastgeberin für die Wissenschaftsgemeinschaft des Kleinen Faches Sporttechnologie und erstmalig für die Fachrichtung Sportinformatik. Gleichzeitig feiert die Studienrichtung Sportgerätetechnik an der Fakultät für Maschinenbau ihr 25-jähriges Jubiläum. Im Wintersemester 1997/98 wurden die ersten Studierenden in das Profil Sportgerätetechnik des Magisterstudiengangs Sportwissenschaft immatrikuliert. Daher möchten wir uns beim Sprecherrat der Sektion bedanken, uns anlässlich dieses Jubiläums mit der Ausrichtung der Tagung betraut zu haben.

Das Ziel von spinfortec^{2022} ist es, den fachlichen Austausch zu Themen an der Schnittstelle von Sportwissenschaft, Informatik, Elektrotechnik und Maschinenbau zu fördern. Insgesamt wurden 22 Beiträge aus Deutschland, Österreich und England eingereicht und in drei Sitzungen zu den Schwerpunkten (i) *Informations- und Feedbacksysteme im Sport*, (ii) *Digital Motion: Datenerfassung, Analyse und Algorithmen* und (iii) *Sportgeräteentwicklung: Werkstoffe, Konstruktion, Testing* sowie einer Postersitzung präsentiert.

Wir sind erfreut, dass das Format *spinfortec* auch außerhalb der akademischen Forschung wahrgenommen wurde. Das spiegelt sich in dem hohen Anteil an Beiträgen aus der Sportartikelindustrie und außeruniversitären Forschungseinrichtungen wieder.

Ein herzliches Dankeschön möchten wir allen Gutachtern für die gewissenhafte Prüfung der eingereichten Beiträge aussprechen.

Prof. Dr.-Ing. Stephan Odenwald

Dr.-Ing. Stefan Schwanitz

Dr.-Ing. Dominik Krumm

Inhaltsverzeichnis

Wissenschaftlicher Ausschuss & Gutachterausschuss

Wissenschaftlicher Ausschuss

Univ.-Prof. Dr.-Ing. Stephan Odenwald
Dr.-Ing. Dominik Krumm
Dr.-Ing. Stefan Schwanitz

Gutachterausschuss

Dr. Ulrich Fehr (Bayreuth)
M. Sc. Aljoscha Hermann (München)
Prof. Dr. Thomas Jaitner (Dortmund)
Dr.-Ing. Dominik Krumm (Chemnitz)
Prof. Dr. Martin Lames (München)
PD Dr. phil. Habil. Daniel Link (München)
Univ.-Prof. Dr.-Ing. Stephan Odenwald (Chemnitz)
Dr.-Ing. Stefan Schwanitz (Chemnitz)
Dr. Peter Wolf (Zürich)

Sitzung I – Informations- und Feedbacksysteme im Sport

https://nbn-resolving.org/urn:nbn:de:bsz:ch1-qucosa2-806704

OpenPose and its current applications in sports and exercise science: a review

Melanie Baldinger[1] & Veit Senner[1]

[1]Technische Universität München, TUM School of Engineering and Design, Professur für Sportgeräte und Materialien, München, Deutschland

Abstract

The aim of this scoping review is to investigate current applications of a markerless human pose estimation (HPE) algorithm in sports and exercise science. 17 studies are selected for this purpose. Results show that HPE is applied already in a variety of sports for different aims and purposes. Even though it provides many advantages over marker-based approaches, it still comes with challenges that need to be tackled in future research.

Keywords: openpose, sports, exercise, application, scoping review

Introduction

In recent years, human pose estimation (HPE) has become a big field in computer vision. One of the most prominent HPE algorithms is OpenPose (Cao et al., 2021). A wide range of validation studies using OpenPose exist (Badiola-Bengoa & Mendez-Zorrilla, 2021), but some questions still remain open: *I) Has OpenPose found its way into being applied in sports and exercise science? II) What are the current applications and research questions when applying OpenPose in sports and exercise science? III) What are the current challenges?*

Methods

To answer these questions a scoping review has been conducted using PubMed as a primary search engine and the following search strategy: *openpose AND ((sport) OR (physical exercise) OR (exercise))*. This search resulted in 20 publications from which 12 were excluded being either review papers, studies with little or no relation to sport or exercise. 9 additional publications were identified through references in the aforementioned publications that were included in this review which resulted in a total of 17 studies that were studied more closely to answer the research questions of this scoping review.

Results

The selected publications that were included in this scoping review can be seen in Table 1. For each study the type of sport investigated and the goal of the study is presented.

Table 1: Publications included in this scoping review (CMJ = counter movement jump, MBMC = marker-based motion capture, NN = neural networks, OP = OpenPose).

Study	Type of sport	Goal
Arbues-Sanguesa, Martin, Fernandez, Rodriguez, et al. (2020)	Soccer	OP is combined with a super-resolution network to obtain the body orientation of players during the game from video data.
Arbues-Sanguesa, Martin, Fernandez, Ballester, and Haro (2020)	Soccer	Estimation of the feasibility of passes using the passing and receiving player's body orientation (obtained using OP).
Baclig et al. (2020)	Elite-level Squash	Estimation of distance traveled, court position, 'T' dominance and average speed.
Echeverria and Santos (2021)	Karate	Extract features of karate movements from OP to identify the postures using machine and deep learning algorithms.
Haralabidis et al. (2020)	Boxing	3D inverse dynamics analysis of punching kinematics using data inputs from wearable sensors and OP.
Hirasawa et al. (2020)	Squats	Detection of key points for evaluation and scoring of squat postures for feedback.
Nakai et al. (2019)	Basketball	Pose estimation as an input for a posture analysis model to predict free throw.
Nakano et al. (2020)	Walking, CMJ, Ball Throwing	Evaluation of differences in joint positions from OP and a MBMC system.
Needham, Evans, Cosker, and Colyer (2021)	Sprinting & Skeleton push start	Evaluation of 3D mass center positions and velocities comparing OP and MBMC.
Needham, Evans, Cosker, Wade, et al. (2021)	Walking, Jumping, Running	Accuracy evaluation for (reconstructed) 3D joint center location of OP and other HPE methods.
Palucci Vieira et al. (2022)	Soccer	Evaluation of OP for obtaining lower limb kicking kinematics comparing to manual digitization.
Park et al. (2020)	Push-Ups	Counting and classification of correct and incorrect push-ups.
Pinheiro et al. (2022)	Soccer	Evaluation of OP to determine body orientation during penalty kicks and investigate its interplay with the goalkeeper strategy.
Shimizu et al. (2019)	Tennis	Prediction of shot direction with NN using OP joint positions and player positions during time of impact as inputs.
Suda et al. (2019)	Volleyball	Prediction of ball trajectory using body joints from OP (2D) and Kinect (3D) applying NN.
Wang and Wang (2022)	Walking, Running, Swimming, Situps, Pullups, Basketball, Rope Jump	Identification and evaluation of movements using OP joint position data as input for a convolutional NN.
Webering et al. (2021)	Vertical Jump	Evaluation of vertical jump height using OP to approximate the body's center of mass.

Discussion

I) Application in sport science: OpenPose is already applied in a diverse range of sports from body-weight exercise (Hirasawa et al., 2020; Park et al., 2020; Wang & Wang, 2022) to walking and running (Nakano et al., 2020; Needham, Evans, Cosker, Wade, et al., 2021; Wang & Wang, 2022) as well as team sports such as Basketball (Nakai et al., 2019), Volleyball (Suda et al., 2019) and soccer (Arbues-Sanguesa, Martin, Fernandez, Ballester, & Haro, 2020; Arbues-Sanguesa, Martin, Fernandez, Rodriguez, et al., 2020; Palucci Vieira et al., 2022; Pinheiro et al., 2022).

II) Current research questions: Some of the studies deal with the validation of the algorithm in determining different parameters, such as joint and mass center positions and velocities (Nakano et al., 2020; Needham, Evans, Cosker, & Colyer, 2021; Needham, Evans, Cosker, Wade, et al., 2021; Wang & Wang, 2022). While in other studies data is used to identify postures (Echeverria & Santos, 2021; Hirasawa et al., 2020; Nakai et al., 2019; Park et al., 2020), to estimate kinematic parameters (Baclig et al., 2020; Haralabidis et al., 2020; Palucci Vieira et al., 2022; Webering et al., 2021) or body orientation (Arbues-Sanguesa, Martin, Fernandez, Ballester, & Haro, 2020; Arbues-Sanguesa, Martin, Fernandez, Rodriguez, et al., 2020; Pinheiro et al., 2022). Some studies use the derived data for predictions of sports-specific parameters (Nakai et al., 2019; Shimizu et al., 2019; Suda et al., 2019).

III) Current challenges: The advantages of OpenPose over conventional marker-based motion capture in sports and exercise science are manifold. On the one hand it only requires one non-specialized camera meaning lower costs (Nakai et al., 2019). On the other hand, limited manual intervention and expertise is required to prove near-time analysis (Baclig et al., 2020). Furthermore, it does not require a laboratory setup which allows to analyze video data from competition or from sports that formerly could not be analyzed. However, there are still challenges that need to be considered. Poor performance can be the result of fast and explosive movements (Shimizu et al., 2019), rare or challenging body poses common in some sports (Badiola-Bengoa & Mendez-Zorrilla, 2021; Needham, Evans, Cosker, & Colyer, 2021) or occlusions and interactions of players with each other or with equipment (Badiola-Bengoa & Mendez-Zorrilla, 2021). In some cases the algorithm fails to correctly detect left and right side of the body which requires either a correction of such failures (Nakano et al., 2020) or 3D instead of 2D motion data (Nakai et al., 2019; Park et al., 2020). Generalization to other sports or applications still needs to be treated with caution and more diverse and sports-specific datasets to train these algorithms are needed.

Conflict of Interest We declare no conflict of interest.

Funding This work was funded by funds of the Professorship of Sports Equipment and Materials.

References

Arbues-Sanguesa, A., Martin, A., Fernandez, J., Ballester, C., & Haro, G. (2020). Using Player's Body-Orientation to Model Pass Feasibility in Soccer. In *2020 IEEE/CVF Conference on Computer Vision and Pattern Recognition Workshops (CVPRW).* IEEE.

Arbues-Sanguesa, A., Martin, A., Fernandez, J., Rodriguez, C., Haro, G., & Ballester, C. (2020). Always Look On The Bright Side Of The Field: Merging Pose And Contextual Data To Estimate Orientation Of Soccer Players. In *2020 IEEE International Conference on Image Processing: Proceedings: September*

25-28, 2020: Virtual conference, Abu Dhabi, United Arab Emirates (pp. 1506–1510). IEEE. https://doi.org/10.1109/ICIP40778.2020.9190639

Baclig, M. M., Ergezinger, N., Mei, Q., Gül, M., Adeeb, S., & Westover, L. (2020). A Deep Learning and Computer Vision Based Multi-Player Tracker for Squash. *Applied Sciences*, *10*(24), 8793. https://doi.org/10.3390/app10248793

Badiola-Bengoa, A., & Mendez-Zorrilla, A. (2021). A Systematic Review of the Application of Camera-Based Human Pose Estimation in the Field of Sport and Physical Exercise. *Sensors (Basel, Switzerland)*, *21*(18). https://doi.org/10.3390/s21185996

Cao, Z., Hidalgo, G., Simon, T., Wei, S.-E., & Sheikh, Y. (2021). Openpose: Realtime Multi-Person 2D Pose Estimation Using Part Affinity Fields. *IEEE Transactions on Pattern Analysis and Machine Intelligence*, *43*(1), 172–186. https://doi.org/10.1109/TPAMI.2019.2929257

Echeverria, J., & Santos, O. C. (2021). Toward Modeling Psychomotor Performance in Karate Combats Using Computer Vision Pose Estimation. *Sensors (Basel, Switzerland)*, *21*(24).

Haralabidis, N., Saxby, D. J., Pizzolato, C., Needham, L., Cazzola, D., & Minahan, C. (2020). Fusing Accelerometry with Videography to Monitor the Effect of Fatigue on Punching Performance in Elite Boxers. *Sensors (Basel, Switzerland)*, *20*(20).

Hirasawa, Y., Gotoda, N., Kanda, R., Hirata, K., & Akagi, R. (2020). Promotion System for Home-Based Squat Training Using OpenPose. In H. Mitsuhara (Ed.), *Proceedings of 2020 IEEE International Conference on Teaching, Assessment, and Learning for Engineering (TALE): Date and venue: 8-11 December 2020, online* (pp. 984–986). IEEE.

Nakai, M., Tsunoda, Y., Hayashi, H., & Murakoshi, H. (2019). Prediction of Basketball Free Throw Shooting by OpenPose. In K. Kojima, M. Sakamoto, K. Mineshima, & K. Satoh (Eds.), *Springer eBooks Computer Science: Vol. 11717. New Frontiers in Artificial Intelligence: Jsai-isAI 2018 Workshops, JURISIN, AI-Biz, SKL, LENLS, IDAA, Yokohama, Japan, November 12–14, 2018, Revised Selected Papers* (1st ed., Vol. 11717, pp. 435–446). Springer. https://doi.org/10.1007/978-3-030-31605-1_31

Nakano, N., Sakura, T., Ueda, K., Omura, L., Kimura, A., Iino, Y., Fukashiro, S., & Yoshioka, S. (2020). Evaluation of 3D Markerless Motion Capture Accuracy Using OpenPose With Multiple Video Cameras. *Frontiers in Sports and Active Living*, *2*, Article 50, 50.

Needham, L., Evans, M., Cosker, D. P., & Colyer, S. L. (2021). Can Markerless Pose Estimation Algorithms Estimate 3D Mass Centre Positions and Velocities during Linear Sprinting Activities? *Sensors (Basel, Switzerland)*, *21*(8). https://doi.org/10.3390/s21082889

Needham, L., Evans, M., Cosker, D. P., Wade, L., McGuigan, P. M., Bilzon, J. L., & Colyer, S. L. (2021). The accuracy of several pose estimation methods for 3D joint centre localisation. *Scientific Reports*, *11*(1), 20673. https://doi.org/10.1038/s41598-021-00212-x

Ota, M., Tateuchi, H., Hashiguchi, T., & Ichihashi, N. (2021). Verification of validity of gait analysis systems during treadmill walking and running using human pose tracking algorithm. *Gait & Posture*, *85*, 290–297. https://doi.org/10.1016/j.gaitpost.2021.02.006

Palucci Vieira, L. H., Santiago, P. R. P., Pinto, A., Aquino, R., Da Torres, R. S., & Barbieri, F. A. (2022). Automatic Markerless Motion Detector Method against Traditional Digitisation for 3-Dimensional Movement

Kinematic Analysis of Ball Kicking in Soccer Field Context. *International Journal of Environmental Research and Public Health*, *19*(3).

Park, H.-J., Baek, J.-W., & Kim, J.-H. (2020). Imagery based Parametric Classification of Correct and Incorrect Motion for Push-up Counter Using OpenPose. In *2020 IEEE 16th International Conference on Automation Science and Engineering (CASE)* (pp. 1389–1394). IEEE.

Pinheiro, G. d. S., Jin, X., Da Costa, V. T., & Lames, M. (2022). Body Pose Estimation Integrated With Notational Analysis: A New Approach to Analyze Penalty Kicks Strategy in Elite Football. *Frontiers in Sports and Active Living*, *4*, 818556.

Shimizu, T., Hachiuma, R., Saito, H., Yoshikawa, T., & Lee, C. (2019). Prediction of Future Shot Direction using Pose and Position of Tennis Player. In R. Lienhart (Ed.), *ACM Digital Library, Proceedings Proceedings of the 2nd International Workshop on Multimedia Content Analysis in Sports* (pp. 59–66). Association for Computing Machinery.

Suda, S., Makino, Y., & Shinoda, H. (2019). Prediction of Volleyball Trajectory Using Skeletal Motions of Setter Player. In *ACM Other conferences, Proceedings of the 10th Augmented Human International Conference 2019* (pp. 1–8). ACM.

Wang, Q., & Wang, Q.-M. (2022). Aided Evaluation of Motion Action Based on Attitude Recognition. *Journal of Healthcare Engineering*, *2022*, 8388325.

Webering, F., Blume, H., & Allaham, I. (2021). Markerless camera-based vertical jump height measurement using OpenPose. In *2021 IEEE/CVF Conference on Computer Vision and Pattern Recognition Workshops (CVPRW)* (pp. 3863–3869). IEEE.

https://nbn-resolving.org/urn:nbn:de:bsz:ch1-qucosa2-806704

Vorhersage des in-game Status im Fußball mit Maschinellem Lernen basierend auf zeitkontinuierlichen Spielerpositionsdaten

Steffen Lang[1], Raphael Wild[1], Alexander Isenko[1], Daniel Link[1]

[1]Technische Universität München, München, Deutschland

Kurzfassung

Diese Studie beschäftigt sich mit der Vorhersage, ausschließlich auf Basis von Spielerpositionsdaten, ob ein Fußballspiel in einem Moment unterbrochen ist oder nicht. Hierfür wurden vier machine-learning Modelle mit Daten von 102 Spielen der Fußball Bundesliga trainiert und ihre Genauigkeit evaluiert. Dabei zeigte sich eine Genauigkeit von bis zu 92% für einen einzelnen Moment und eine Präzision von 81% für ganze Unterbrechungen.

Schlüsselwörter: Fußball, Maschinelles Lernen, Spielerpositionsdaten, in-game Status

Einleitung

Die Information, ob ein Spiel unterbrochen ist oder nicht, ist ein zentrales Strukturierungsmerkmal eines Fußballspiels. Dieser sogenannte in-game Status ist notwendig, um bspw. Leistungsindikatoren relativ zur Nettospielzeit zu berechnen oder Standardsituationen in Positionsdaten oder Videomaterial finden und analysieren zu können. Während der in-game Status im Profifußball von Datendienstleistern manuell erhoben wird, steht er im Amateurbereich nicht zur Verfügung. Allerdings werden auch hier zunehmend Spielerpositionsdaten über GPS erhoben[1]. Unter der Annahme, dass die Bewegungsaktivität der Spieler vom in-game Status abhängig ist, untersucht unsere Studie, in welchem Ausmaß sich diese Variable aus zeitkontinuierlichen Spielerpositionen bestimmen lässt.

Methode

Es wurden vier etablierte machine-learning Verfahren verwendet: AdaBoost (AD), Logistic Regression (LR), Decision Tree (DT) und Random Forest (RF)[2]. Training und Evaluation der Modelle erfolgte auf Basis von xy-Positionsdaten von Spielern (25Hz, TRACAB Corp.) sowie dem manuell annotierten in-game Status in 102 Spielen der deutschen Fußball Bundesliga[3]. Der Datensatz, zur Verfügung gestellt durch die Deutsche Fußball Liga, wurde geteilt in Trainings- (45 Spiele) / Validierungsset (10) und Testset (47). Für unsere Experimente wurden die Implementierungen für diese Algorithmen mit der scikit-learn-Bibliothek[4] (v0.20.3) für Python verwendet.

Aus den Rohdaten haben wir eine Reihe von Features für jeden Frame in einem Spiel mit einer Frequenz von 25 Hz abgeleitet. Jede Stichprobe enthält die Informationen zu den 22 Spielern auf dem Feld und deren Positionen (x,y), Geschwindigkeit und Beschleunigung. Anschließend wurde jede Stichprobe mit Merkmalen aus den vergangenen und zukünftigen Frames ergänzt, um den Modellen mehr Kontextinformationen zu liefern. Genauer gesagt enthält jede Stichprobe zusätzliche Informationen von 0,4, 0,8, 2, 4, 20, 40 und 80 Sekunden aus der Vergangenheit und der Zukunft. Der Grund für die Wahl dieser Werte ist die Bereitstellung von Informationen über die Handlungen der Spieler unmittelbar vor und nach der aktuellen Situation sowie über den langfristigen Kontext, wobei die Auswahl der wichtigen Informationen dem Lernalgorithmus überlassen wird. Zusammenfassend lässt sich sagen, dass alle Modelle dieselben Eingabemerkmale verwendeten: Die vier individuellen Merkmale aller 22 Spieler auf dem Spielfeld sind die x- und y-Koordinaten jedes Spielers in Metern, die Geschwindigkeit in m/s und die Beschleunigung in m/s². Diese Stichprobe für jeden Frame wurde um 14 weitere erweitert, sowohl sieben aus der Vergangenheit und der Zukunft. Daraus ergibt sich, dass jede Stichprobe aus 1.320 (22 × 4 × 15) Eingabemerkmalen besteht.

Wir haben die Leistung der endgültigen Modelle anhand von vier Ansätzen evaluiert. 1) Durchführung einer frame-wise Evaluierung, die den in-game Status in der Ground Truth (GT) mit der Vorhersage in jedem Frame vergleicht. Als Leistungskennzahlen berechneten wir die Genauigkeit und den F1-Score für jedes Modell. 2) Die Leistung des Modells wurde auch auf Basis vollständiger Unterbrechungen evaluiert. Die Grundidee besteht darin, aus den Originaldaten und den Vorhersagen Spielunterbrechungen zu extrahieren. 3) Überprüfung, ob die vorhergesagten Anfangs- und Endpunkte der Unterbrechungen nicht zu stark von den tatsächlichen abweichen. 4) Berechnung und Evaluierung des Leistungsindikators Total Distance Covered (TDC) in der Netto-Spielzeit (TDC_E). TDC ist einer der gebräuchlichsten Leistungsindikatoren zur Schätzung der Arbeitsbelastung[5,6]. TDC_E stellt die Laufaktivität dar, wenn der Ball im Spiel ist, und kann als Spielintensität interpretiert werden. Da der Fehler bei der Vorhersage des in-game Status einen Fehler in den TDC_E mitbringt, haben wir geprüft, ob dieser Fehler für die Leistungsanalyse noch akzeptabel ist.

Ergebnisse

Die Validierung für die Vorhersage des in-game Status auf Frameebene (1) ergab eine Genauigkeit von 85% - 92%. Tabelle 1A zeigt den durchschnittlichen F1-Score und die Genauigkeit unserer Modelle für alle 47 Testspiele. Hier zeigt AD die besten Ergebnisse bei der Genauigkeit mit 92,0 ± 2,1% und dem F1-Score mit 93,1 ± 2,4% insgesamt.

Die Erkennung von Phasen (länger als 2s) in denen das Spiel unterbrochen war (2), erfolgte beim besten Verfahren (AD) mit einer Precision von PPV=.81, einem Recall von TPR=.79 und einem mittleren absoluten zeitlichen Fehler von 1.79 s beim Startpunkt und 1.68 s beim Endpunkt. AD hat einen um 12 % höheren mittleren F1-Score für alle Spiele (F1 = 79,8 ± 5,8%) im Vergleich zu den anderen drei Modellen, die zwischen 67,9 ± 5,1% (RF) und 61,2 ± 6,1% (LR) liegen (Tab. 1B). AD übertraf bei der Vorhersage die anderen Modelle in 42 von 47 Spielen.

Außerdem haben wir die Länge der zeitlichen Verschiebungen überprüft (3). Hier war bei mehr als 51 % (Start) und 58 % (Ende) die Abweichung vom realen Punkt ≤1s, und mehr als 78 % (Start) und 80 % (Ende) aller Unterbrechungen hatten eine Verschiebung von ≤2s. Die mittlere absolute Verschiebung betrug 1,79 ± 3,44s (99% CI [1,65, 1,94]) für den Startpunkt und 1,68 ± 3,47s (99% CI [1,54, 1,83]) für den Endpunkt.

Tabelle 2 vergleicht den TDC_E, der unter Verwendung des auf der GT basierenden in-game Status berechnet wurde, mit der AD-Vorhersage und einem naiven Ansatz (4). Die Ergebnisse zeigen, dass die Unterschiede zwischen dem TDC_E der GT und AD geringer sind, als die Unterschiede zwischen dem TDC_E von GT und dem naiven Ansatz. Zur Interpretation der Fehlergröße unter Berücksichtigung der Leistungsanalyse haben wir den von Hopkins eingeführten, so genannten "smalles worthwhile change" (SWC)[7], verwendet. SWC bezieht sich auf die kleinste Änderung einer Leistungsvariable innerhalb einer Messreihe, die im Sport praktische Bedeutung hat. Für den Fußball wird in der Literatur ein SWC von 20 % der Variation eines Laufleistungsindikators innerhalb oder zwischen den Athleten empfohlen[8]. Dieser Empfehlung folgend beträgt die SWC für TDC_E 326 m und ist somit höher als die Standardabweichung des mittleren Fehlers der AdaBoost Vorhersage (273 m).

Tab. 1: Vorhersageergebnisse für A) Frame-wise und B) Unterbrechungen der vier ausgewählten ML-Modelle in 47 Testspielen. Genauigkeit, Precision, Recall und F1-Score in Prozent mit Standardabweichung. In B) werden nur Unterbrechungen mit einer Mindestdauer von 2 s berücksichtigt. Die besten Ergebnisse sind fett gedruckt.

	Random Forest	**Logistic Regression**	**Decision Tree**	**AdaBoost**
		A) Frame-wise		
Genauigkeit	89.3 (±2.0)	86.7 (±2.0)	84.6 (±1.9)	92.0 (±2.1)
Precision	88.1 (±4.0)	88.3 (±3.9)	85.8 (±4.3)	93.4 (±2.6)
Recall	94.6 (±2.2)	89.4 (±3.4)	88.8 (±3.0)	93.0 (±4.0)
F1 Score	91.2 (±2.3)	88.7 (±2.3)	87.2 (±2.3)	93.1 (±2.4)
		B) Unterbrechungen		
Precision	68.8 (±6.4)	58.9 (±7.6)	68.6 (±7.2)	81.1 (±7.4)
Recall	67.4 (±5.6)	64.5 (±6.7)	61.6 (±6.4)	78.9 (±5.7)
F1-Score	67.9 (±5.1)	61.2 (±6.1)	64.7 (±5.8)	79.8 (±5.8)

Tab. 2: Gesamtdistanz, die pro Spieler in der Netto-Spielzeit zurückgelegt wurde, berechnet mit dem in-game Status der Ground Truth, der AdaBoost-Vorhersage und einem naiven Ansatz für 751 Spieler, ohne Torhüter, die nur das volle Spiel gespielt haben. Unterschiede zwischen der Ground Truth, der AdaBoost-Vorhersage und dem naiven Ansatz.

	TDC_E pro Spieler in der Netto Spielzeit		
	Ground Truth (GT)	**AdaBoost**	**Naiver Ansatz**
Durchschnitt [m]	7939 (± 1631)	8041 (± 1683)	6348 (± 1099)
Mittlerer Fehler zur GT [m]		-102 (± 273)	1590 (± 683)
Mittlerer absoluter Fehler (MAE) zur GT [m]		238 (± 169)	1594 (± 674)
99% Konfidenz Intervall (MAE) [m]		[222 ; 254]	[1531 ; 1658]
Inter-Klassen Koeffizient (ICC)		0.985	0.532
R (Pearson)		0.987	0.949

Diskussion

Unsere Daten zeigen, dass das trainierte AD-Modell eine geeignete technologische Lösung für die Bestimmung des in-game Status anhand der zeitkontinuierlichen Spielerpositionen darstellt. Das AD-Modell kann mehr als 78 % der Anfangs- und Endpunkte von Spielunterbrechungen mit einem zeitlichen Verschiebungsfehler von weniger als 2 s vorhersagen, was für Videoanalysen gut genug sein sollte. Am Beispiel des TDC zeigt unsere Analyse, dass in-game Status basierende Leistungsindikatoren mit einem akzeptablen Fehler berechnet werden können. In Szenarien, in denen Mannschaften nur Zugang zu Spielerpositionen haben (z. B. von GPS/LPM-Systemen), aber nicht zu von manuell erhobenen in-game Status- und/oder Ballpositionsdaten, z. B. im Amateur- oder Jugendfußball, kann unser Ansatz die Spielanalyse verbessern.

Interessenskonflikt Wir erklären keine Interessenskonflikte.

Literatur

1. Goes FR, Kempe M, van Norel J, Lemmink KAPM. Modelling team performance in soccer using tactical features derived from position tracking data. *IMA J Management Math*. 2021;32(4):519–533. doi:10.1093/imaman/dpab006
2. Bonaccorso G. Machine Learning Algorithms: Popular Algorithms for Data Science and Machine Learning. Second Edition. Birmingham, Mumbai: Packt; 2018.
3. DFL. How is the official match data collected? | DFL Deutsche Fußball Liga. Available from: https://www.dfl.de/en/innovation/how-is-the-official-match-data-collected/. Updated October 30, 2020. Accessed January 20, 2022.
4. Pedregosa F, Varoquaux G, Gramfort A, et al. Scikit-learn: Machine Learning in Python. *Journal of Machine Learning Research*. 2011;12:2825–2830.
5. Clemente F, Silva R, Arslan E, Aquino R, Castillo D, Mendes B. The effects of congested fixture periods on distance-based workload indices: A full-season study in professional soccer players. *bs*. 2021;38(1):37–44. doi:10.5114/biolsport.2020.97068
6. Rojas-Valverde D, Gómez-Carmona CD, Bastida Castillo A, et al. A longitudinal analysis and data mining of the most representative external workload indicators of the whole elite Mexican soccer clubs elite Mexican soccer clubS. *International Journal of Performance Analysis in Sport*. 2021:1–16. doi:10.1080/24748668.2021.1996131
7. Hopkins W. How to interpret changes in an athletic performance test. *Sportscience*. 2004;8:1–7. Available from: https://ci.nii.ac.jp/naid/10025270469/.
8. Buchheit M. Magnitudes matter more than Beetroot Juice. *Sport Performance & Science Reports*. 2018;15. Available from: https://sportperfsci.com/magnitudes-matter-more-than-beetroot-juice/.

https://nbn-resolving.org/urn:nbn:de:bsz:ch1-qucosa2-806704

Exercise assessment in trampoline sport by automated jump classification

Lucas Woltmann[1], Katja Ferger[2], Claudio Hartmann[1] & Wolfgang Lehner[1]

[1]Technische Universität Dresden, Dresden Database Research Group, Dresden, Germany

[2]Justus Liebig University Giessen, Institute of Sport Science, Giessen, Germany

Abstract

The results of the presented work show that machine learning (ML) can be used to support correct training logging in order to improve technical performance in trampoline gymnastics. They indicate considerable potential for expanding mobile applications in a sport with complex movement requirements.

Keywords: trampoline sport, machine learning, tool, training support

Introduction

Trampoline competitions consist of different routines with ten elements in each routine. A set drill and a voluntary drill are conducted in the qualifying rounds, while a voluntary drill is conducted in the finals. The first exercise in the preliminary round (set) contains ten predetermined skills. In competitions, the judges' job is to score a particular routine and establish an overall score for that routine based on the Overall Difficulty Rating (DD), Overall Skill Execution (E), Time of Flight (ToF) measurement and the newly added Measurement of horizontal displacement (HD; cf. Regulations of the International Gymnastics Federation, FIG, 2021). Time of flight and horizontal displacement are automatically recorded by a measuring system, whereas several judges evaluate the execution of the exercise. The difficulty of each element is calculated by a referee on the basis of the amount of twist and somersault rotation.

At present, there is no known reliable method for the automated detection and recognition of the various gymnastic elements for determining the difficulty of an exercise in trampoline gymnastics. And the use of machine learning methods for the detection of complex jump movements, such as those occurring in trampoline gymnastics, has been insufficiently explored up to now (Helten et al. 2011, Woltmann et al. 2022).

The aim of the presented tool is to use sensor-based data and the machine learning approach to make it utilisable for technical training and to automate the detection of the jumps within an exercise and, in the long term, for competitions.

In the remainder of this work, we present three scenarios in which our tool is used and give illustrative examples on how they improve everyday work of athletes and trainers. Furthermore, we discuss the possibility to use our tool for automatic difficulty determination in competitions.

Methods

In order to improve the assessment of exercises in trampoline sport, we present a tool that is able to give athletes the opportunity to analyse their jumps based on sensor data. The data is obtained by equipping the athletes with a single gyroscopic sensor on their back. For the assessment, the user interface of the tool provides three scenarios. Every scenario individually covers one major aspect of the self-assessment process by displaying the most important information for that particular analysis. The three scenarios are: (1) the jump protocol diary with automated jump classification, (2) the jump analysis with the visualization of the sensor data, and (3) the scientific analysis providing further information about the model used for automatic jump classification. In the following, we describe each of the three scenarios and their implementation in the tool. In general, the tool and its scenarios are presented to athlete and trainer as a website.

Firstly, we present the jump protocol scenario pictured in (Fig. 1a). Here, the athletes can upload the measurements from the gyroscopic sensor and the exercise protocol, which contains all jumps of the current exercise. After the upload, the jumps are automatically classified using a neural network (NN), which analyses the sensor data as presented in previous work (Woltmann et al., 2022). In our case, jump classification means the automated labelling of a jump in respect to one of the 148 jump types as defined by the FIG. In addition to the jump type, the NN returns a confidence score (0-100%) for each jump. This score tells the athlete, how certain the classification is.

The second scenario, as illustrated in (Fig. 1b), shows the quantitative analyses of a single jump from the jump protocol. For this, the tool plots all measurement channels as line plots. With the dynamic selection of plotted channels, athlete and trainer can do a detailed analysis for all aspects of the jump. Additionally, the plot shows an average representation of all measurements of the recognized jump type. This allows for a quality assessment on how close the jump was to either the previous jumps or an ideal execution of the jump.

Lastly, the third scenario contains a scientific analysis of the behaviour of the NN for each classified jump. NNs are black boxes by nature meaning a direct interpretation of their inner workings is not possible. Therefore, we use feature importance that calculates the direct impact of each measured channel on the classification decision. For our scenario, we use Shapley Additive Explanation (SHAP) values, as they are known to perform very well with NNs (Lundberg et al., 2017). The SHAP values are visualised as an ordered bar chart where each gyroscopic measurement channel receives a SHAP value showing its quantitative influence on the final jump classification. This leads to the opportunity for discussing the expressiveness of certain channels for a jump type. The third scenario is targeted towards a scientific user and not primarily towards the athlete.

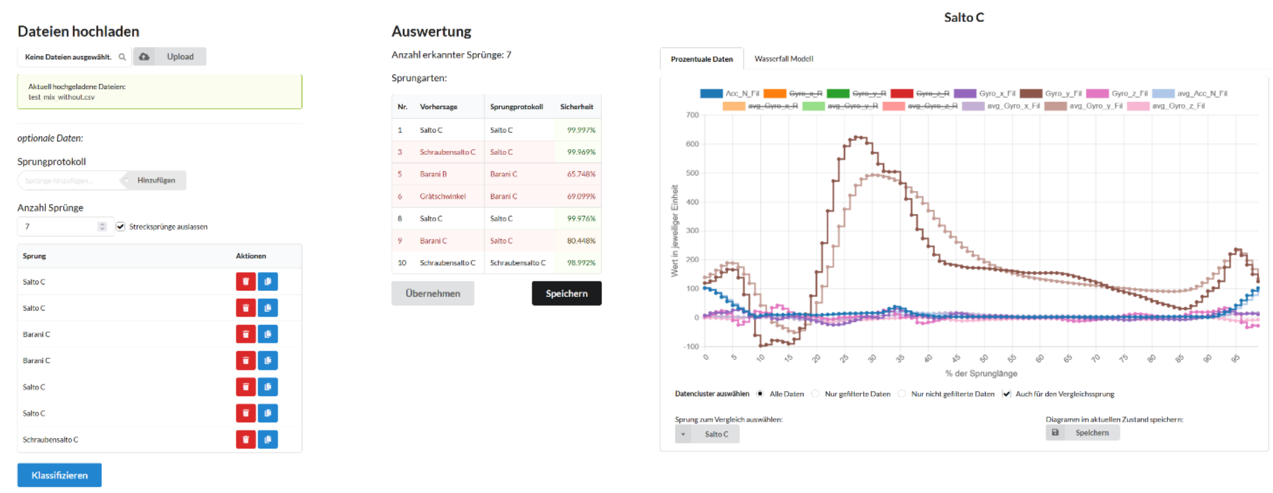

(a) (b)

Fig. 1 (a) The jump protocol screen (scenario 1); (b) The quantitative analysis screen (scenario 2).

Results

Given the three scenarios we described in the previous section, we now illustrate their advantages in the everyday work of athletes and trainers. Our tool can help to prevent and correct common mistakes in protocoling the daily training and adapt training routines.

The automated jump classification for the jump protocol from the first scenario can help in two ways. First, if the athlete has noted the incorrect jump in the protocol, the model would predict the correct jump type with a high confidence score. This indicates a high probability that the jump is incorrect in the jump protocol and may be corrected. Second, if the athlete executes a jump incorrectly, the model would predict the same jump type as in the protocol but with a low confidence score. Therefore, the jump is correct in the jump protocol but the sensor data is not consistent with previous executions of the same jump. In conclusion, the execution of the jump must have been sub-optimal.

The quantitative analysis of the second scenario provides a more detailed view for the error analysis. Sticking to the example of the incorrect jump execution, the quantitative analysis can help to find the erroneous part of the jump. The athlete can go through all plotted measurements to find anomalies, compare their measurements to the average representative of that particular jump type, and search for deviations from an ideal jump.

The scientific analysis in the third scenario helps to get a deeper understanding of the use of Machine Learning in the field of automated athlete data analysis, i.e., trampoline jump classification. SHAP values improve the understanding of the decision making of NNs making them more transparent. In our case, the analysis is used to identify expressive measurement channels for jump types. For example, previous work has shown that the NN correctly identifies the rotation around the athlete's y-axis as the most expressive part for a back tucked somersault (Woltmann et al., 2022). Additionally, this can again be used for error analysis. If a jump is classified wrongly or with a low confidence score, the SHAP values show what channel (and therefore which movement) led to the incorrect classification. From this, athletes can include this information in their next training by actively modifying the particular movement.

Discussion

This study shows that ML methods can be used to detect jumps using sensor data. However, the application of mobile sensors in combination with prediction models for jump detection has been insufficiently studied so far. The approach proposed herein shows considerable potential for expanding mobile applications in sports with complex movement requirements.

In addition to the automated logging of the training data and the quality assessment of various jumps, the automated determination of the difficulty of jumps according to international evaluation rules is a special challenge. The approach presented here shows perspectives for supporting the difficulty judges and enables a phase-specific assessment of individual jumps by using the first scenario in a real-time environment.

For example, currently there is a problem regarding the recognition of combinations of double somersaults and double twists. Here, the exact distinction between “Full in Full out” (one twist in the first somersault, one twist in the second somersault - 822) and “Half in rudy out Fliffis” (half twist in the first somersault, one and a half twists in the second somersault - 813) seems to be possible in the future by using automated jump classification based on sensor data. Finally, this approach seems to be promising for other technical-compositional sports that also calculate the difficulty of elements based on twists, somersaults and twist rotations, such as gymnastics, diving, and rhythmic gymnastics.

Conflict of interest We declare no conflicts of interest.

Funding No special funding was received for this work.

References

FIG Executive Committee. (2021). 2021–2022-2024 Code of Points. https://www.gymnastics.sport/publicdir/rules/files/en_TRA%20CoP%202022-2024.pdf.

Woltmann, L., Hartmann, C., Lehner, W., Rausch, P. & Ferger, K. (2022). Sensor-based jump detection and classification with Machine Learning in trampoline gymnastics. *German Journal of Exercise and Sport Research*, under review.

Helten, T., Brock, H., Müller, M. & Seidel, H.-P. (2011). Classification of trampoline jumps using inertial sensors. *Sports Engineering, 14*(2-4), 155–164. https://doi.org/10.1007/s12283-011-0081-4

Lundberg, S. M., & Lee, S. I. (2017). A unified approach to interpreting model predictions. *Advances in neural information processing systems*, 30.

https://nbn-resolving.org/urn:nbn:de:bsz:ch1-qucosa2-806704

Reinforcement learning estimates muscle activations

Gheorghe Lisca[1,2,3], Cristian Axenie[3], Thomas Grauschopf[2,3] & Veit Senner[1]

[1]Technical University of Munich, TUM School of Engineering and Design, Munich, Germany

[2]Technische Hochschule Ingolstadt, Faculty of Computer Science, Ingolstadt, Germany

[3]Audi Konfuzius-Institut Ingolstadt Laboratory, Ingolstadt, Germany

Abstract

A digital twin of the human neuromuscular system can substantially improve the prediction of injury risks and the evaluation of the readiness to return to sport. Reinforcement learning (RL) algorithms already learn physical quantities unmeasurable in biomechanics, and hence can contribute to the development of the digital twin. Our preliminary results confirm the potential of RL algorithms to estimate the muscle activations of an athlete's moves.

Keywords: neuromuscular control, neuromechanical simulation, reinforcement learning

Introduction

A detailed assessment of the human neuromuscular system (NMS) can drastically improve the prediction of injury risks for a healthy athlete and the evaluation of the readiness to return to sports for an injured one. Furthermore, such a detailed assessment will bring us one step closer to an accurate digital twin (Barricelli Barbara Rita et al., 2020) of the human NMS and significantly improve the personalization and efficiency of neuromuscular training. Neuromechanical simulators (Seth et al., 2018) already estimate the muscle activations of an athlete and reproduce a captured movement on the athlete's musculoskeletal model. Unfortunately, trajectory optimization techniques, on which they rely, constrain their usage for simple movements and with simplified musculoskeletal models. These constraints limit the neuromechanical simulators from accurately modelling the NMS of an athlete. However, the recently developed RL algorithms show great potential for overcoming these limitations (Song et al., 2021). They are already capable of reproducing complex captured movements on torque actuated skeletal models within physics simulators (Peng et al., 2022). We envision to employ them to reproduce the muscle activations necessary for the generation of the captured movements of an athlete on the athlete's personalized musculoskeletal model within a neuromechanical simulator. Since this is an ambitious endeavor, it is essential to validate at small scale that RL algorithms learn plausible muscle activations.

Methods

We designed our experiment that the learned muscle activations are directly comparable with the ones optimized by the state-of-the-art Moco optimizer (Dembia et al., 2021).

Neuromechanical simulators enable the research of the connections between the brain and the body while dynamically interacting with the world. They encompass computational models of different fidelity for each of them.

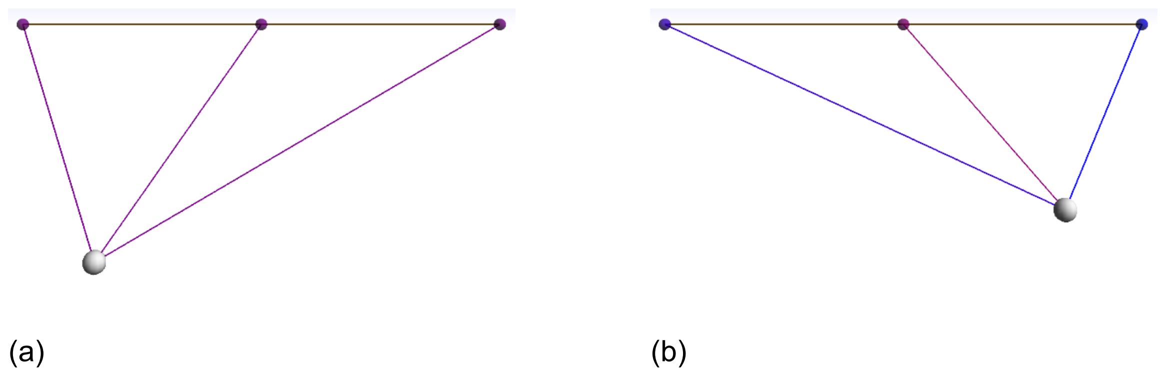

Fig. 1 (a) The point mass in its initial position; (b) The point mass in its final position.

A mass suspended by three muscles depicted in Fig. 1 is one of the first experiments performed with Moco to validate that the muscle activations which it optimizes are plausible. We reproduced the same simulation setup to validate that the RL algorithms learn muscle activations which resemble the ones optimized by Moco, using optimal control theory. The simulation setup consists of a point mass of 1 kg which moves only in a vertical plane, is suspended by three muscles, and is under the influence of gravity. We want to find the activations which will command the three muscles to move the point mass from its initial position (Fig. 1a) to its desired one (Fig. 1b) with minimum energy and within the defined time interval (0.4 seconds). The simulation setup runs in OpenSim, which simulates the three muscles using the De Groote implementation of the Hill's muscle model.

The dynamic optimizer of Moco leverages the advantages of the direct collocation method used in trajectory optimization techniques, automatically generates a nonlinear problem which it solves using the IPOPT solver (Wächter & Biegler, 2006). For this simulation setup, Moco receives the initial and desired positions of the point mass, the time interval and outputs the optimized muscle activations.

Reinforcement Learning has its roots in the theory of animal learning, and its core component is the learning from the interaction with the environment. During the last decade the RL algorithms obtained multiple spectacular results, mostly by leveraging the breakthroughs of Deep Learning (DL) ones which became very successful at training highly complex Artificial Neural Networks (ANNs). In contrast to the dynamic optimization algorithms which optimize for muscle activations relative to the provided costs and constraints, the RL algorithms, by repeated trial-and-error, learn to generate improved muscle activations. This generative capability is particularly valuable for our experiments.

Behavioral cloning (BC) (Ho et al., 2016) is one of the simplest RL which trains an ANN to map the set of context to the one of actions provided as training examples. The Cartesian trajectory of the point mass obtained from the forward simulation of Moco's optimized activations represents the set of contexts, and the optimized activations represents the one of actions. BC runs multiple forward simulations of the muscle activations which the ANN generates. It selects the ones which best resemble the optimized muscle activations and uses them to retrain the ANN. After a few iterations, the ANN becomes increasingly better and generates muscle activations which mirror with precision the optimized ones. The ANN is a multilayer perceptron with 4 sequential layers, each composed of 64 neurons with hyperbolic tangent as the activation function.

Results

The first three plots of Fig. 2 present the activations of the three muscles over time. The dashed lines depict Moco's optimized muscle activations, and the continuous ones depict the BC's learned ones. The fourth plot presents the two Cartesian trajectories of the point mass obtained from forward simulating the optimized and learned muscle activations.

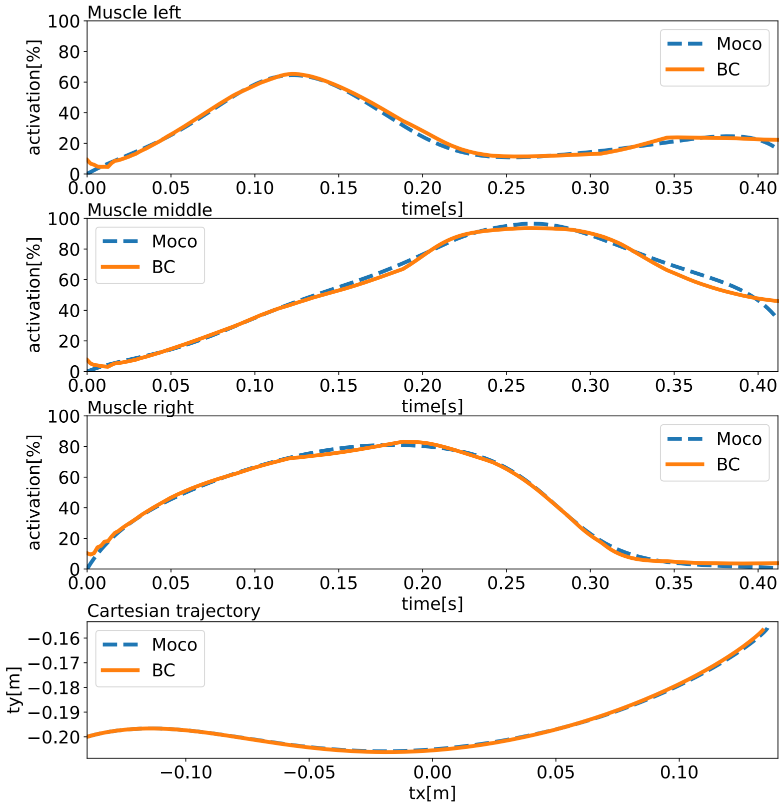

Fig. 2 The activations of the three muscles and the Cartesian trajectory of the point mass.

The first three plots share the same horizontal axis - the time axis. The horizontal axis of the fourth plot is aligned and has the same scale with the horizontal axis of the first three plots. It represents the horizontal Cartesian coordinate of the position of the point mass. These preliminary results validate that RL algorithms estimate plausible muscle activations because the learned muscle activations mirror the optimized ones very well and the two Cartesian trajectories are very similar.

Discussion

The generative capabilities of BC are limited because the ANN which it trains is unable to predict the muscle activations for a new Cartesian position of the point mass, which is not provided in the training sets. This is mainly due to the weak generalization capability of the BC algorithm and the deterministic nature of the ANN. From this perspective, BC is very similar to the supervised learning algorithms. Nevertheless, Proximal Policy Optimization (PPO) (Schulman et al., 2017) is a better alternative. It trains a stochastic ANN, and hence has significantly increased generalization and generative powers. Our future reports will present the performance of PPO on learning the muscle activations, which the musculoskeletal model of an athlete's lower body needs in order to reproduce athlete's gait in OpenSim.

The learning power of the RL algorithms is still only minimally used. In addition to their capability of estimating physical quantities unmeasurable in biomechanics, RL algorithms can test complex models of the human motor control (Merel et al., 2019).

Conflict of interest We declare no conflicts of interest.

Funding This work was funded by the Audi-Konfuzius Institut Ingolstadt, Ingolstadt, Germany.

References

Barricelli Barbara Rita, Casiraghi Elena, Gliozzo Jessica, Petrini Alessandro, & Valtolina Stefano (2020). Human Digital Twin for Fitness Management. *IEEE Access*, *8*, 26637–26664. https://doi.org/10.1109/ACCESS.2020.2971576

Dembia, C. L., Bianco, N. A., Falisse, A., Hicks, J. L., & Delp, S. L. (2021). OpenSim Moco: Musculoskeletal optimal control. *PLOS Computational Biology*, *16*(12), 1–21. https://doi.org/10.1371/journal.pcbi.1008493

Ho, J., Gupta, J. K., & Ermon, S. (2016). Model-Free Imitation Learning with Policy Optimization. Advance online publication. https://doi.org/10.48550/ARXIV.1605.08478

Merel, J., Botvinick, M., & Wayne, G. (2019). Hierarchical motor control in mammals and machines. *Nature Communications*, *10*(1), 5489. https://doi.org/10.1038/s41467-019-13239-6

Peng, X. B., Guo, Y., Halper, L., Levine, S., & Fidler, S. (2022). ASE: Large-Scale Reusable Adversarial Skill Embeddings for Physically Simulated Characters. *ACM Trans. Graph.*, *41*(4). https://doi.org/10.1145/3528223.3530110

Schulman, J., Wolski, F., Dhariwal, P., Radford, A., & Klimov, O. (2017). *Proximal Policy Optimization Algorithms*. arXiv.

Seth, A., Hicks, J. L., Uchida, T. K., Habib, A., Dembia, C. L., Dunne, J. J., Ong, C. F., DeMers, M. S., Rajagopal, A., Millard, M., Hamner, S. R., Arnold, E. M., Yong, J. R., Lakshmikanth, S. K., Sherman, M. A., Ku, J. P., & Delp, S. L. (2018). OpenSim: Simulating musculoskeletal dynamics and neuromuscular control to study human and animal movement. *PLOS Computational Biology*, *14*(7), 1–20. https://doi.org/10.1371/journal.pcbi.1006223

Song, S., Kidziński, Ł., Peng, X. B., Ong, C., Hicks, J., Levine, S., Atkeson, C. G., & Delp, S. L. (2021). Deep reinforcement learning for modeling human locomotion control in neuromechanical simulation. *Journal of NeuroEngineering and Rehabilitation*, *18*(1), 126. https://doi.org/10.1186/s12984-021-00919-y

Wächter, A., & Biegler, L. T. (2006). On the implementation of an interior-point filter line-search algorithm for large-scale nonlinear programming. *Mathematical Programming*, *106*(1), 25–57. https://doi.org/10.1007/s10107-004-0559-y

https://nbn-resolving.org/urn:nbn:de:bsz:ch1-qucosa2-806704

Sports Scene Searching, Rating & Solving using AI

Robert Marzilger, Fabian Hirn, Raul Aznar Alvarez & Nicolas Witt

Fraunhofer Institute for Integrated Circuits IIS, Germany

Abstract

This work shows the application of artificial intelligence (AI) on invasion game tracking data to realize a fast (sub-second) and adaptable search engine for sports scenes, scene ratings based on machine learning (ML) and computer-generated solutions using reinforcement learning (RL). We provide research results for all three areas. Benefits are expected for accelerated video analysis at professional sports clubs.

Keywords: AI, ML, RL, tracking data, invasion games

Introduction

Video analysis of invasion games like soccer, ice hockey, and basketball, despite available software tools, is still a quite manual and challenging task, but very important for game preparation & post-game analysis. Identification of meaningful scenes for trainers, preparation for the playing style of opponents, as well as discussing different solutions for certain scenes are repeating tasks that could be supported by omnipresent tracking data and the use of machine learning techniques (ML). The following sections explain the use of ML for *Scene Search*, a scheme for *Scene Rating,* and the use of reinforcement learning for *Scene Solving*, which generates new solutions for scenes played in real games never seen before.

Methods and Results

Scene Searching is realized with a similarity-based search, that retrieves the most similar scenes to a query scene within fractions of a second using deep representation learning (Löffler et al., 2022a) and that adapts to expert annotations.

Fundamental problems with similarity search stem from a lack of available labels and are threefold (Löffler et al., 2022a). First, the unordered structure of samples from team sports like football is caused by the lack of a generalized role assignment between the two teams. Every player's position may change dynamically throughout the game. This affects the similarity calculation because the assignment between players of two scenes is undefined. Second, the high dimensionality of positional tracking sampled at 25Hz for 23 targets in football, and the combinatorial complexity of pairwise computations, limit the scalability of searching with raw samples.

In our search component, we address the assignment problem by calculating optimal assignments between pairs of scenes $(Scene_1, Scene_2)$ with the Hungarian algorithm (Kuhn, 1955). This produces pairwise optimal assignments of players from one scene to their counterparts in the other scene. However, while this necessary step solves the assignment, its computational complexity of $\mathcal{O}(n^3)$ is still infeasible, and the scalability problem even intensifies.

Hence, we jointly learn to estimate the assignment problem and a lower dimensional representation of the complex raw tracking data to solve the three fundamental problems. We employ Deep Siamese Metric Learning to learn both i) a distance preserving lower-dimensional embedding $f()$ and ii) an estimation of the assignment problem. We use the Euclidean distance $d()$ as a proxy for semantic similarity, since Sha et al. (2016) showed its efficacy despite its apparent simplicity, with the Siamese loss that minimizes the difference between the embedding and raw distances:

$$Loss_{Siamese}(Scene_1, Scene_2) = (\|f(Scene_1) - f(Scene_2)\|_2 - d(Scene_1, Scene_2))^2 \quad (1)$$

However, we individualize the similarity metric in a second step. Even though the Siamese embedding preserves the Euclidean well and accelerates search by orders of magnitude (Reeb et al., 2020), we seek to improve upon it. Specifically, the Euclidean distance suffers from the Curse of Dimensionality (Bellman, 1961), and in practice does not differentiate semantically, e.g., no weighting of ball or player trajectories. We propose to learn a metric from human annotations using triplets (Hoffer et al., 2015) of query $Scene_a$, similar $Scene_p$, and dissimilar $Scene_n$. This extends our Siamese Network by learning experts' notions of similarity, which may resemble semantics more closely. We implement this cost-effectively by leveraging transfer-learning and furthermore by only querying the most informative samples through Active Learning (Löffler et al., 2022b). We fine-tune via triplet loss:

$$Loss_{Triplet}(Scene_a, Scene_p, Scene_n) = max\left(\|f(Scene_a) - f(Scene_p)\|_2 - \|f(Scene_a) - f(Scene_n)\|_2 + 1, \quad 0\right) \quad (2)$$

Despite inconsistent annotations from noisy oracles, we see an increase in triplet accuracy of 5-10% triplet accuracy after only 20 queries.

Scene Rating of soccer scenes is done using three method types: i) distance functions such as the distance to the goal and the distance won (between the last and the first frame). ii) formation spread, average distance of players to the formation's center of mass. This is based on the tactical idea, that an increased distance between defenders makes it harder to defend and an attacking team must position itself to spread the opposing formation (Rafelt, 2021). iii) pressure metric, as proposed by Link et al. (2016). In addition, we implement an Expected Goals (xG) metric based on the distance to goal (Altman, 2015), and the pitch control metric (Fernandez et al., 2018).

We provide statistical breakdowns of scenes for professional soccer analysts. We can choose scenes in two different ways. The first lists 5s scenes that are pre-filtered scenes to satisfy the criteria that one team possesses the ball for at least 90% of the time. Alternatively, scenes can be selected before or after an annotated event (1s to 10s). We provide visualizations of the scene and rating, and the video clip. In Fig. 1, we show trajectories of players and ball (a), and radar plot with rating metrics (b). In addition, we show (animated dynamic) plots of the scene and an animation of the pitch control metric (c).

These animations can be played forwards and backward to allow analysts to gain insight into the play of either the attacking or defending team.

(a) (b) (c)

Fig. 1 (a) Scene trajectory plot; (b) Radar chart with rating; (c) Pitch control.

It is planned to extend the rating to data-driven models for the prediction (in the next five seconds) of box entry, shot on goal, and scoring for attacking scenes.

Scene Solving is realized using the Google Research Football Environment (Kurach et al., 2020) and Reinforcement Learning (RL) techniques to generate new solutions from real scenes. The generated artificial solutions can then be sorted by different rating criteria described above, to identify valuable new proposals. The RL-agent consists of a Multilayer-Perceptron (MLP) of two layers [512,512], trained for 15 million steps using Proximal Policy Optimization (PPO) (Schulman et al., 2017). The state is represented using a 169-dimensional vector (see Fig 2) and extends previous work by adding relative positions from the active player to other entities.

Agent Team	Opponent Team	Team ball owner	Ball Information	Controlled player	Sticky actions	Controlled player	Controlled player
Position & Direction	Position & Direction	One-hot encoder	Position & Direction	One-hot encoder	Binary	Relative pos&dir to all players	Relative pos&dir to ball & ref.points
44	44	3	6	11	9	42	10

Fig. 2 State space representation

In soccer not losing the ball is of utmost importance. When risky actions are taken, the chance of losing the ball increases. Hence, we made the agent risk aware by defining constraints whenever the agent is in danger of losing the ball. Our risk estimator uses past transitions generated from the environment. The risk estimator allows the user of our application to tune the willingness of the playing agent to take a risk in its solutions. *Risk-tolerant* agents solutions advance faster, but the agents also lose the ball more easily, leading to counterattacks. *Risk-averse* agents focus on keeping the ball in possession which can be helpful if the team is already winning the match.

In Fig 3, we show the average safety value for passing and directional actions. Passing actions carry a higher risk than directional actions, especially when the agent is closer to the opponent's goal. Consequently, risk-averse agents do not pass when they are close to the goal, whereas risk-tolerant agents may perform a pass in such situations.

Conclusion

We think that a fast and adaptable search engine based on scene ratings and tracking data in combination with advances in computer aided scene solving will help to make video analysis more effective and may lead to new playing strategies.

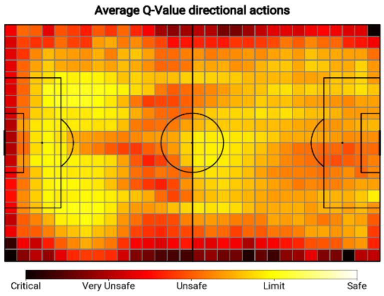

(a)

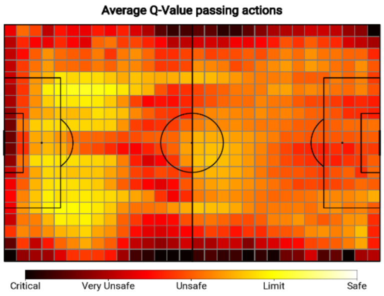

(b)

Fig. 3 (a) Safety values of directional actions; (b) Safety values of passing actions.

Conflict of interest We declare no conflicts of interest.

Funding We would like to acknowledge support for this project from the Bavarian Ministry of Economic Affairs, Infrastructure, Energy and Technology as part of the Center for Analytics-Data-Applications (ADA) within the framework of “BAYERN DIGITAL II”.

References

D. Altman. (2015). Beyond Shots: A new approach to quantifying scoring opportunities. OptaProForum. https://northyardanalytics.com/Dan-Altman-NYA-OptaPro-Forum-2015.pdf

J. Fernandez, & L. Bornn. (2018). Wide Open Spaces: A statistical technique for measuring space creation in professional soccer. *MIT Sloan Sports Conference*.

D. Link, S. Lang, & P. Seidenschwarz. (2016). Real Time Quantification of Dangerousity in Football Using Spatiotemporal Tracking Data. *PLoS ONE 11*(12).

M. Rafelt. (2021, March 27). Wie Guardiolas 3-2-2-3 (letztlich) das Abwehrspiel löst. *Spielverlagerung.de.* https://spielverlagerung.de/2021/03/27/wie-guardiolas-3-2-2-3-letztlich-das-abwehrspiel-loest/

Löffler, C., Reeb, L., Dzibela, D., Marzilger, R., Witt, N., Eskofier, B. & Mutschler, C. (2022a). Deep Siamese Metric Learning: A Highly Scalable Approach to Searching Unordered Sets of Trajectories. *ACM Transactions of Intelligent Systems and Technology, 13*(1), Article 6.

Sha, L., Lucey, P., Yue, Y., Carr, P., Rohlf, C. & Matt hews, I. (2016). Chalkboarding: A New Spatiotemporal Query Paradigm for Sports Play Retrieval. *21st International Conference on Intelligent User Interfaces*, pp. 336–347.

Reeb, L., Dzibela, D., Marzilger, R., & Witt, N. (2020) Effiziente Suche und Bewertung von Szenen in Spielsportarten. *spinfortec digital*, pp. 16-17.

Bellman, R. (1961). Adaptive Control Processes. A Guided Tour. *Princeton University Press, 255*.

Hoffer, E. & Nir A. (2015). Deep Metric Learning Using Triplet Networks. Similarity-Based Pattern Recognition SIMBAD. Lecture Notes in Computer Science, 9370.

Löffler, C., Fallah, K., Fenu, S., Zanca, D., Eskofier, B., Rozell, C. J., Mutschler, C. (2022b) *Active Learning of Ordinal Embeddings: A User Study on Football Data. ArXiv.* 2207.12710

Kuhn, H. (1955). The Hungarian Method for the Assignment Problem. *Naval Research Logistics Quarterly, 2*, pp. 83-97.

Kurach, K., Raichuk, A., Stanczyk, P., Zajac, M., Bachem, O., Espeholt, L., Riquelme, C., Vincent, D., Michalski, M., & Bousquet, O. (2020). Google research football: A novel reinforcement learning environment. *AAAI Conference on Artificial Intelligence, 34*(4), pp. 4501–4510.

Schulman, J., Wolski, F., Dhariwal, P., Radford, A., & Klimov, O. (2017). Proximal Policy Optimization Algorithms. *ArXiv*. 1707.06347

https://nbn-resolving.org/urn:nbn:de:bsz:ch1-qucosa2-806704

Near-infrared spectroscopy wearable biosensor for monitoring exhaustion in sports climbing

Carlo Dindorf[1], Eva Bartaguiz[1], Jonas Dully[1], Max Sprenger[1], Anna Merk[1], Stephan Becker[1], Oliver Ludwig[1] & Michael Fröhlich[1]

[1]Technische Universität Kaiserslautern, Department of Sports Science, Kaiserslautern, Germany

Abstract

Monitoring exhaustion using near-infrared spectroscopy (NIRS) wearable biosensors seems promising in sports climbing. However, there is a lack of research regarding climbing specific muscular exhaustion and muscle oxidative metabolism. The current study analyses how exhaustion affects muscle oxidative metabolism and deduces to what extent measurements using NIRS are suitable for an objective monitoring as well as feedback of exhaustion.

Keywords: fatigue, training, fingerboard, grip strength, bouldering

Introduction

The continuous monitoring of physiological signals using wearable devices or wearable biosensors plays an important role in modern sports practice. One promising application, which seems highly feasible for monitoring local forearm oxygenation in climbing, is the near-infrared spectroscopy (NIRS). This is a non-invasive technique for monitoring muscle oxygen saturation (SmO_2) in vivo (Hamaoka et al., 2011). It might be used as an indicator of training status in sports climbing (Fryer et al., 2016), relates to the overall climbing performance (e.g. oxidative capacity predicts red-point grade (Feldmann et al., 2022)) and possibly form the basis for an objective feedback system of exhaustion (see, e.g. Muramatsu and Kobayashi (2013) in muscular context of biceps brachii). Nevertheless, there is still a need for research regarding the use of NIRS in the context of climbing specific exhaustion, especially since most studies only analyse experienced climbers (Baláš et al., 2018; Feldmann et al., 2022). Therefore, the current study analyses how climbing specific exhaustion affects finger flexor muscle oxygenation of regularly and non-climbing subjects. The overall aim is to discuss whether the use of NIRS for measuring SmO_2 is suitable for an objective monitoring of acute exhaustion (caused during isometric muscle contraction) and cumulative exhaustion (result of multiple, intermittent isometric muscle contractions) in the context of the maximal climbing specific holding time (CSHT).

Methods

42 healthy subjects (gender: 22 female, 20 male, 0 divers; age: M = 22.45, SD = 3.13; height: M = 173.08, SD = 8.96; weight: M = 69.90, SD = 12.39; body fat: M = 20.04, SD = 8.24; 8 subjects with experiences in sports climbing) underwent an anthropometric analysis as well as maximal pull-up test before the experiments. After 15 minutes of rest, the CSHT was measured three times with about 90 seconds in between to assess the influence of exhaustion. For this purpose, subjects were advised to hold themselves as long as possible without touching the ground on a four centimetre deep crimp with rounded edges and structuring (see Fig. 1) of a MOON fingerboard

(Moon Climbing Limited, Seffield, England). Before the exercise, as well as during the 90 seconds in between the CSHT measurements, hand grip strength (HGS) was assessed according to the instructions of Mathiowetz et al. (1984) using the Jamar hydraulic hand dynamometer (JLW Instruments, Chicago, IL, USA).

In parallel, the muscle oxygen level was measured using the Moxy NIRS biosensor (Moxy Monitor, Huttchinson, Minnesota, USA). According to Philippe et al. (2012), the sensor was placed at the forearm of the handiness side using kinesio tape. The recording interval was set to two seconds and data was smoothed using a ten second moving average. For the statistical analysis the following parameters were extracted: initial SmO_2 before hanging, SmO_2 at the termination time (fall off event), the average slope of SmO_2 reduction, SmO_2 ten seconds after termination time (recovery). Statistical analysis was performed using IBM SPSS (version 16, SPSS Inc. Chicago, USA).

Fig. 1 Hand positioning on the fingerboard.

Results

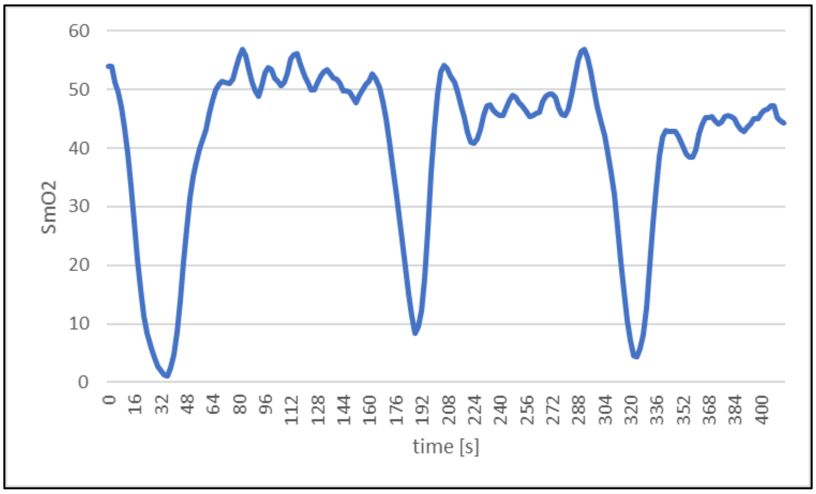

Fig. 2 Waveform SmO_2 data of an exemplary subject with an initial CSHT of 21.83 s. (second CSHT: 11.00 s; third CSHT: 13.79 s) during the test procedure.

A significant reduction of CSHT ($F(1.29,60.72) = 12.43$, $p < .001$, $\eta_p^2 = .21$) as well as HGS ($F(1.60,75.32) = 50.84$, $p < .001$, $\eta_p^2 = .52$) along the different measurements could be found. Post-hoc analysis shows that all HGS measurements were different between each other ($p \leq .001$). For the CSHT the first and second as well as first and third measurements were different ($p < .05$).

Between the second and third measurement, no significant differences was found for the CSHT (p = .21).

Significant differences were present between pre, termination as well as recovery SmO_2 saturation level (F(1.47,60.05) = 284.33, p < .001, η_p^2 = .87). Exemplary waveform SmO_2 data of one subject is presented in Fig. 2. There were no differences in initial SmO_2 level, SmO_2 level at fall off, SmO_2 recovery (F(2,82) = 0.54, p = .58) and mean negative slope of the SmO_2 reduction between the different measuring times (F(1.46,65.79) = 1.46, p = .24).

Visually, subjects with relative longer holding times do not appear to have a higher basal O_2 saturation. However, they seem to be able to better and deeper drain their SmO_2 level and seem to show less variability in their SmO_2 level at the fall-off events (see Fig. 3).

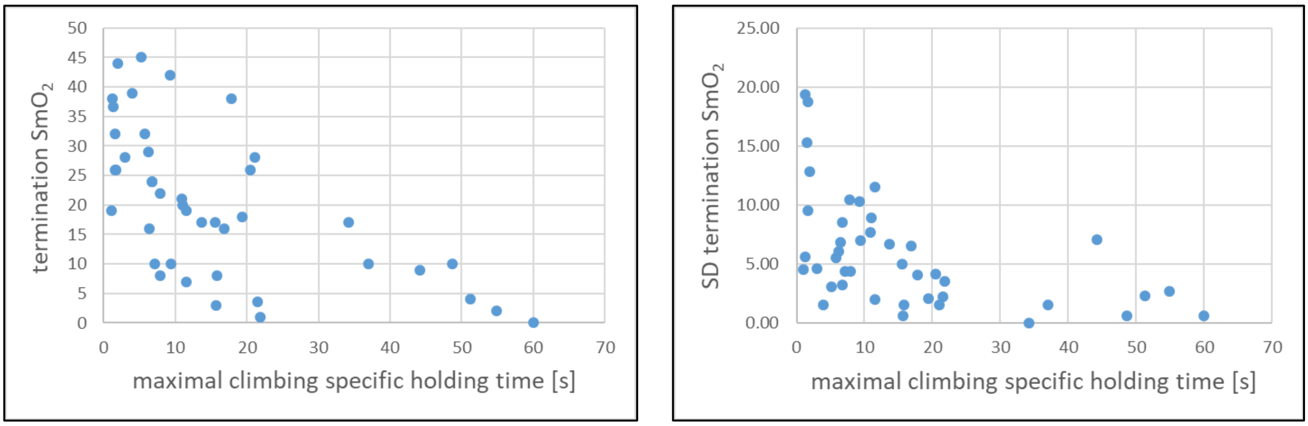

(a) (b)

Fig. 3 (a) SmO_2 levels at the first termination event in dependence of the maximal holding time; (b) Standard deviation (SD) of the SmO_2 levels at termination events in dependence of the maximal holding time.

Discussion

The significant decreases in both CSHT and HGS shows that consecutive maximal isometric holding introduces cumulative exhaustion of the finger flexors. However, the current study indicates that SmO_2 level in the different regarded conditions (initial SmO_2 before hanging, SmO_2 at the termination time, average slope of SmO_2 reduction, SmO_2 ten seconds after termination time) does not change under the different measuring times. Therefore, monitoring cumulative exhaustion during intermittent isometric climbing specific muscle contractions using SmO_2 level does not seem useful. Contrary, Feldmann et al. (2022) showed using regularly climbing subjects that the climbing specific force production correlates negatively with the minimal attainable muscle oxygenation in the forearms in climbers in the context of HIT training. A possible explanation for the current studies results might be the consideration of subjects that are unexperienced in climbing.

Significant differences between pre, termination and recovery SmO_2 level indicates the potential usefulness of NIRS as an indicator for acute exhaustion. Visually, the individual SmO_2 profiles show that even with a relative short holding time, SmO_2 seems to be sensitive enough to map a load. Subjects with relatively long CSHT seem to show less variability in their SmO_2 level at fall off events. This is in accordance with the work of Baláš et al. (2018), which showed that NIRS provides a reliable measure of oxygenation during intermittent contractions to fall off in the forearm flexors of climbers. Therefore, SmO_2 level seems preferable for monitoring acute exhaustion for subjects with relative long CSHT. The fall off SmO_2 level seems to be highly individual and possibly dependent on the training status of the subjects. For monitoring acute exhaustion, it seems necessary to perform a fit on the individuals' drop-off SmO_2 level. Furthermore, it must be considered that the Moxy biosensor only covers a small area, while the finger flexors responsible for gripping take up a large volume of the forearm. Missing statistical correlations can therefore also be due to the isolated observation of a small muscle section.

Conflict of interest We declare no conflicts of interest.

Funding This research was funded by Offene Digitalisierungsallianz Pfalz, BMBF [03IHS075B] and Ministerium für Wissenschaft und Gesundheit Rheinland-Pfalz (project: LLL@U.EDU).

References

Baláš, J., Kodejška, J., Krupková, D., Hannsmann, J., & Fryer, S. (2018). Reliability of Near-Infrared Spectroscopy for Measuring Intermittent Handgrip Contractions in Sport Climbers. *Journal of strength and conditioning research*, *32*(2), 494–501. https://doi.org/10.1519/JSC.0000000000002341

Feldmann, A., Lehmann, R., Wittmann, F., Wolf, P., Baláš, J., & Erlacher, D. (2022). Acute Effect of High-Intensity Climbing on Performance and Muscle Oxygenation in Elite Climbers. *Journal of Science in Sport and Exercise*, *4*(2), 145–155. https://doi.org/10.1007/s42978-021-00139-9

Fryer, S., Stoner, L., Stone, K., Giles, D., Sveen, J., Garrido, I., & España-Romero, V. (2016). Forearm muscle oxidative capacity index predicts sport rock-climbing performance. *European Journal of Applied Physiology*, *116*(8), 1479–1484. https://doi.org/10.1007/s00421-016-3403-1

Hamaoka, T., McCully, K. K., Niwayama, M., & Chance, B. (2011). The use of muscle near-infrared spectroscopy in sport, health and medical sciences: recent developments. *Philosophical Transactions of the Royal Society*, *369*(1955), 4591–4604. https://doi.org/10.1098/rsta.2011.0298

Mathiowetz, V., Weber, K., Volland, G., & Kashman, N. (1984). Reliability and validity of grip and pinch strength evaluations. *The Journal of Hand Surgery*, *9*(2), 222–226. https://doi.org/10.1016/S0363-5023(84)80146-X

Muramatsu, Y., & Kobayashi, H. (2013). Assessment of local muscle fatigue by NIRS. In *2013 Seventh International Conference on Sensing Technology (ICST)* (S. 1-4). IEEE. https://doi.org/10.1109/ICSensT.2013.6727728

Philippe, M., Wegst, D., Müller, T., Raschner, C., & Burtscher, M. (2012). Climbing-specific finger flexor performance and forearm muscle oxygenation in elite male and female sport climbers. *European Journal of Applied Physiology*, *112*(8), 2839–2847. https://doi.org/10.1007/s00421-011-2260-1

Sitzung II – Digital Motion: Datenerfassung, Analyse und Algorithmen

https://nbn-resolving.org/urn:nbn:de:bsz:ch1-qucosa2-806704

Data Quality Knowledge in Sport Informatics: A Scoping Review

Wolfgang Kremser[1]

[1]Salzburg Research Forschungsgesellschaft, Human Motion Analytics, Salzburg, Austria

Abstract

As sport informatics research produces more and more digital data, effective data quality management becomes a necessity. This systematic scoping review investigates how data quality is currently understood in the field. Results show the lack of a common data quality model. Combining data quality approaches from related fields such as Ambient Assisted Living and eHealth could be the first step toward a data quality model for sport informatics.

Keywords: data quality, data quality model, sport informatics, data management

Introduction

More and more national and international scientific funding bodies require research projects to generate sharable and high-quality research data (Corti et al., 2019). The modern understanding of data quality (DQ) is multi-dimensional and goes beyond data's intrinsic accuracy. For example, the FAIR guidelines adopted by the European Union require data to be findable, accessible, interoperable, and reusable (Corti et al., 2019). This trend also affects the sport informatics research community that relies on wearable digital sensors to generate data.

Batini & Scannapieco (2016) distinguish three types of knowledge required for DQ assessment and management: (i) organizational knowledge describes the organizations, processes and rules involved in creating and using data, (ii) technological knowledge on relevant data flows, databases, and data sources and (iii) quality knowledge, i.e. an understanding of the dimensions and characteristics of data quality.

This work is concerned with identifying the current state of data quality knowledge in sport informatics. In particular, it searches for DQ models or assessment methodologies specific to sports science data, and applications of existing DQ frameworks. Furthermore, it investigates how the term 'data quality' is currently used in sport science literature and related fields such as eHealth and AAL. This work contributes to sport informatics research by identifying possible knowledge gaps in data and DQ management practices that, when addressed in future work, could help to produce more readily sharable and higher-quality datasets.

Methods

This work investigates the current state of quality knowledge in sport informatics through a systematic scoping review (Peters et al., 2015). The review has the following research questions:

RQ 1: How is the term DQ used in sport informatics and related literature?

RQ 2: What DQ models and assessment methods exist specifically for sport science?

Four literature databases, (Pubmed, SportDISCUS, Scopus, Web of Science), were searched on June 10th, 2022 with the following query over the articles' titles, abstracts, and keywords:

"data quality" AND ("wearable*" OR "sensor*")

The results of Scopus and Web of Science were further limited to the subject areas related to sports (Scopus: *SUBJAREA (heal OR medi)*; Web of Science: "*Research Area = Medical Informatics"*) due to a large number of results unrelated to sport informatics (e.g. environment monitoring, industry 4.0, traffic monitoring).

After duplicate removal, the articles' titles and abstracts were screened for relevance using the Rayyan web application (Ouzzani et al., 2016). The remaining articles' full texts were screened for inclusion in the final dataset. Table 1 shows the list of inclusion and exclusion criteria used for both screening rounds.

Table 1 Inclusion / exclusion criteria.

Inclusion Criteria	**Exclusion Criteria**
In the field of sports science or a related field (e.g. eHealth, AAL)	Reviews
It is clear what is meant by DQ when authors use the term	Sensor validation studies
Not older than 6 years	
English language	
Published in a peer-reviewed journal or conference proceedings	

The included articles were categorized based on their topics. When the article discussed DQ, the corresponding DQ dimensions were either explicitly stated (e.g. 'records were checked for consistency with other records'), or they were derived from the context (e.g. 'records that contained at least twelve hours of continuous data' was assigned to the 'completeness' DQ dimension).

Results

The query resulted in 176 records over all four databases. After deduplication, 161 articles remained. After applying the exclusion criteria in the subsequent abstract and full-text screening, a total of 43 records remained for inclusion. Of the included articles, 38 (88%) were published in journals, and 5 (12%) were published in conference proceedings. Their research questions were distinguished into the categories listed in Table 2. Furthermore, Fig. 1 lists the extracted DQ dimensions and how often they were mentioned among the included articles. Most often mentioned was *accuracy* (49% of articles), followed by *completeness* (30%) and *signal quality* (23%). Other dimensions occurred only occasionally.

Table 2 Identified topics of the included articles.

Category	Count	Description
mHealth	17 (40%)	Collection of health data without supervision
Physiology	7 (16%)	Supervised collection of physiological data
Electronic Medical Records	7 (16%)	Maintainance of an athlete's digital health record
Eventdetection	5 (12%)	Experts label events like injury or game maneuvers
IoT	3 (7%)	Relevant uses of methods from the Internet-of-Things
Positioning	3 (7%)	Use of global navigation satellite systems (GNSS) to position athletes in 3D space
Social Psychology	1 (2%)	Social psychology in relation to sports science

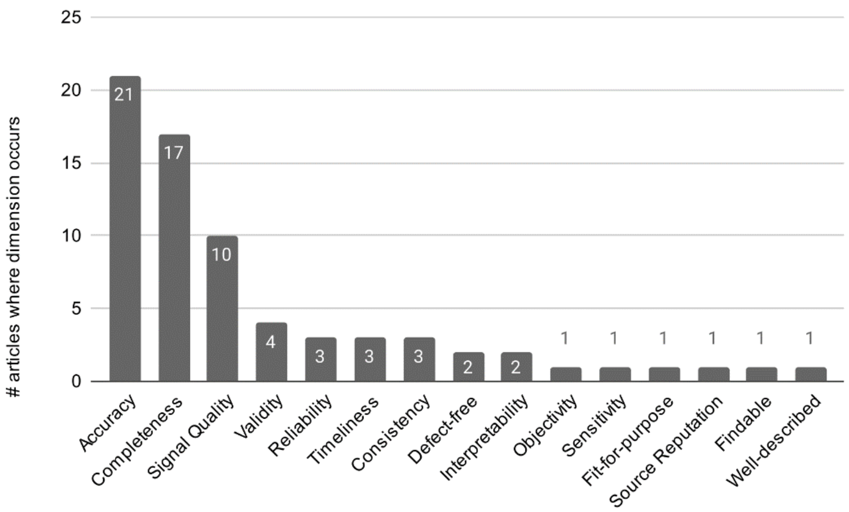

Fig. 1 The DQ dimensions mentioned in the included articles. An article can include multiple DQ dimensions.

Discussion

We will now address the research questions posed above in order.

Ad RQ 1: Based on our results, we can identify four understandings of data quality. The first and most prevalent is what we call *data quality as signal quality*. It exists when digital sensors are involved and means that data quality is high if the sensors' output signals have a high signal-to-noise ratio, signal continuity, sample rate, and resolution. The second is *data quality as compliance*. This understanding comes from unsupervised, in-field data collection, where subjects are asked to generate data without the supervision of an expert. Here, data quality is high if the compliance is high, i.e. the subjects use the sensor hardware correctly for the specified amount of time. Third is *data quality as expert agreement*, which appears in articles about event detection where experts identify and label events. Consequently, the data (= labels) is of high quality if multiple experts assign the same label to each event. Fourth, we want to mention *data quality as consistency*. In articles discussing electronic medical records of athletes and patients, the goal is to ensure accuracy by cross-referencing data sources and to ensure completeness by enforcing conformity to standards.

Ad RQ2: There are no reports of a DQ model or assessment method in the included articles. Only two articles explicitly are about DQ. One is Towse et al. (2021) which propose guidelines for good quality data in the context of data sharing in psychology. They include findability, accessibility, completeness, and being well-described. Abdolkhani et al. (2019) interviewed various stakeholders in remote patient monitoring and find that interpretability, consistency, relevancy, accessibility, and timeliness are most important in this context.

A limitation of this study is the somewhat arbitrary mapping of DQ dimensions since they lack a formal definition. While this reflects the loose usage of DQ terms in literature, future studies should use already existing definitions if available to avoid ambiguity (e.g. ISO 8000). We tried to resolve this issue by summarizing the different understandings of DQ.

We conclude that sport informatics lacks formalized and shared DQ knowledge. To develop this knowledge, we propose combining the methodologies used in (Cho et al., 2021) and (Erazo-Garzon et al., 2020). Cho et al. use a multi-method study design, consisting of a literature review, an expert survey, and focus group discussions, to identify relevant DQ dimensions for person-generated wearable device data for biomedical research. Erazo-Garzon et al. demonstrate how to define and apply formal metrics that make DQ dimensions measurable. Combining these two approaches can yield a DQ model that is both centered on the needs of data consumers (sports and data scientists) and applicable in practice.

Conflict of interest: I declare no conflicts of interest.

Funding This work was partly funded by the Austrian Federal Ministry for Transport, Innovation and Technology, the Austrian Federal Ministry for Digital and Economic Affairs, and the federal state of Salzburg under the research program COMET in the project DiMo.

References

Abdolkhani, R., Gray, K., Borda, A., & DeSouza, R. (2019). Patient-generated health data management and quality challenges in remote patient monitoring. *JAMIA Open*, *2*(4), 471–478.

Batini, C., & Scannapieco, M. (2016). *Data and Information Quality: Dimensions, Principles and Techniques* (1st ed.). Springer International Publishing.

Cho, S., Weng, C., Kahn, M. G., & Natarajan, K. (2021). Identifying Data Quality Dimensions for Person-Generated Wearable Device Data: Multi-Method Study. *JMIR MHealth and UHealth*, *9*(12), e31618.

Corti, L., den Eynden, V. Van, Bishop, L., & Woollard, M. (2019). *Managing and Sharing Research Data: A Guide to Good Practice*. SAGE Publications Ltd.

Erazo-Garzon, L., Erraez, J., Illescas-Peña, L., & Cedillo, P. (2020). A Data Quality Model for AAL Systems. In *Advances in Intelligent Systems and Computing* (Vol. 1099, pp. 137–152). Springer.

Ouzzani, M., Hammady, H., Fedorowicz, Z., & Elmagarmid, A. (2016). Rayyan—a web and mobile app for systematic reviews. *Systematic Reviews*, *5*(1), 210.

Peters, M. D. J., Godfrey, C. M., Khalil, H., McInerney, P., Parker, D., & Soares, C. B. (2015). Guidance for conducting systematic scoping reviews. *International Journal of Evidence-Based Healthcare*, *13*(3), 141–146.

Towse, A. S., Ellis, D. A., & Towse, J. N. (2021). Making data meaningful: guidelines for good quality open data. *The Journal of Social Psychology*, *161*(4), 395–402.

https://nbn-resolving.org/urn:nbn:de:bsz:ch1-qucosa2-806704

Ein neuer Algorithmus zur Zeitsynchronisierung von Ereignis-basierten Zeitreihendaten als Alternative zur Kreuzkorrelation

Christoph Schranz[1] & Sebastian Mayr[1]

[1]Salzburg Research Forschungsgesellschaft m.b.H., Salzburg, Österreich

Kurzfassung

Mit der Verwendung von Sensordaten aus mehreren Quellen entsteht oft die Notwendigkeit einer Synchronisierung der entstandenen Messreihen. Ein Standardverfahren dazu ist die Kreuzkorrelation, die jedoch übereinstimmende Zeitstempel voraussetzt und empfindlich gegenüber Ausreißern reagiert. In diesem Paper wird daher ein alternativer Algorithmus für die Synchronisierung von Ereignis-basierten Zeitreihendaten vorgestellt.

Schlüsselwörter: Ereignis-basierte Zeitreihendaten, Synchronisierung, Kreuzkorrelation

Einleitung

In vielen praktischen Anwendungen, wie zum Beispiel beim Vergleich eines neuartigen Sensors mit der etablierten Messmethode, liegen zwei oder mehrere Messungen derselben oder einer korrelierenden Metrik mit versetztem Zeitstempel vor. Ursachen für einen solchen Zeitversatz können unter anderem Synchronisierungsprobleme der unterschiedlichen Geräte sein. In diesem Fall muss der Zeitunterschied zwischen den Messungen ermittelt und die Zeitstempel der als nicht synchron angenommen Messung korrigiert werden.

Das Standardverfahren zur Synchronisierung von Ereignis-basierten Zeitreihen ist es, die jeweiligen Datenpunkte auf eine konstante Abtastrate zu interpolieren um anschließend die Kreuzkorrelation für einzelne Zeitversätze zwischen den Messungen zu berechnen. Eine Verringerung der Laufzeit kann dabei durch die Verwendung der Fast Fourier-Transformation (FFT) erreicht werden (Lyon, 2010). Dieses Standardverfahren besitzt jedoch mehrere Nachteile: Falls die inhärente Frequenz der Signaländerung geringer ist als jene der auftretenden Ereignisse, sinkt die Präzision des ermittelten Zeitversatzes. Zusätzlich zeigt sich auch eine geringe Robustheit der Ergebnisse bei kurzen Zeitreihen sowie bei fehlenden oder falschen Werte, wodurch oft eine aufwändige Korrektur erforderlich ist. (Pearson, 2005)

In dieser Arbeit wird ein neues Verfahren für die Synchronisierung Ereignis-basierter Zeitreihendaten vorgestellt. Der Fokus bei der Entwicklung dieses Verfahrens war eine hohe Präzision des resultierenden Zeitversatzes und Robustheit.

Methode

Die hier vorgestellte Methode zur Synchronisierung Ereignis-basierter Zeitreihendaten basiert auf einem Reißverschlussprinzip, angelehnt an den effizienten Stream-Stream-Join Algorithmus von Schranz 2020. Grundsätzlich wird für jedes Ereignis der Abstand zum jeweils Nächsten der anderen Zeitreihe berechnet. Der Mittelwert aller dieser Abstände dient als Maß für die Synchronität der Zeitreihen für einen gegebenen Zeitversatz φ. Aufgrund des iterativen Vergleichs der Zeitstempel zum jeweils nächsten Gegenüber wird der Algorithmus im Rahmen dieser Arbeit als *nearest_advocate* bezeichnet.

```
def nearest_advocate(arr_1, arr_2, time_delta=0.0, max_distance=0.5):
    arr_2 = arr_2 - time_delta       # apply time shift
    cum_distance = 0.0; counter = 0  # initialize cumulative values
    i1, i2 = forward_until_first_intersection(arr_1, arr_2)  # skip indices
    for ts_2 in arr_2[i2:]:          # iterate over all timestamps in arr2
        while arr_1[i1+1] <= ts_2:   # forward i1 until arr_1[i1+1] > ts_2
            i1 += 1
            if i1 + 1 > len(arr_1):  # array 1 is finished, return
                return cum_distance / counter
        if arr_1[i1] <= ts_2:
            # here the invariance arr_1[i1] <= ts_2 < arr_1[i1+1] holds
            cum_distance += min(ts_2-arr_1[i1], arr_1[i1+1]-ts_2,
                                max_distance)
            counter += 1
    return cum_distance / counter
```

(a)

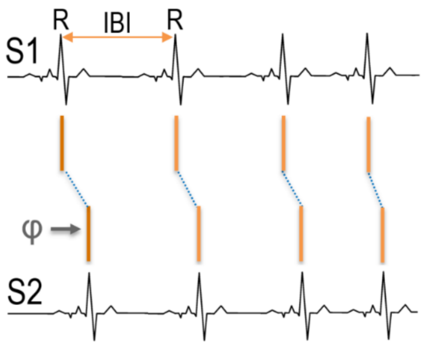

Abb. 1 (a) Pseudocode des *nearest_advocate*; (b) Zwei idente um φ versetzte EKG (schwarz) mit deren charakteristischen Schläge (R-peaks, orange) und den minimalen Abständen (blau strichliert).

In Abbildung 1a wird der Pseudocode dargestellt: Gegeben zwei sortierte Reihen aus Zeitstempeln der Ereignisse mit überlappenden Zeitabschnitten, berechnet *nearest_advocate* den mittleren Abstand von jedem Zeitstempel in Reihe 2 zu dem jeweils nächsten Gegenüber in Reihe 1 (siehe Abb. 1b). Der Parameter *‚time_delta'* gibt dabei den zu evaluierenden Zeitversatz an und *‚max_distance'* den maximal akzeptierten Abstand zwischen zwei gegenüberliegenden Ereignissen.

Der Algorithmus besitzt eine lineare Laufzeit- und Speicherkomplexität für einen zu prüfenden Zeitversatz. Insgesamt beträgt die Laufzeitkomplexität somit $|time\_deltas| \cdot (|arr_1| + |arr_2|)$. Für die Wahl der zu testenden Zeitversätze ist zu beachten, dass für die Erkennung der Form und somit des Optimums der Ergebniskurve etwa die 10- bis 20-fache Rate der erwarteten Nyquist- oder Signalfrequenz empfohlen wird (Wescott, 2018).

Experiment

Für das Experiment wurden EKG-Daten (siehe Abb. 1b) verwendet, die innerhalb des Projektes Virtual Sleep Lab während des Schlafs erhoben wurden (siehe Finanzierung). Die Zeitreihe 1 wurde mit dem laborüblichen Polysomnographen Brainvision BrainAmp ExG aufgenommen, die Zeitreihe 2 mit dem Suunto Movesense Sensor HR+. Beide Reihen liegen in Form von Arrays vor, wobei die Elemente die Zeitstempel der charakteristischen R-peaks der jeweiligen Herzschläge sind. Die Messdauer betrug etwa 30,000 Sekunden.

Folgende Algorithmen wurden im Experiment verglichen: (1) Eine Kreuzkorrelation mit FFT auf linear interpolierte Abstände der R-peaks (*interbeat intervals, IBI*). Zusätzlich (2) eine Kreuzkorrelation mit FFT auf, mittels Dreiecken der Breite 0.5s, interpolierten R-peaks, um die Präzision der Zeitversätze zu verbessern. Der hier vorgestellte Algorithmus *nearest_advocate* wird mit einer Maximaldistanz von 0.5s (3) auf alle R-peaks angewandt sowie (4) dünn besetzt (*sparse*) mit nur jedem 100sten R-peak der Zeitreihe 2. Der Suchraum für den Zeitversatz beträgt ±60 Sekunden bei einer Auflösung von 0.1 s.

In Abbildung 2 werden typische Ergebnisse für die Synchronisation dargestellt: In (a) das charakteristische Schwingen der jeweiligen Distanz (blau) um das Optimum (rot), das in den Algorithmen (2), (3) und (4) auftritt. In (b) das markante Maximum (blau) über einer dreieckigen Approximation für die Kreuzkorrelation (1). Aus dem Median der mittleren Distanzen (a) bzw. der Annäherung der Korrelationskoeffizienten mit einer Dreiecksform über zwei lineare Theil-Sen Regressoren (b) wird die Grundlinie (schwarz) bestimmt. Um das Hintergrundrauschen zu filtern, werden nur jene Kurvenanteile extrahiert, welche signifikanter als 50% des Optimums sind. Dieser Anteil wird auf eine Wahrscheinlich-keitsverteilung (türkis punktiert) normiert. Das Maß für die Präzision ist die Breite des 90%-Konfidenzintervalls dieser Wahrscheinlichkeitsverteilung (schwarz strichliert).

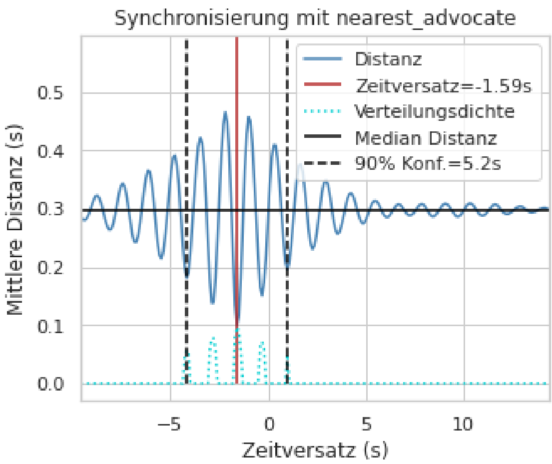

(a)

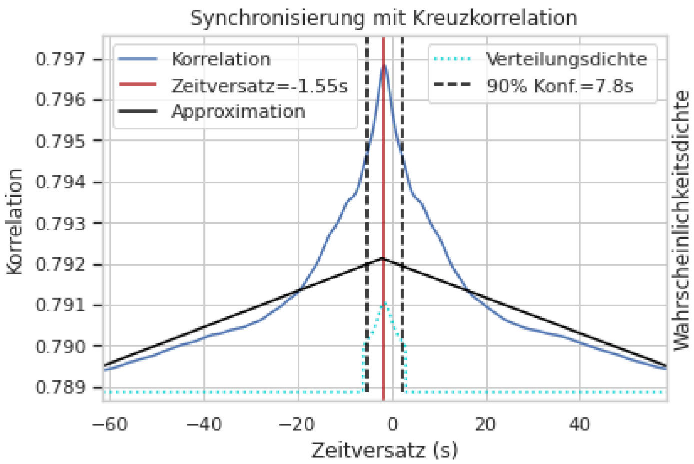

(b)

Abb. 2 (a) Bei der Synchronisierung mit *nearest_advocate* treten um den Versatz φ (in rot) charakteristische Schwingungen auf; (b) Bei der Kreuzkorrelation eine markante Spitze um φ.

Die Experimente wurden in Python 3.9 durchgeführt. Für die Kreuzkorrelation wurde die Methode *signal.correlate* des Pakets *scipy* mit Version 1.7.3 verwendet. Um für *nearest_advocate* ebenfalls vergleichbare Laufzeiten wie in C zu erzielen, wurde dieser in der JIT-Kompilierungsumgebung *numba* 0.55.0 implementiert. (Lam, 2015)

Ergebnisse

In Abbildung 3 werden für die Synchronisierungen der jeweiligen Algorithmen (a) die Präzision als Breite der 90%-Konfidenzintervalle der Wahrscheinlichkeitsdichten und (b) Laufzeiten für unterschiedliche maximale Längen der Zeitreihen dargestellt. Für den Fall mit maximaler Länge von 100,000s wurde die Zeitreihe synthetisch vervielfacht.

Die Streubreiten nehmen mit steigender Länge tendenziell ab und die Laufzeiten zu. Der Algorithmus *nearest_advocate* lieferte die präzisesten und robustesten Ergebnisse. Die schnellere *sparse*-Variante liefert für längere Zeitreihen ebenfalls präzise Ergebnisse und besitzt sogar die günstigste asymptotische Laufzeitkomplexität, womit diese für die Länge von 100,000s sogar schneller als die

Kreuzkorrelation mit FFT (mit Laufzeitkomplexität von $n \cdot log(n)$ (Lewis, 1995)) ist. Die Kreuzkorrelation mit Kernelapproximation liefert ebenfalls sehr präzise Lösungen, allerdings wird die rechenintensive Interpolation nicht für die hier als sehr niedrig erscheinende Laufzeit berücksichtigt.

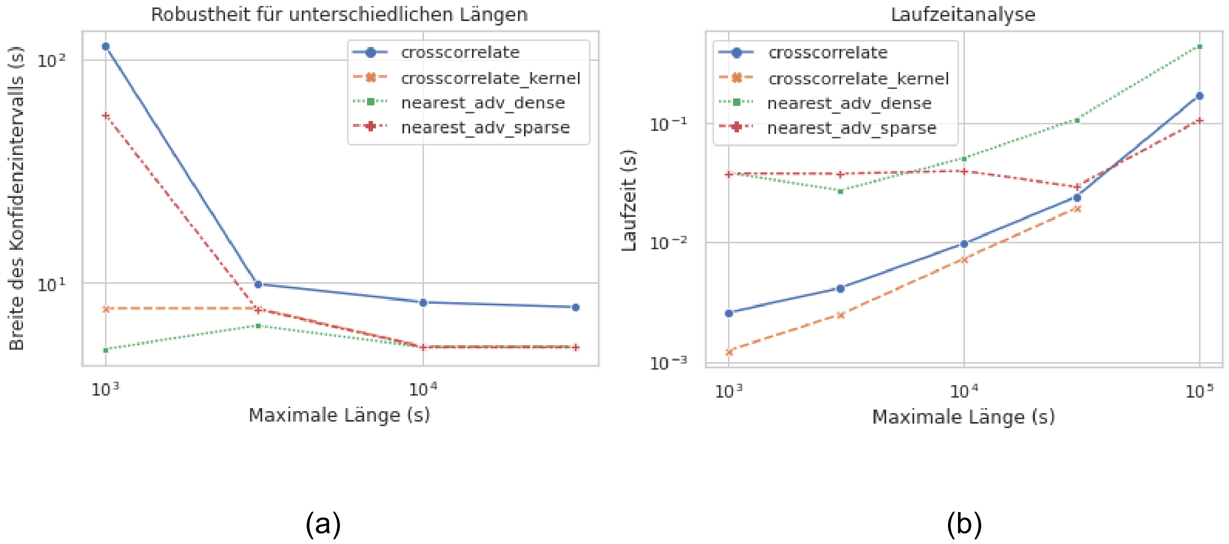

Abb. 3 (a) Breite der 90%-Konfidenzintervalle der Wahrscheinlichkeitsdichten und (b) die Laufzeiten der Algorithmen für unterschiedliche maximale Längen der Zeitreihen.

Diskussion

In diesem Paper wurde exemplarisch für R-peaks als Ereignis-basierte Zeitreihen gezeigt, dass das hier vorgestellte Synchronisierungsverfahren *nearest_advocate* für alle getesteten Längen eine höhere Präzision als das Standardverfahren Kreuzkorrelation liefert. Für kurze Zeitreihen demonstriert dieser eine sehr hohe Robustheit. Die *sparse*-Variante verspricht trotz geringerer Präzision für kurze Reihen, eine asymptotisch sehr gute Laufzeit.

In zukünftigen Analysen soll die Robustheit insbesondere gegenüber fehlender und falscher Ereigniswerte genauer untersucht werden. Außerdem wäre es sinnvoll, zusätzliche Algorithmen wie z.B. die Kreuzkorrelation mit beschränktem Suchraum zu betrachten.

Interessenskonflikt Ich bzw. wir erklären keine Interessenskonflikte.

Finanzierung Wir bedanken uns für die finanzielle Unterstützung durch das Land Salzburg innerhalb des WISS 2025 Projekt Virtual Sleep Lab (VSL-Lab) (20102-F2002176-FÜR).

Literatur

Pearson, R. (2005). Mining Imperfect Data. In *SIAM*, 250, https://doi.org/10.1137/1.9780898717884.

Lewis, J. P. (1995). "Fast Normalized Cross-Correlation." In *Industrial Light & Magic,* http://scribblethink.org/Work/nvisionInterface/nip.pdf.

Lyon, D. (2010). The Discrete Fourier Transform, Part 6: Cross-Correlation. In *The Journal of Object Technology, 9*(2), 17. https://doi.org/10.5381/jot.2010.9.2.c2

Wescott, Tim. (2018). Sampling: What Nyquist Didn't Say, and What to Do About It. In *Wescott Design Services,* https://www.wescottdesign.com/articles/Sampling/sampling.pdf.

Lam, S. K. (2015). Numba: A llvm-based python jit compiler. In Proceedings of the Second Workshop on the LLVM Compiler Infrastructure in HPC, (pp. 1–6).

Schranz, C. (2020). Deterministic Time-Series Joins for Asynchronous High-Throughput Data Streams, In *ETFA,* pp. 1031-1034, https://doi.org/10.1109/ETFA46521.2020.9211958.

https://nbn-resolving.org/urn:nbn:de:bsz:ch1-qucosa2-806704

Verwendung von künstlicher Intelligenz und Computer Vision bei der Bewegungsanalyse von Hochleistungskanuten/innen - die nächste Ausbaustufe

Marc Schuh[1], Jonas Mayer[1], Thomas Endres[1]

[1]TNG Technology Consulting, Unterföhring, Germany

Kurzfassung

In unserem Vortrag stellen wir die verbesserte Version des vor zwei Jahren präsentierten Kanu KI Analysators vor. Die automatische Paddel- und Paddelwinkelerkennung ist mit einer Trefferquote von über 99% sehr robust geworden. Die Erkennung der Paddelposen des Technikleitbildes hat sich von 37% auf 60% verbessert.

Schlüsselwörter: Kanu, KI, Computer Vision

Einleitung

Die visuelle Technik-Analyse im Hochleistungs-Kanusport ist bislang ein manueller und zeitaufwändiger Prozess. Hierbei werden zunächst die Athleten von einem Beiboot aus im Kanu gefilmt, das Videomaterial wird im Nachgang durch Sportwissenschaftler*innen ausgewertet. Untersucht wird der Winkel des Paddels zur Wasseroberfläche bei der Paddelbewegung, genauer gesagt in vier diskreten Positionen (siehe Abb. 1), im nachfolgenden auch vereinfachend "Paddelposen" genannt. Die erzielten Paddelwinkel werden mit jeweiligen Sollwinkeln des Technik-Leitbilds verglichen, um Rückmeldung zur Verbesserung der Paddeltechnik an die Kanutin / den Kanuten zu gegeben.

Hierfür muss aktuell das gesamte Video Einzelbild für Einzelbild nach den Paddelposen durchsucht werden, um anschließend händisch Wasserlinie und Paddellinie einzuzeichnen. Dies kommt einem menschlichen Aufwand von 15 Minuten pro analysiertem Athleten gleich. Unser Ziel ist es, diese manuelle Arbeit zu automatisieren.

Bei der Konferenz Spinfortec 2020 konnten wir einen ersten Prototypen zeigen, der die Paddelposen findet, sowie den Paddelwinkel via Wasser- und Paddellinie erfasst. Bei der Vorstellung 2020 berichteten wir, dass die Paddelwinkel-Erkennung robust funktionierte, aber dennoch in 20 - 30% Fälle fehlerhaft war. Die Paddelposen-Erkennung entsprach hingegen nur in 37% der Fälle auf +/- 1 Bild der menschlichen Auswertung.

In diesem Vortrag stellen wir die Verbesserungen vor, die dazu geführt haben, dass die Paddelwinkel-Erkennung in >99% der Fälle funktioniert und die Paddelposen-Erkennung im angegebenen Intervall zu 60% korrekt ist.

Abb. 1 Die vier Paddelposen zeigen das Einstechen, vollständige Eintauchen, Auftauchen, Ausstechen. Die Soll-Winkel sind eine Leitbildvorlage des IAT, welches aktuell noch einmal überprüft wird

Methode

Wie auch in unserem ersten Prototypen haben wir die Analyse-Aufgabe in 3 unabhängige Unteraufgaben zerteilt:

1. Bestimmung der Wasserlinie
2. Bestimmung der Paddellinie
3. Finden der Paddelposen

Im Folgenden gehen wir auf den Ansatz, die technische Umsetzung, sowie die Verbesserungen der einzelnen Teilschritte ein.

Bestimmung der Wasserlinie

Wir orientieren uns hier an der Lösung von Braun et al [1]: Zunächst wird das Kanu mithilfe eines eigens trainierten neuronalen Netzes (MaskRCNN [2]) vom Hintergrund segmentiert, was eine Bestimmung der Kanu-Umrisse erlaubt.

Mithilfe der gefunden Umrisse, kann die Wasserlinie durch eine Gerade am unteren Rand des Kanus approximiert werden.

Abb. 2 Es wird eine Kanu-Athletin auf dem Wasser gezeigt. Der durch das MaskRCNN als Vordergrund erkannte Kanuteil ist hell hervorgehoben.

Bestimmung der Paddellinie

Zunächst muss die Position der Handmittelpunkte schrittweise bestimmt werden: Im ersten Schritt wird die Athletin / der Athlet grob mithilfe eines Personendetektors (YOLOv3 [3]) geortet. Auf diesen Bildausschnitt wird eine Körperposen-Erkennung (TransPose [4]) angewandt, die insbesondere die genaue Position der Handgelenke bestimmt. In einem letzten Schritt wird mittels einer Handposen-Erkennung (DeNa [5]) die Position der Handmittelpunkte erkannt.

Abb. 3 Die Heatmap des Personendetektors TransPose zeigt auf der Athletin die verschiedenen Gelenke. Für uns besonders interessant sind die Positionen der Handgelenke.

Um eine robuste Schätzung der Handposition zu gewährleisten, auch wenn die Hand kurzzeitig nicht sichtbar ist, werden die Handpositionen über die zeitliche Historie gefiltert. Dazu nähern wir ein Polynom mindestens dritten und maximal achten Grades auf diskrete Zeitfenster der Handpositionen an. Durch Gewichtung der einzelnen Beobachtung anhand der Sicherheit des Posen-Erkenners, können unsichere und fehlende Detektionen herausgefiltert werden.

Unsere Erfahrungen aus dem ersten Prototypen haben gezeigt, dass eine Approximation des Paddels nur über die Handposition in einzelnen Randfällen erhebliche Ungenauigkeiten verursachen kann. Um diese zu minimieren setzen wir jetzt auch eine weitere, direkte Erkennung des Paddels. Unsere Paddelerkennung basiert auf der Annahme, dass ein Paddel in der Regel gerade und ungefähr parallel zur Linie zwischen den beiden Händen ist. Wir nutzen diese beiden Annahmen um mit einer Linienerkennung zwischen den Händen direkt die Umrisse des Paddels im Bild zu finden. Das Paddel wird als Durchschnitt der gefundenen Linien festgelegt.

Auch die Position und Rotation des Paddels wird wieder über ein zeitliches Fenster interpoliert. Die Gewichtungen der einzelnen Beobachtungen ergeben sich aus der Anzahl der gefundenen Linien. Dies ermöglicht uns eine robuste Approximation der Paddelposition, auch wenn das Paddel gerade verdeckt, oder die Hände nicht zu sehen sind.

Aus der Paddellinie und der Wasserlinie kann nun der Einstichwinkel berechnet werden.

Finden der Paddelpose

Das Problem, die Paddelpose zu finden, reduzieren wir wie im ersten Prototypen wieder auf das Erkennen von einzelnen Paddelzuständen. Wir unterscheiden hier zwischen drei möglichen Paddelzuständen:

1. Paddel komplett über Wasser (a)
2. Paddelblatt teilweise eingetaucht (p)
3. Paddelblatt komplett eingetaucht (u)

Die vier möglichen Übergänge zwischen diesen Zuständen korrespondieren zu den vier Paddelposen des Technikleitbilds. Zur Erkennung des Paddelzustands haben wir einen temporär konsistenten ZustandsErkenner basierend auf MobilenetV2 [6]. In unserem Training kommt unser Zustanderkenner auf 95% Präzision auf zuvor ungesehenen Daten.

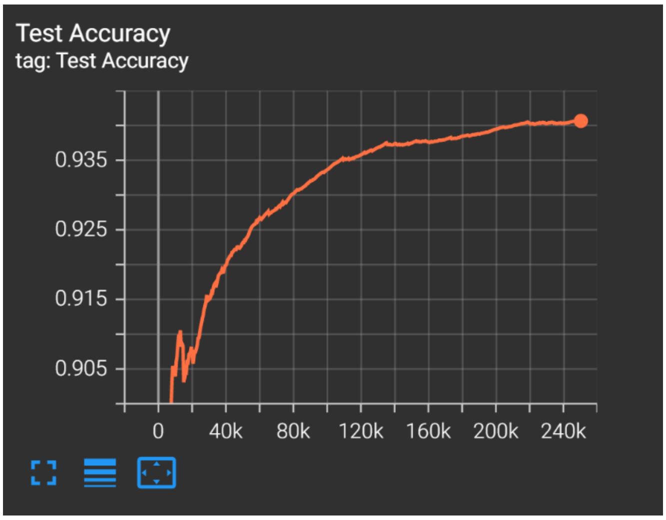

Abb. 4 Es zeigt die Genauigkeit des neuronalen Netzes in der Erkennung der Paddelzustände in einem Trainingsvideo im Verlauf über verschiedene Trainingsiterationen.

Mithilfe der bereits erkannten Paddellinie und der Position der Hände kann als erstes ein grober Ausschnitt des Paddels vorgenommen werden. Um zeitliche Zusammenhänge abbilden zu können, werden die Paddelausschnitte von drei aufeinander folgenden Einzelbildern als Input in den Paddelzustands-Erkenner gegeben.

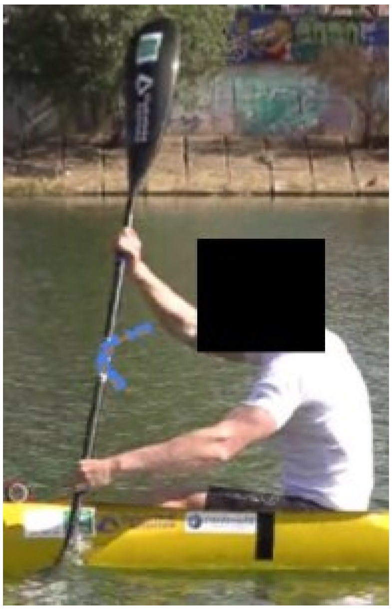

Abb. 5 Durch die Paddelmitte verläuft eine parabelförmige braune Linie mit blauen Punkten. Dies ist die interpolierte Bewegung der Paddelmitte.

Um vereinzelte Fehldetektionen auszugleichen und eine robuste Erkennung des Zustandsübergangs zu ermöglichen, filtern wir auch über die zeitliche Historie der Paddelzustände. Unter der Annahme, dass nur bestimmte Zustandsübergänge physikalisch möglich sind (z.B. p → u) und ein Zustand auch für eine gewisse Mindestzeit gehalten werden muss, können wir die Zustandsverteilungen über das zeitliche Fenster mit Sigmoiden annähern. Dadurch werden einzelne Falschdetektionen (a→ p → a) und unmögliche Zustandsübergänge (a→u) effektiv herausgefiltert. Auch wird für alle Einzelbilder mit einem nach oben zeigenden Paddel angenommen, dass das Paddel über Wasser ist.

Die vier Paddelposen werden von unserem System im Einzelbild vor einem Zustandsübergang erkannt.

Technische Umsetzung

Unsere Software ist in Python implementiert und verwendet einige Open Source Libraries wie OpenCV und TensorFlow. Im Gegensatz zum ersten Prototypen arbeitet unser Analysator nicht Bild für Bild, sondern in mehreren Analyse-Schritten über das gesamte Video. Dies ermöglicht das Berücksichtigen von zeitlichen Abhängigkeiten.

Die einzelnen Analyse-Schritte sind als Module implementiert, die nacheinander über das zu analysierende Video laufen und teilweise mit vorherigen Zwischenergebnissen arbeiten. Die Zwischenergebnisse mit sämtlichen Analysedaten werden in einem persistenten Speicherstand gehalten.

Am Ende der Analyse wird eine Zusammenfassung mit Paddelwinkeln, Paddelzuständen und Zeitstempeln im csv-Format ausgegeben. Zusätzlich werden die ausgewählten Einzelbilder der Paddelposen mit Wasserlinie, Paddellinie, Soll- und Ist-Winkel annotiert.

Ergebnisse

Das neuronale Netz wurde auf zehn Videos, die nicht im Trainingssatz enthalten waren, angewendet und verglichen, um wie viele Bilder der detektierte Paddelzustandwechsel von einer menschlichen Detektion abweicht (siehe Tab 1).

Tab 1 Vergleich der automatischen Paddelzustandserkennung mit einer manuellen Auswertung. Der Fehler in der Winkelbestimmung liegt bei etwa 3° pro Bild.

	Exakt	**+/-1**	**+/-2**	**Mehr als 2**	**Verpasste Detektion**	**TOTAL**
Summe	54	87	60	35	16	236
Prozent	22.88%	36.86%	25.42%	14.83%	6.78%	

Diskussion

Gegenüber der im September 2020 vorgestellten Software konnten wir wesentliche Verbesserungen erreichen. Die Paddelschafterkennung ist robust und fällt nur noch in Extremsituationen, wenn zum Beispiel mehrere Kanuten im Bild sind aus. Die Paddelzustandserkennung hat sich von 37% auf 60% verbessert, wenn weiterhin angenommen werden kann, dass auch der Mensch bei einer manuellen Annotation gelegentlich ein Bild falsch liegt. Besonders der Wechsel in den vollständig eingetauchten Zustand bzw. gerade auftauchend ist selbst bei menschlichen Analysen fehleranfällig.

Insgesamt ist die Paddelzustandserkennung jedoch noch nicht vollständig zufriedenstellend. Auch wenn das neuronale Netz im Training 95% der Bilder richtig erkannt, bezieht sich dies aber auf den kompletten Zyklus der Paddelbewegung. Die für uns interessanten und scheinbar auch schwieriger zu analysierenden Einzelbilder um die vier Paddelposen herum sind in unserem bisherigen Datensatz nur zu 5-10% repräsentiert. Unsere Beobachtungen zeigen, dass sich aber gerade hier Fehler in der Detektion häufen. Weitere Faktoren wie unterschiedliche Bewegungsunschärfe, Kanu- und Wasserfarbe sowie eine reflektierende Wasseroberfläche bringen weitere Veränderungen in die Bilder, mit denen das neuronale Netz umgehen muss.

Um die Paddelposen-Findung zu verbessern, schlagen wir eine direkte neuronale Detektion der Paddelposen vor, ohne über einen Paddelzustand zu gehen. Außerdem könnte das Training stark von mehr Trainingsdaten und konsistenteren Aufnahmebedingungen profitieren.

Interessenskonflikt Keine Angabe.

Finanzierung Keine Angabe.

Literatur

[1] von Braun, M., Frenzel, P., Käding, C., Fuchs, M., 2020, https://arxiv.org/abs/2004.09573

[2] He, K., Gkioxari, G., Dollár, P., Girshick, R., 2017, https://arxiv.org/abs/1703.06870

[3] Redmon, J., Farhadi, A, 2018, https://arxiv.org/abs/1804.02767

[4] Yang, S., Quan, Z., Nie, M., Yang, W., 2020, https://arxiv.org/abs/2012.14214

[5] Cao, Z., Simon, T., Wei, S., Sheikh, Y., 2016, https://arxiv.org/abs/1611.08050

[6] Sandler, M., Howard, A., Zhu, M., Zhmoginov, A., Chen, L., 2018, https://arxiv.org/abs/1801.04381

[7] Chen, L., Papandreou, G., Kokkinos, I., Murphy, K., Yuille, A. L., 2017, IEEE Transactions on Pattern Analysis and Machine Intelligence, vol. 40, 2018

[8] Shi, J., Tomasi, C. 1994 https://ieeexplore.ieee.org/document/323794

[9] Cao, Z., Hidalgo, G., Simon, T., Wei, S., Sheikh, Y., 2018, https://arxiv.org/abs/1812.08008

[10] Sandler, M., Howard, A., Zhu, M., Zhmoginov, A., Chen, L.C., 2018, https://arxiv.org/abs/1801.04381

https://nbn-resolving.org/urn:nbn:de:bsz:ch1-qucosa2-806704

Relationship between local ski bending curvature, lean angle and radial force in alpine skiing

Christoph Thorwartl[1], Josef Kröll[1], Michael Lasshofer[1], Helmut Holzer[2], Andreas Tschepp[3] & Thomas Stöggl[1,4]

[1]University of Salzburg, Department of Sport and Exercise Science, Hallein/Rif, Austria

[2]Atomic Austria GmbH, Department of Anticipation & Advanced Research, Altenmarkt, Austria

[3]Joanneum Research Forschungsgesellschaft mbH, Materials, Weiz, Austria

[4]Red Bull Athlete Performance Center, Thalgau, Austria

Abstract

The deflection of the ski is a prerequisite for carved turns. The more the ski is edged, the more the ski has to deflect and the more radial force has to be realised in order to keep the whole edge in contact with the snow. To verify this relationship, local ski bending curvature, the lean angle and the radial force were correlated with each other. Characteristic curvature patterns as well as very large correlations (r > 0.7) between the variables were identified.

Keywords: curvature, flexion, lean angle, PyzoFlex, ski bending, ski deflection

Introduction

The hourglass shape (known as sidecut) of alpine skis allows carving turns, meaning changes of direction on the snow with reduced lateral skidding. In order to define the radius (R) of a carving turn, the equipment-related sidecut and the ski deflection are essential (Federolf, Roos, Lüthi, & Dual, 2010). A deflection of the ski is only possible when the ski is edged and a sufficiently large radial force (RF) is applied. Therefore, the higher the lean angle (LA), the more RF must be realised and the more the ski must deflect to reduce R so that the entire edge remains in contact with the snow (Fig. 1).

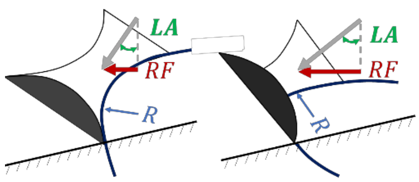

Fig. 1 Relationship between lean angle (LA) turn radius (R) and radial force (RF) during a carved turn (based on LeMaster, 2009)

However, the assumption that bending radius is homogeneous over the entire length of the ski is an oversimplification, as there are segmental differences in the local ski bending curvature (w'') (Thorwartl et al., 2021). To measure the characteristic progression of $w''(x)$ along the ski, a prototype based on PyzoFlex® technology was utilised. In laboratory investigations, the novel demonstrator has been shown to provide both reliable and valid w'' progressions in a quasi-static (Thorwartl et al., 2021) as well as in a dynamic setting (Thorwartl et al., 2022).While studies have shown that larger edge angles (corresponds to the LAs for flat terrain) as well as larger RFs lead to better carving performance (Cross et al., 2021; Jentschura & Fahrbach, 2004), w'' has not yet been investigated in this context because there has been no measurement instrument available for it. Therefore, the main aim of this work is to verify the relationship between w'', LA and the RF for different skiing styles.

Methods

One skier (A-level ski instructor) performed different skiing techniques (carving long radii (CL), carving short radii (CS), parallel ski steering long radii (PSSL) and parallel ski steering short radii (PSSS)) on a uniform slope section. 24 turns of each skiing style were included in the analysis. For the determination of the turn switch points (TSPs), the recordings of a follow cam were used. Furthermore, OpenGo (Moticon GmbH, Munich, Germany) sensor insoles with a sampling rate of 100 Hz were utilised. The insoles have an integrated Inertial Measurement Unit (IMU), which was used to determine LA by integrating the rotational velocity (ω_x) around the x-axis (roll axis) over time (t) according to the procedure of Snyder, Martinez, Strutzenberger, and Stöggl (2021) (Fig. 2). To calculate RF, the foot force measured by the pressure insole was multiplied by the sinus of $|LA|$. It should be mentioned that the effective force between the ski and the binding system is greater than the estimated force from the sensor insoles (Nakazato, Scheiber, & Müller, 2011). Since the absolute values of the RF, which is affected by a systematic bias, are not crucial for this study, the sensor soles serve their intended purpose. A novel PyzoFlex® technology prototype (Joanneum Research Forschungsgesellschaft m.b.H, Weiz, Austria, 215 Hz) was employed to capture w'' during skiing. The PyzoFlex® sensors are intrinsically piezoelectric and pyroelectric and produces a charge $Q(t)$ which is converted to a mean segmental curvature (w_i'') using a two-point calibration method (Thorwartl et al., 2021).

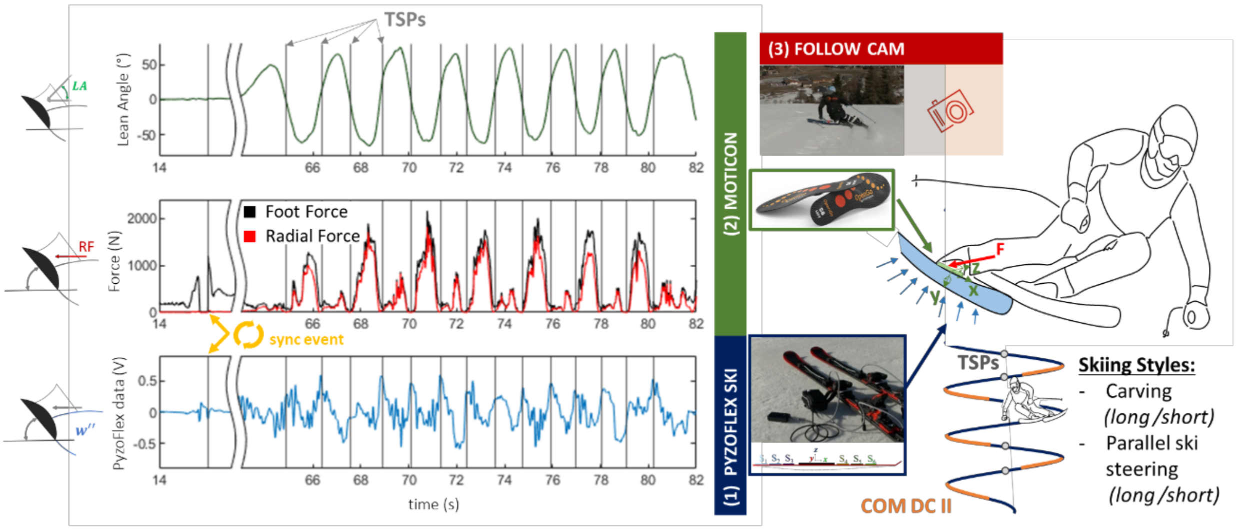

Fig. 2 Experimental setup with (1) PyzoFlex® ski with sensor S_1 to S_6, (2) Moticon system and (3) Follow cam. TSPs: Turn switch points; COM DC II: Centre of Mass of direction change II.

However, before calibration, the sensor signal was postanalytically filtered, linearly drift-corrected, and processed via a custom-developed zero-update algorithm using MATLAB (R2018B, MathWorks, Natick, MA, USA). For the qualitative description, the PyzoFlex® data were time normalised over a left-right turn combination. The second half of the turn phase was defined as the Centre of Mass Direction Change II (COM DC II) and is assumed to be between 25% to 42.5% and 75% to 92.5% of a total left-right turn combination (Spörri, Kröll, Schwameder, Schiefermüller, & Müller, 2012). For this section, the mean w'' from the middle segment $(\overline{w''_{2-4}} = (w''_2 + w''_3 + w''_4)/3)$, mean LA $(\overline{LA})$, and mean RF $(\overline{RF})$ were calculated for each left turn and used for the correlation. Thus, only the right outer ski and the data from the right sensor insole were considered for the investigation. The magnitude of agreement was assessed using Pearson's correlation coefficient (r) with thresholds of 0.1, 0.3, 0.5, and 0.7 for small, moderate, large, and very large correlation, respectively (Hopkins, Marshall, Batterham, & Hanin, 2009).

Results

The time normalised mean w_i'' ± standard error (SE) of left-right combinations is shown in Fig. 3. At 0% and 100% is the TSP from a right to a left turn and at 50% from a left to a right turn. The curvature is greatest between the TSPs (at about 25% and 75%). The sensor element behind the binding system (S_3) is curved mostly, followed by the neighbouring element S_2 and the sensor S_4 in front of the binding. In carved turns, the w'' signal was higher at sensor S_2, S_3 and S_4 than in parallel ski steering turns. However, there were hardly any differences in the decentralised sensors (S_1, S_5 and S_6) with respect to skiing style; therefore, these sensors were excluded for the correlation analysis.

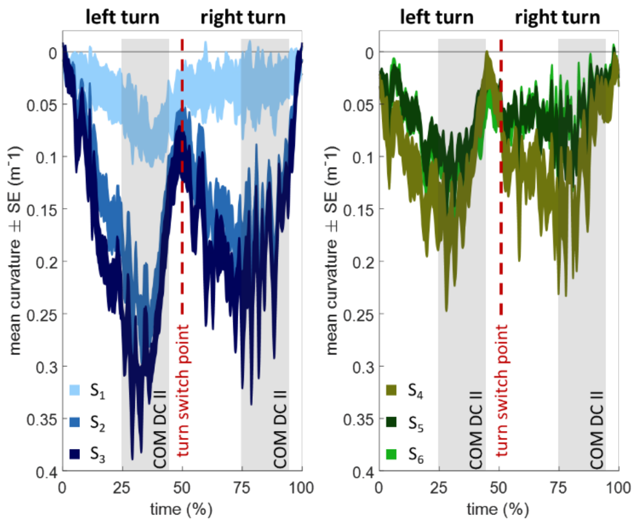

Fig. 3 Time normalized mean curvature ± standard error (SE) for carving long radii turns. Rear sensors (S_1 to S_3) in blue and front sensors (S_4 to S_6) in green. COM DC II: Centre of Mass Direction Change II.

As can be seen in Fig. 4a, there was a positive relationship between $\overline{RF}$ and $\overline{LA}$ (r = 0.81) in COM DC II across all skiing styles. A differentiated consideration with respect to technique still shows positive correlations, but r varies between 0.17 and 0.71. It was found that $\overline{w''_{2-4}}$ increases with both $\overline{LA}$ (r = 0.81) (Fig. 4b) and $\overline{RF}$ (r = 0.70) (Fig. 4c) across all skiing styles, but there were also large differences in r within techniques.

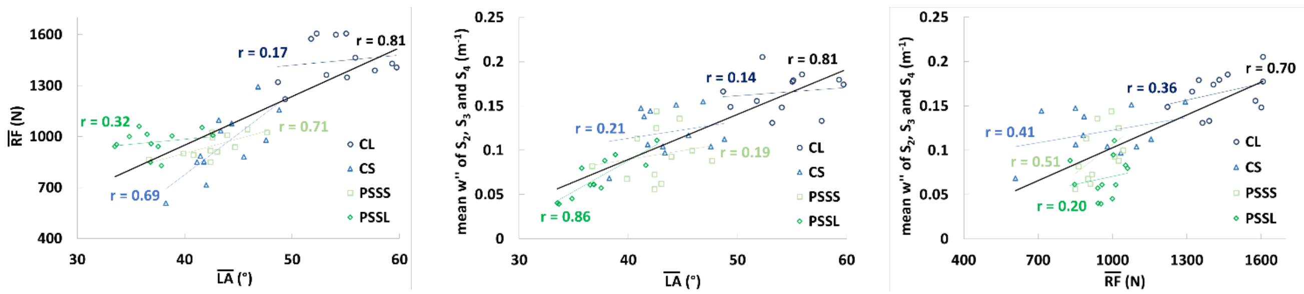

(a) (b) (c)

Fig.4 Correlations of the mean values in the Centre of Mass Direction Change II (COM DC II) for different skiing styles (CL: carving long radii; CS: carving short radii; PSSS: parallel ski steering short radii; PSSL: parallel ski steering long radii) of the outer ski. r: Correlation coefficient. (a) Mean radial force ($\overline{RF}$) vs. mean lean angle ($\overline{LA}$). (b) Mean curvature of S_2, S_3 and S_4 in the middle segment ($\overline{w''_{2-4}}$), vs. $\overline{LA}$. (c) $\overline{w''_{2-4}}$ vs. $\overline{RF}$.

Discussion

The purpose of this research was, first, to perform a descriptive analysis of the PyzoFlex® field data and, second, to investigate the relationship between $\overline{w''_{2-4}}$, $\overline{LA}$ and $\overline{RF}$ for different skiing techniques. The w'' data of the prototype shows a characteristic pattern with the largest w'' between the TSPs. The rapidly fluctuating w'' within a turn (Fig. 3) is consistent with the finding by Yoneyama, Scott, Kagawa, and Osada (2008) that the ski shape changes rapidly over time. There is a very large correlation for $\overline{RF}$ vs. $\overline{LA}$ (r = 0.81), as well as for $\overline{w''_{2-4}}$ vs. $\overline{LA}$ (r = 0.81), and $\overline{w''_{2-4}}$ vs. $\overline{RF}$ (r = 0.70) (Hopkins et al., 2009). Higher $\overline{LA}$ lead to greater local ski bending curvature and accordingly to a smaller R of a turn, which is in line with Jentschura and Fahrbach (2004). Within skiing styles, the correlations vary between small to very high (Fig. 4 (a-c)). It seems that patterns can already be recognised from the existing dataset. More extensive analyses are needed to define possible technique-specific patterns and features.

Conflict of interest We declare no conflicts of interest.

Funding This work was partly funded by the Austrian Federal Ministry for Transport, Innovation and Technology, the Federal Ministry for Digital and Economic Affairs, and the federal state of Salzburg.

References

Cross, M. R., Delhaye, C., Morin, J.-B., Bowen, M., Coulmy, N., Hintzy, F., & Samozino, P. (2021). Force output in giant-slalom skiing: A practical model of force application effectiveness. *Plos one, 16*(1).

Federolf, P., Roos, M., Lüthi, A., & Dual, J. (2010). Finite element simulation of the ski–snow interaction of an alpine ski in a carved turn. *Sports Engineering, 12*(3), 123-133.

Hopkins, W., Marshall, S., Batterham, A., & Hanin, J. (2009). Progressive statistics for studies in sports medicine and exercise science. *Medicine+ Science in Sports+ Exercise, 41*(1), 3.

Jentschura, U. D., & Fahrbach, F. (2004). Physics of skiing: The ideal carving equation and its applications. *Canadian journal of physics, 82*(4), 249-261.

LeMaster, R. (2009). *Ultimate skiing*: Human kinetics.

Nakazato, K., Scheiber, P., & Müller, E. (2011). A comparison of ground reaction forces determined by portable force-plate and pressure-insole systems in alpine skiing. *Journal of sports science & medicine, 10*(4), 754.

Snyder, C., Martinez, A., Strutzenberger, G., & Stöggl, T. (2021). Connected skiing: Validation of edge angle and radial force estimation as motion quality parameters during alpine skiing. *European Journal of Sport Science*, 1-9.

Spörri, J., Kröll, J., Schwameder, H., Schiefermüller, C., & Müller, E. (2012). Course setting and selected biomechanical variables related to injury risk in alpine ski racing: an explorative case study. *British journal of sports medicine, 46*(15), 1072-1077.

Thorwartl, C., Kröll, J., Tschepp, A., Holzer, H., Teufl, W., & Stöggl, T. (2022). Validation of a Sensor-Based Dynamic Ski Deflection Measurement in the Lab and Proof-of-Concept Field Investigation. *Sensors, 22*(15), 5768.

Thorwartl, C., Kröll, J., Tschepp, A., Schäffner, P., Holzer, H., & Stöggl, T. (2021). A novel sensor foil to measure ski deflections: Development and validation of a curvature model. *Sensors, 21*(14), 4848.

Yoneyama, T., Scott, N., Kagawa, H., & Osada, K. (2008). Ski deflection measurement during skiing and estimation of ski direction and edge angle. *Sports Engineering, 11*(1), 3-13.

Sitzung III – Sportgeräteentwicklung: Werkstoffe, Konstruktion, Testing

https://nbn-resolving.org/urn:nbn:de:bsz:ch1-qucosa2-806704

A Fuzzy Controller Design for a Mechatronic Ski Binding

Aljoscha Hermann[1], Dirk Baumeister[1], Patrick Carqueville[1] & Veit Senner[1]

[1]Professorship of Sport Equipment and Materials, TUM School of Engineering and Design, Technical University of Munich, Garching, Germany

Abstract

Mechatronic Ski Bindings are the most promising technical solution to reduce knee injuries in alpine skiing. The key to a successful system is the algorithm controlling the bindings adaption of the retention values. A fuzzy controller has advantages compared to classical controllers due to missing information about injury mechanisms and the complex dynamics of the skier. We present a controller structure and test it using the injury case reported in the literature.

Keywords: Mechatronic Ski Binding, Injuries, Alpine Skiing, Algorithm, Fuzzy Controller

Introduction

Previous publications report on the advantage of integrating a mechatronic component in the ski binding concerning possible reductions in knee injuries while skiing [1, 2]. In our previous work [1] we proposed a mechatronic system that uses five input parameters: the knee flexion angle, the muscle activity of the thigh, the loads acting on the foot, the skiing velocity, and information about the skiing individual (e.g. gender) and presented prototypes for measurement systems to record these parameters [1, 3–6]. In this work, we propose an algorithm based on fuzzy controllers to determine a risk of injury by processing the input variables and providing an output signal to control allowing the adaption of the retention settings of the binding or releasing the ski.

Methods

In a literature study, the relationship between the input parameters and injury mechanisms of the knee in skiing was derived. The gained knowledge was used to define the structure of the algorithm and to define fuzzy membership functions and fuzzy rules. The final algorithm was applied to a data set of case studies of six patients who have suffered an ACL injury while skiing which was published by Fischer et al. [7]. The data set provides information about the skier and the injury mechanism. No information about muscle activation and binding loads is provided. Therefore, assumptions were made for the missing input parameters concerning the described injury mechanisms and the defined fuzzy membership functions.

Results

A total of 30 load cases were defined and respective risk values for these load cases were assessed. The proposed fuzzy controller algorithm includes three independent Mamdani fuzzy controllers providing each a respective risk level as output (Fig.1). The first controller determines a risk due to the combination of an internal or external torque on the knee, a varus, or valgus moment, the knee flexion angle and the muscle activation. The second controller determines a risk level due to a backward or forward leaning position of the skier derived by the My, the knee flexion angle, and the muscle activation. The third controller determines a risk level due to the speed of the skier. In the overall algorithm, the gender and measurement accuracies are also taken into account. The different risk levels are aggregated to define the output signal. The simulative application of the algorithm on the six case studies results in a reduction of the retention settings of the binding in four cases.

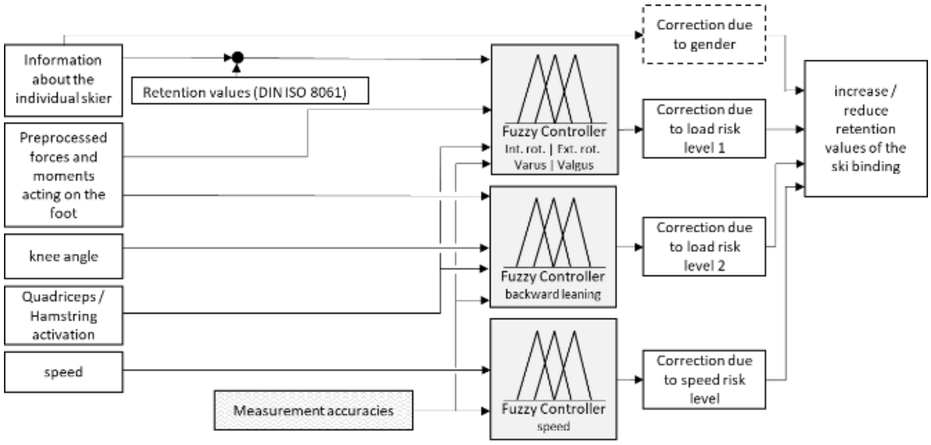

Fig. 1: Proposal for a structure of a Fuzzy controller algorithm for a mechatronic ski binding.

Discussion

The design of the algorithm is based on knowledge about injury mechanisms described in the literature. The available information is still incomplete and further research is encouraged. Besides using expert knowledge from different disciplines and results from further scientific investigations, artificial intelligence may help to allow a better definition of the various parameters of the algorithm. The application of the algorithm on the case studies just allows the demonstration of the principal workings of the algorithm. The main challenge will be the real-life validation of the algorithm for which data from many skiing days is needed. For ethical reasons, the data collection must be done with traditional binding and the sensor systems alone. The data can then be used to adapt the algorithm iteratively and only when a safe behaviour of the mechatronic system can be guaranteed can the algorithm and the active element be implemented.

Conflict of interest We declare no conflicts of interest.

Funding Bayerische Forschungsstiftung AZ-1375-19

References

1. Hermann A, Senner V (2020) Knee injury prevention in alpine skiing. A technological paradigm shift towards a mechatronic ski binding. *J Sci Med Sport*. https://doi.org/10.1016/j.jsams.2020.06.009
2. Senner V, Michel FI, Lehner S et al. (2013) Technical possibilities for optimizing the ski-binding-boot functional unit to reduce knee injuries in recreational alpine skiing. *Sports Eng* 16:211–228. https://doi.org/10.1007/s12283-013-0138-7
3. Hermann A, Ostarhild J, Mirabito Y, et al. (2020) Stretchable piezoresistive vs. capacitive silicon sensors integrated into ski base layer pants for measuring the knee flexion angle. *Sports Eng* 23. https://doi.org/10.1007/s12283-020-00336-9

4. Kiefmann A, Krinninger M, Lindemann U, et al. (2006) A New Six Component Dynamometer for Measuring Ground Reaction Forces in Alpine Skiing. In: *The Engineering of Sports 6,* vol 21. Springer, New York, NY, pp 87–92
5. Hermann A, Senner V (2020) EMG-pants in Sports: Concept Validation of Textile-integrated EMG Measurements. In: Pezarat-Correia P, Vilas-Boas J, Capri J (eds) *Proceedings of the 8th International Conference on Sport Sciences Research and Technology Support*. SCITEPRESS - Science and Technology Publications, pp 197–204
6. Hermann A, Senner V (2019) Sensing the Skier: Towards a Mechatronic Ski Binding. *23rd International Congress on Snow Sports Trauma and Safety*, Squaw Valley, California, USA
7. Fischer JF, Loureiro O, Leyvraz PF, et al. (1996) Injury mechanism of the anterior cruciate ligament in alpine skiing: Case studies. ASTM Special Technical Publication 1266

https://nbn-resolving.org/urn:nbn:de:bsz:ch1-qucosa2-806704

Saddle-pressure distribution and perceived comfort during inclined and upright cycling

Johanna Freunek[1], Stefan Litzenberger[1] & Frank Michel[2]

[1]Fachhochschule Technikum Wien, Department of Life Science Engineering, Vienna, Austria

[2]VAUDE Sport GmbH & Co. KG, Innovation Team, Tettnang, Germany

Abstract

To gather further information on the issue of discomfort and its prevention during seated bicycle riding, different seating conditions were tested during short term indoor cycling trials. The pressure distribution on the bicycle saddle for an upright position on a wide, cushioned saddle and an inclined position on a narrow, sporty saddle as well as the riders' subjective feedback revealed significant differences between these scenarios.

Keywords: bicycle saddle, indoor trials, pressure distribution, subjective feedback

Introduction

The rise in the popularity of cycling in recent years encourages scientific approaches to investigate the issue of discomfort and its prevention during seated riding. Regardless of whether discomfort is perceived, the matter of protection to health hazards is ever-present. Frequent complaints are related to the entrapment of the pudendal nerve that could lead to disorders like genital numbness or even sexual dysfunction (Sommer et al. 2001). To increase both comfort and protection during cycling, different saddle constructions and paddings in cycling shorts were investigated by saddle pressure measurements in former studies (Marcolin et al. 2015; Bressel and Larson 2003; Lowe et al. 2004; Larsen et al. 2018).

The review of these studies revealed the complexity of the influencing factors. Research showed that the main impact on pressure distribution was caused by saddle geometry and its materials, the posture by means of the pelvic tilt, cycling time, individual subject parameters (gender, age, body weight, riding experience and individual anatomy), the position of hands on the handlebar, applied workload and the seat pad.

Most of these studies were conducted using sporty saddles, sitting-positions and subjects. Hence this work focuses on the differences between an inclined and an upright riding scenario.

Methods

A cross-sectional study was performed to examine possible relationships between the pressure distribution and the discomfort perception for upright and inclined riding. All tests were performed on a stationary bike-trainer (KICKR Smart Bike 2021, Wahoo Fitness, LLC, Atlanta, USA) in two sitting positions (upright and inclined) with either a narrow (for the inclined condition) and a broader upholstered saddle (for the upright condition). 24 subjects (12 male, 12 female, age: 26±4 yrs, weight: 70.45±11 kg, height: 177±8 cm) participated in the study. They were mainly recruited from the community of the University and gave their informed consent to participate in the study.

The saddle-height of the stationary trainer was adapted using the subjects' inner leg length and the saddle width was chosen by measuring the subjects' seat bone distance. Two saddle-models in two widths (large, regular) each were used for the experiments, the wider comfort saddle CUBE Shen (CUBE, Pending System GmbH & Co. KG, Waldershof, GER) and the narrow, sporty saddle CUBE Venec.

Participants rode in two conditions: (1) upright (comfort saddle) where the handlebar and stem were set to achieve a very upright trunk angle of 80° and participants were asked to pedal at a cadence of 70 rpm and a power of 1.5 W/kg bodyweight; (2) inclined (sporty saddle) where trunk angle was set to 50° and participants pedalled at 80 rpm and a power of 2.25 W/kg. The subjects completed each condition seven times, first wearing short tights without any padding and then with six cycling shorts with different seat-pads. The tests consisted of a 2 min warmup-phase and 15 s of pressure-data acquisition each.

Pressure data were recorded at a frequency 120 Hz using a medilogic® saddle pressure mat (T&T medilogic Medizintechnik GmbH, Schönefeld, GER). While still sitting on the bike, the subjects answered a questionnaire on the perceived pressure strength, pressure sense, stability and the overall feeling. The obtained data were analysed using MATLAB R2021b (MATLAB®, The MathWorks, Inc., USA). Mean pressure p_{mean} (mean of each sensor averaged over time and participants), maximum pressure p_{max} (maximum of each sensor averaged over time and participants) and contact area A were calculated. Additionally, the pressure patterns were represented graphically in heat maps and the area of the saddle mat was divided in a “front”, “mid” and “back” zone. It was calculated how often the maximum of the three parameters (p_{mean}, p_{max}, A) occurred in each zone. Statistical tests were performed on both pressure and non-parametric survey data to observe differences between the upright and the inclined sitting scenario using a Friedman test.

Results

The averaged pressure values of p_{max} tested without seat pad (reference measurement) are represented graphically in Fig. 1. Comparison among the sitting scenarios shows higher pressure values for the inclined sitting scenario. Upright riding indicates pressure centres less distributed along the lateral curvature of the mat but more focused to the line between back and mid zone whereas in inclined cycling, the maximum pressure is mainly occurring in the mid zone.

The classification of each trial using predefined zones “front”, “mid” and “back” is displayed in Table 1. For all three - p_{max}, p_{mean} and A - similar tendencies could be observed. In the inclined sitting scenario, five or less trials (p_{max}: 5, p_{mean}: 1, A: 0) were evaluated for exhibiting maximum values in the front zone. The majority of counts (152, 154, 123) was registered for the mid zone. Fewer trials

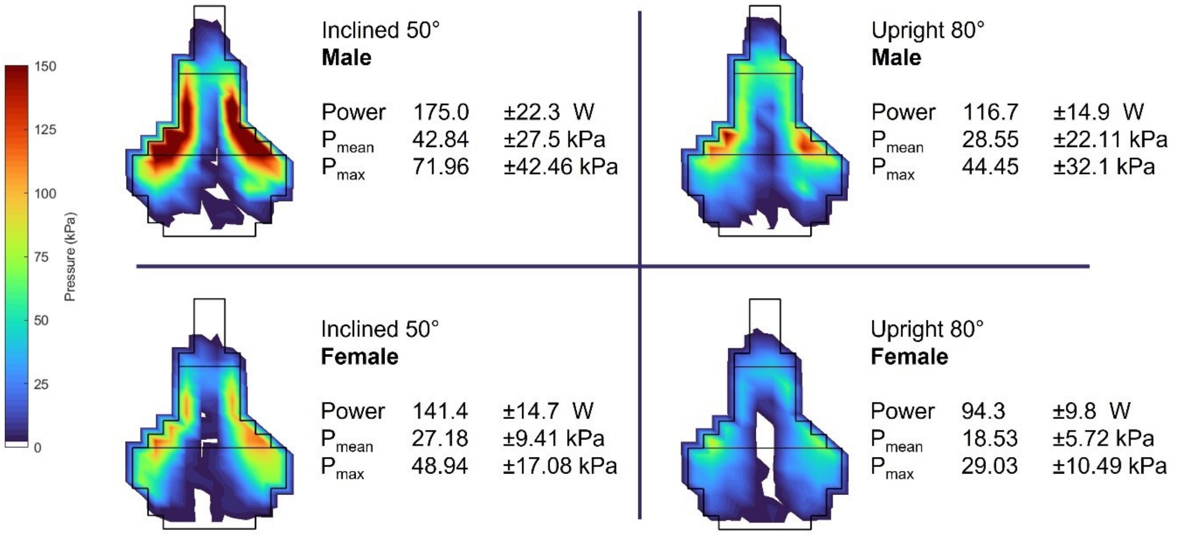

Fig. 1: Averaged pressure distribution patterns of pmax distinguishing gender and sitting position; “front”, “mid” and “back” zones are divided by horizontal black lines

(11, 13, 45) were assigned to the back zone. During upright cycling, p_{max} and p_{mean} still emphasize the mid zone (p_{max}: 111, p_{mean}: 113) but show a larger number of counts in the front zone (44, 38). The back zone (13, 17) is nearly unchanged. The contact area again does not exhibit any case with the maximum contact area in the front zone, but 91 in the mid and 77 in the back zone.

Table 1 Occurrences of the zones “front”, “mid” and “back” as locations of the maximum calculated from p_{max}, p_{mean} and A for the inclined and upright condition

	p_{max}		**p_{mean}**		**A**	
	inclined	**upright**	**inclined**	**upright**	**inclined**	**upright**
front	5	44	1	38	0	0
mid	152	111	154	113	123	91
back	11	13	13	17	45	77

For the perception data collected with the questionnaire, the Friedman analysis was run for all data grouped for upright and inclined riding. Significant differences between inclined and upright was found for perceived pressure strength, pressure sense and overall impression (all $p<0.001$) but not for the stability rating ($p=0.574$). Whether the upright or inclined condition was rated better depended mainly on the combination of individual preferences regarding cycling short worn and the saddle used. No statistical proof was found favouring one specific combination.

Discussion

For the first time in scientific research, a wide and upholstered saddle was integrated to a setup with an *upright* trunk posture and compared to an *inclined* sitting scenario featuring a narrow and less cushioned saddle. The more *inclined* sitting posture in the described scenario leads to higher absolute pressure values (Fig. 1). These findings did not match the recent literature that mainly associates increased workloads and more inclined postures with decreasing pressure. However, former research is based on comparing upright and inclined on the same narrow and sportive saddle types. The *upright* scenario according to the acquired data is furthermore associated with the emphasis of sitting on the seat bones rather than the pubic bones during *inclined* sitting and the subjects shifting their weight considerably more often to the front zone than in the *inclined* position. This finding did not match the expectations and requirements usually associated with broad and well-cushioned saddle designs.

Although different influencing factors were not kept constant in this work, strong evidence exists that in seat pad design for cycling shorts differentiation into customer types according to e.g., weight class and cycling segment is conceivable and personal preferences such as saddle type, trunk inclination or power output should be considered additionally to - or even more than - gender differences.

Conflict of interest We declare no conflicts of interest.

Funding Cycling shorts were funded by the company VAUDE. This study was conducted within the framework of the Alliance for Sports Engineering Education (A4SEE) project, co-funded by the Erasmus+ Programme of the European Union.

References

Bressel, Eadric; Larson, Brad J. (2003): Bicycle seat designs and their effect on pelvic angle, trunk angle, and comfort. In: *Medicine and science in sports and exercise 35*(2), S. 327–332. DOI: 10.1249/01.MSS.0000048830.22964.7c.

Larsen, Anna Sofie; Larsen, Frederik G.; Sørensen, Frederik F.; Hedegaard, Mathias; Støttrup, Nicolai; Hansen, Ernst A.; Madeleine, Pascal (2018): The effect of saddle nose width and cutout on saddle pressure distribution and perceived discomfort in women during ergometer cycling. In: *Applied ergonomics 70,* S. 175–181. DOI: 10.1016/j.apergo.2018.03.002.

Lowe, Brian D.; Schrader, Steven M.; Breitenstein, Michael J. (2004): Effect of bicycle saddle designs on the pressure to the perineum of the bicyclist. In: *Medicine and science in sports and exercise 36*(6), S. 1055–1062. DOI: 10.1249/01.mss.0000128248.40501.73.

Marcolin, Giuseppe; Petrone, Nicola; Reggiani, Carlo; Panizzolo, Fausto A.; Paoli, Antonio (2015): Biomechanical Comparison of Shorts With Different Pads: An Insight into the Perineum Protection Issue. In: *Medicine 94*(29), e1186. DOI: 10.1097/MD.0000000000001186.

Sommer, F.; Schwarzer, U.; Graf, C.; Klotz, T.; Engelmann, U. (2001): Veränderungen der penilen Durchblutung beim Radsport - wie verhindert man eine Minderdurchblutung? In: *Dtsch Med Wochenschr 126*(34-35), S. 939–943. DOI: 10.1055/s-2001-16582.

https://nbn-resolving.org/urn:nbn:de:bsz:ch1-qucosa2-806704

Influence of the Vergence-Accommodation-Conflict by Using HMDs with Augmented Reality for Sport and Exercises – First Results

Eva Bartaguiz[1], Sergey Mukhametov[1,2], Carlo Dindorf[1], Oliver Ludwig[1], Jochen Kuhn[3] & Michael Fröhlich[1]

[1]Technische Universität Kaiserslautern, Department of Sports Science, Kaiserslautern, Germany

[2]Technische Universität Kaiserslautern, Department of Physics Education, Kaiserslautern, Germany

[3]Ludwig-Maximilians-Universität München, Faculty of Physics, Munich, Germany

Abstract

To improve the performance and capabilities of athletes, augmented reality could play an important role in exercise training. During training, these technologies support athletes in analyzing their training over all phases. Regardless of all potential advantages, the vergence-accommodation-conflict (VAC) could affect the effectiveness of training and performance. This work is aimed to evaluate the effect of VAC in different conditions.

Keywords: vergence-accommodation-conflict, augmented reality, HMD, sport sciences, sports education, training, performance

Introduction

Due to the multiple ways of generating environmental and perceptual stimuli, the application and use of virtual and augmented reality (VR and AR) is gaining more and more popularity. To enhance and extend the efficiency of training methods, learning experiences and realize novel learning exercise scenarios, these technologies are also increasingly considered in the context of exercises and sports science (Loila & Orciuoli, 2019). Existing AR solutions are mainly used for enhancing training sessions, observing athletes' data or providing additional information during training. This allows the athletes and also patients in their rehabilitation phase to improve their specific physical behaviour. By adding relevant goals, the monotonous parts of the training should become more attractive and social cooperation should be promoted (Kajastila und Hämäläinen, 2014). Improving the mental, perceptual skills, coordination, and further reaction times, the AR-based devices could be useful to reduce errors (Loila & Orciuoli, 2019).

However, besides the potential to create new supporting training settings and generate potential solutions for enhancing performance, head- or helmet-mounted displays (HMDs) also have drawbacks in this context that could affect training success. Thus, the vergence-accommodation conflict (VAC) is a well-known phenomenon in this context (Cakmakci & Rolland, 2006). Especially women are prone to symptoms of VAC (Grassini & Laumann, 2021). This effect is exacerbated in AR when a relatively close real object is augmented by additional virtual information (Duchesne & Coubard, 2021). Furthermore, visual processes responsible for clear and simple binocular vision can thus interfere with cognitive processes and attentional conduction, thus affecting learning and training success in its entirety (Daniel & Kapoula, 2019). Therefore, this study aims to investigate the influence of such AR headsets with simple virtual and real objects on vergence, well-being as well as concentration ability of students. Based on the findings, training and exercise environments can be designed in a method-appropriate manner without the success of performance being influenced by the VAC. In this study, we focus on the first results for the well-being and possible symptoms, caused by being in an environment with AR-elements.

Methods

A total of 45 healthy subjects (gender: 28 female, 17 male, 0 divers; age *M* = 23.26, *SD* = 3.10) underwent the experiment. Subjects had to have the normal or corrected-to-normal vision, which was checked in advance with a visual acuity chart, followed by the baseline measurement of HRV and the applications in AR. Data on gaze behavior using eye trackers were collected continuously throughout the usage of the AR-application. In addition, symptoms and sensitivities were queried after each app (VAC 1, 2, 3, and 4) (Fig. 1). The order of the apps was randomized using a randomization list. As HDM, we used the HoloLens 2 (Microsoft Corporation, Redmond, Washington, USA).

(a)

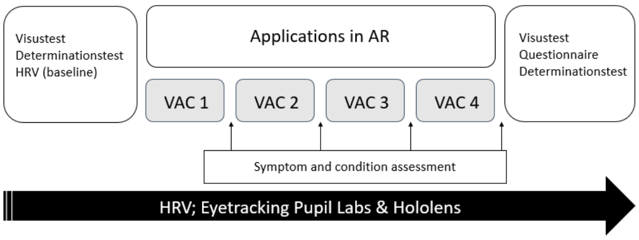

Fig. 1 Set-up and

(b)

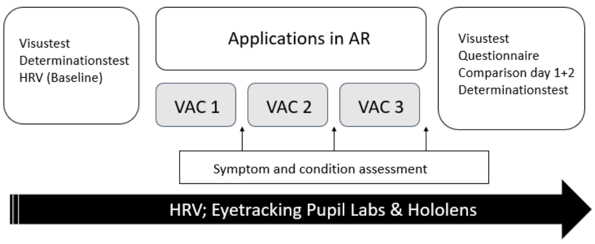

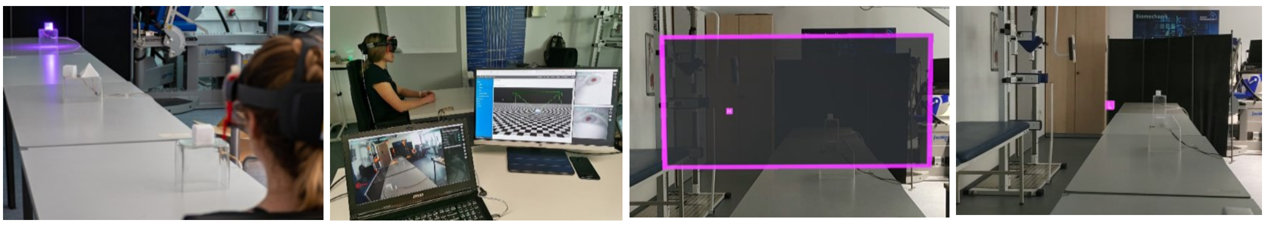

schematic representation of the study procedure of day 1 (a) and day 2 (b)

We developed four types of interventions for the 1st day with variable distances: VAC 1: display/watching of real and virtual boxes; VAC 2: watching letters and numbers with sequential writing; VAC 3: boxes in motion: reading sequence at different distances; VAC 4: boxes in motion with constantly changing distance; and three types of interventions for the 2nd day analog to day 1 (VAC 1-3), but with a fixed distance. On day two all subjects were randomly assigned to the two groups with different distances (distance 2.5 m: *n* = 23; age: *M* = 23.48, *SD* = 3.66 / distance 0.7 m: *n* = 22; age: *M* = 22.82, *SD* = 2.01). This assignment was done single-blinded, using a randomization list. To measure the symptoms after the intervention, we used the adaption of Visual Fatigue Questionnaire (VFQ) (Bangor, 2000; Spilski et al., 2019), which consists of 17 items with a 5 Likert scale (1-5). During the intervention, eye tracking data will be collected to calculate the real vergence angle (Daniel & Kapoula, 2019), as well as heart rate variability (HRV) to measure stress. The real vergence angle data are then compared with the mathematically postulated vergence angle, and the HRV is compared with baseline measurements. Symptoms of VAC are additionally queried via two symptom questionnaires.

Results

Gender specific differences were only found for the item “Ich habe Kopfschmerzen" (I've headaches) (F(1,43) = 5.41, p = .02, η_p^2 = .1118). On day 2, when the subjects were randomly assigned to the two distance groups, a significant difference was only found for the item "Mein Gesicht ist schweißnass" (my face is wet with sweat) (F(1,43) = 4.26, p = .04; η_p^2 = .09). The multivariate comparisons showed no significance between the groups and the two test days.

Discussion

Our first results, which indicate almost no symptoms when using the Microsoft HoloLens, confirm the findings of Vovk, Wild, Guest & Kuula (2018). One explanation for the significant result from day 1 can be found in the changing distances on day 1. Thus, the VAC is provoked by continuous refocusing and accommodation. This could be the first indication of how training and exercise sessions can be designed and which arrangement (e.g. fixed distances) of virtual objects is more suitable.

At this point, we want to point out the pending analysis of the eye tracking and HRV data across the complete cohort and the individual level. During the execution of the experiment, it became apparent that consideration of individual cases could be interesting in this context. Nevertheless, the study contains a few limitations. For example, the subjects completed the questionnaire only a few minutes after the intervention in the AR environment, which means that delayed symptoms are no longer recorded. In addition, the subjects were in the AR environment for 30 minutes. The after-effects of prolonged exposure to AR, especially in connection with sporting activities, are still unclear. Further research should aim to evaluate AR to induce an external associative focus and investigate its effectiveness in enhancing performance and physical capabilities.

Summarising, AR can enable situations that are not readily available in physical reality. This includes training and realistic preparation for possible stressful situations in competition, as well as direct feedback to improve individual skills and movements. Based on the insights gained, training and exercise environments can be designed in a method-appropriate way without success being influenced by the VAC.

Conflict of interest: The authors declare no conflict of interest.

Funding: The project Health.Holo.Lab as a sub-project of "U.EDU: Unified Education – Medienbildung entlang der Lehrerbildungskette" is part of the “Qualitätsoffensive Lehrerbildung”, a joint initiative of the Federal Government and the Länder which aims to improve the quality of teacher training. The program is funded by the Federal Ministry of Education and Research. The authors are responsible for the content of this publication. BMBF [01JA2029].

References

Bangor, A. W. (2000). *Display technology and ambient illumination influences on visual fatigue at VDT workstations* (Doctoral dissertation, Virginia Polytechnic Institute and State University).

Cakmakci, O. & Rolland, J. (2006). Head-Worn Displays: A Review. *Journal of Display Technology, 2*(3), 199–216. https://doi.org/10.1109/JDT.2006.879846

Daniel, F. & Kapoula, Z. (2019). Induced vergence-accommodation conflict reduces cognitive performance in the Stroop test. *Scientific Reports, 9*(1), 1247. https://doi.org/10.1038/s41598-018-37778-y

Duchesne, J. & Coubard, O. A. (2021). Measuring vergence and fixation disparity in 3D space. *The European Journal of Neuroscience, 53*(5), 1473–1486. https://doi.org/10.1111/ejn.14929

Grassini, S., & Laumann, K. (2021, April). Immersive visual technologies and human health. In *European Conference on Cognitive Ergonomics 2021* (pp. 1-6).

Kajastila, R. & Hämäläinen, P. (2014). *Augmented climbing: interacting with projected graphics on a climbing wall.* In M. Jones, P. Palanque, A. Schmidt & T. Grossman (Hrsg.), CHI '14 Extended Abstracts on Human Factors in Computing Systems (S. 1279–1284). New York, NY, USA: ACM.

Loila, V. & Orciuoli, F. (2019). ICTs for exercise and sport science: focus on augmented reality. *Journal of Physical Education and Sport, 2019*(5). https://doi.org/10.7752/jpes.2019.s5254

Spilski, J., Exner, J. P., Schmidt, M., Makhkamova, A., Schlittmeier, S., Giehl, C., ... & Werth, D. (2019, November). Potential of VR in the vocational education and training of craftsmen. In Proceedings of the 19th International Conference on Construction Applications of Virtual Reality.

Vovk, A., Wild, F., Guest, W., & Kuula, T. (2018, April). *Simulator sickness in augmented reality training using the Microsoft HoloLens.* In Proceedings of the 2018 CHI conference on human factors in computing systems (pp. 1-9).

https://nbn-resolving.org/urn:nbn:de:bsz:ch1-qucosa2-806704

Position detection in Ultimate Frisbee using Drones

Tiago G. Russomanno[1], Patrick Blauberger[2], Marc Schmid[2], Otto Kolbinger[2] & Martin Lames[2]

[1]Universidade de Brasilia, Faculty of Physical Education, Brasilia, Brazil

[2]Technical University of Munich, Chair of Performance Analysis and Sports Informatics, Department of Sport and Health Sciences, Munich, Germany

Abstract

Drones are widely used in different applications, with different models, like quadcopters, or military drones. But so far little has been done in sports regarding performance analysis, based on this, the aim of this work is to present a position detection in Ultimate Frisbee using drones.

Keywords: Ultimate frisbee, Position detection, Drone

Introduction

Currently, video-based systems that use image recognition are popular for live sports broadcasts and rely on several fixed cameras set up around the field of play. However, there are several constraints regarding the location of these systems. For example, the cameras must be placed at a sufficient height, which is often only possible in arenas and other well-equipped training facilities (Torres-Ronda et al., 2022). Besides, previous studies have found that video-based electronic performance and tracking systems (EPTS) for outdoor sports share some limitations, like occlusion during corner kicks in soccer (Baysal and Duygulu, 2016; Kim et al., 2018), that can only be overcome by human corrections or the use of more cameras, consequently increasing the cost. One option to alleviate these problems might be using a bird eye view perspective of a drone presented by Russomanno et al. 2022. As we know, drones are widely used in different applications, but most of those applications are focused on agriculture, inspections, and defence. But so far little has been done in sports regarding performance analysis, most of the applications in sports are related to enhance the spectator experience during broadcast (Ayranci, 2017). Based on this, the aim of this work is to present the likelihood to use drones for position detection in Ultimate Frisbee once the sport is played in open fields without any adjacent structure for fixing cameras or antennas and still been played in amateur level with low budget compared with other outdoor sports (football).

Methods

A sample of 14 Ultimate frisbee players, including current or former players from the German national team (age:28.35 ± 2.46 years) took part in the study. All procedures performed in the study were in accordance with the Declaration of Helsinki. The drone used in this study was a Mavic Air 2 Model (SZ DJI Technology Co., Ltd DJI. As the flight duration of this drone is around 34 minutes, we used a second drone of the same model to replace the first one and to ensure continuous data acquisition in case we exceeded this duration. The chosen height during stationary flight was determined based on the size of the field, weather conditions and was in accordance with the legal regulations for UAV, in our case the German regulations (www.gesetze-im-internet.de/luftvo_2015/).

All these variables were set to optimize the safety of the participants and the quality of the video footage through the unique bird's-eye view perspective.

The data was collected on an Ultimate Frisbee field (97.11 m x 36.25 m) with the drone at a height of 85 m. Data was recorded from a bird’s eye view with the drone positioned at the centre of the field, enabling a full view of the field and the players, including the surrounding areas of interest, as shown in Fig. 1.

Fig. 1 Bird eye view from the drone, hovering at 85 m

Tracking was done using a flexible software interface developed in the Python programming language (Python Software Foundation, https://www.python.org/). Figure 2 presents the block diagram of the tracking system, in which multiple object tracking was performed (Bewley et al., 2016; Milan et al., 2016). This was conducted with a 2 Phase System. A Faster-RCNN object detection neural network was trained to recognize players from a bird’s eye view (Ren et al., 2015). Next, we tracked the initial players’ bounding boxes with a generic object tracker called Atom (Danelljan et al., 2019), which performs at the top of specific tracking benchmarks such as UAV123 and TrackingNet.

The X and Y positions of the players were defined as the center point of the bounding box enclosing the respective player’s outline. Following the tracking procedure, the X and Y positions of the players were reconstructed based on the four corner points extracted for calibration in MATLAB (R2020b, The MathWorks Inc., Natick, MA, USA) using 2D homography (Corke, 2017). Due to slight movements of the drone, the calibration was performed frame by frame to reduce errors.

Results

Some exemplar results are presented in figures 2 and 3, as examples of performance indicators of the players during an Ultimate match that can be obtained based on the position detection from a drone.

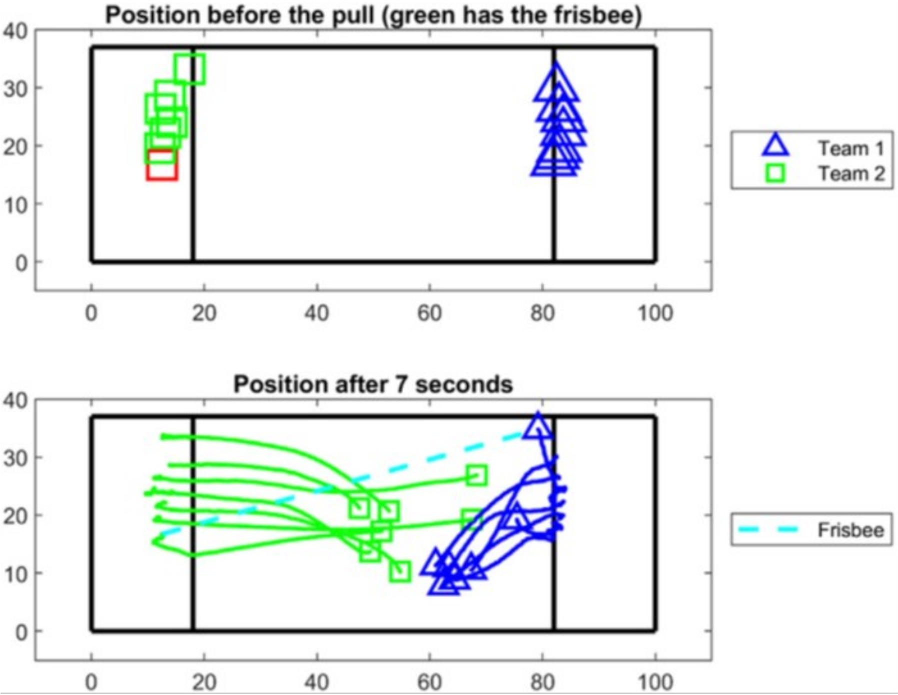

Fig. 2 position of the players before and after the pull

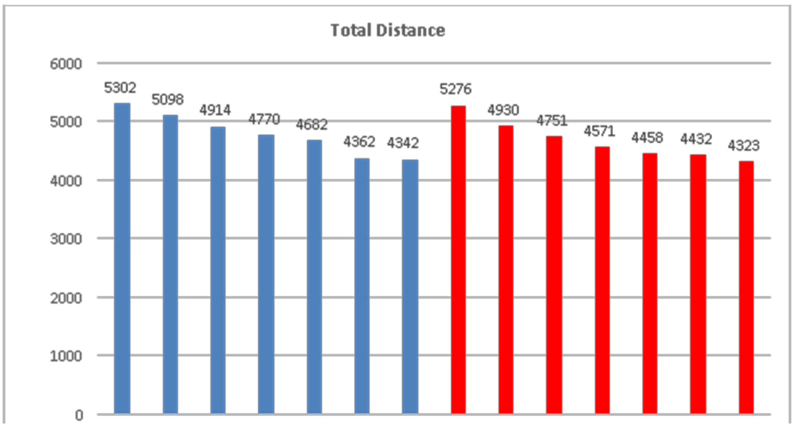

Fig. 3 Total disctance coverd by the players during the match.

Discussion

The position detection system based on drones, for ultimate frisbee presented in this work, shows as a reliable option for the sport, in this case Ultimate frisbee. As most of the games are played on open fields without any adjacent structure to fix cameras or other EPTS. Furthermore, drones can be an optimum option for neglect sports like Ultimate that do not rely on any kind of EPTS for performance analysis of their players. The current work presented some examples of results that can be used in Ultimate. Besides that, the system was able to track all the players using only one camera with a bird eye view perspective and provide basic performance indicators based on X and Y position of the players. The results in this paper are just a small sample off the possible performance indicators that can be calculated from the data regarding physical demands of the match like covered distance, speeds, number of sprints as well some tactical analysis position for Ultimate Frisbee.

Future research can build upon the findings of this work by further testing the drone-based system in more matches and compare with other tracking systems available in the market.

Conflict of interest: We declare no conflicts of interest.

Funding This work was funded by the Federal Institute for Sports Science (BISp) under grant ZMVI4-071501/20. The authors declare that they do not have any financial interest or benefit arising from the direct applications of their research.

References

Ayranci, Z.B. (2017). Use of Drones in Sports Broadcasting *Ent. & Sports Law,* (3), 79-93.

Baysal, S., and Duygulu, P. (2016). Sentioscope: A Soccer Player Tracking System Using Model Field Particles. *IEEE Transactions on Circuits and Systems for Video Technology* 26(7), 1350-1362. doi: 10.1109/TCSVT.2015.2455713.

Bewley, A., Ge, Z., Ott, L., Ramos, F., and Upcroft, B. (Year). "Simple online and realtime tracking", in: *2016 IEEE international conference on image processing (ICIP)*: IEEE), 3464-3468.

Danelljan, M., Bhat, G., Khan, F.S., and Felsberg, M. (Year). "Atom: Accurate tracking by overlap maximization", in: *Proceedings of the IEEE/CVF Conference on Computer Vision and Pattern Recognition*), 4660-4669.

Kim, W., Moon, S.-W., Lee, J., Nam, D.-W., and Jung, C. (2018). Multiple player tracking in soccer videos: an adaptive multiscale sampling approach. *Multimedia Systems* 24(6), 611-623. doi: 10.1007/s00530-018-0586-9.

Milan, A., Leal-Taixé, L., Reid, I., Roth, S., and Schindler, K. (2016). MOT16: A benchmark for multi-object tracking. *arXiv preprint arXiv:1603.00831*.

Ren, S., He, K., Girshick, R., and Sun, J. (2015). Faster r-cnn: Towards real-time object detection with region proposal networks. *arXiv preprint arXiv:1506.01497*.

Russomanno, T.G., Blauberger, P., Kolbinger, O., Lam, H., Schmid, M., and Lames, M. (2022). Drone-Based Position Detection in Sports—Validation and Applications. *Frontiers in Physiology* 13. doi: 10.3389/fphys.2022.850512.

Torres-Ronda, L., Beanland, E., Whitehead, S., Sweeting, A., and Clubb, J. (2022). Tracking Systems in Team Sports: A Narrative Review of Applications of the Data and Sport Specific Analysis. *Sports Medicine - Open* 8. doi: 10.1186/s40798-022-00408-z.

https://nbn-resolving.org/urn:nbn:de:bsz:ch1-qucosa2-806704

Characterisation of thermoplastic polyurethane (TPU) for additive manufacturing

Daniel Matthias Haid[1], Olly Duncan[2], John Hart[1] & Leon Foster[1]

[1]Sports Engineering Research Group, Sheffield Hallam University, Faculty of Health and Wellbeing, AWRC, Olympic Legacy Park, 2 Old Hall Road, S9 3TU, Sheffield, UK

[2]Department of Engineering, Manchester Metropolitan University, Manchester, M15 6BH, UK

Abstract

Despite increasing use, many 3d printing material properties are not openly available, which causes barriers to simulation and application. Four additively manufactured thermoplastic polyurethanes were characterised at low (0.006 s^{-1}) to high (16 s^{-1}) compressive and tensile strain rates, and during stress relaxation. Quasi-static Young's moduli were determined to be 24 – 247 MPa, increasing by up to 183% at 16 s^{-1}.

Keywords: Material characterisation, 3d printing, digital image correlation

Introduction

Additive manufacturing (AM) is a rapidly growing industry, with applications from creation of prototypes during design and development to mass manufacturing. AM is being used for technological advancements in sports to enhance athletes' performance or safety (Kajtaz et al., 2019). One area of interest lies in mechanical metamaterials, made available through advances in AM. Thermoplastic polyurethanes (TPU), used in these designed architectures can facilitate novel properties such as extreme, pentamode, or auxetic behaviour (Zadpoor, 2016).

An efficient way of optimising and designing complex mechanical metamaterial forms is finite element analysis (FEA). Print material data, required for FEA, is often not available, or it can be unsuitable as print material changes with printing parameters (Johnston & Kazancı, 2021). Here, we provide print material characteristics for defined printing parameters, following a characterisation protocol that has been previously suggested for FEA modelling of mechanical metamaterials for sports applications (Shepherd et al., 2020).

Methods

Four commercially available filaments (with a diameter of 2.85 mm) were selected to represent the range of flexible materials (Table 1). Test samples were produced on an Ultimaker S5 (Ultimaker, NLD; nozzle diameter 0.4 mm) 3d printer with a Bowden drive extruder. Samples were printed with a 0.12 mm layer height, and with 100% infill. All other print settings (Table 2) were determined through an iterative refinement of the print process for each material. Twelve type 1 dumb-bell samples (International Organization for Standardization, 2017) and 27 cubic samples (side length 10 mm) were produced and tested for each material (Fig. 1a). All testing was conducted using an Instron Universal testing machine (Instron, UK) with a 5 kN load cell (Fig. 1b).

Table 1 TPU material parameters according to manufacturers' technical data sheet.

Material	Density [kg/m^3]	Hardness	Tensile Modulus [MPa]
Flex Medium, Extrudr, AT	1190	98 A	40
MD Flex, Copper 3D, CHL	1160	98 A	150
TPU 95A, Ultimaker, NLD	1220	95 A	26
NinjaFlex, Ninjatek, USA	1190	85 A	12

Quasi-static tensile tests (grip distance 70 mm; engineering strain 0.5 (35 mm); strain rate 0.006 s^{-1} (0.42 mm/s)) and compression tests (engineering strain 0.5 (5 mm); strain rate 0.008 s^{-1} (5 mm/min); pre-load 10 N) were carried out. Machine force and displacement data and sample dimensions were used to compute engineering stress (σ) and strain (ε). A linear trend line was fitted between strains of 0 and 0.1 to obtain Young's Modulus (E). To assess the effects of print layer building direction on final mechanical properties, cubic samples were compressed in their building direction (Z-direction) and perpendicular to building direction (X-direction), with each test repeated three times. For full-field strain measurements using Digital Image Correlation (DIC), a spray paint speckle pattern was applied to the narrow portion of all tensile samples (Fig. 1c) and to one face of all cubic samples (undercoat: matt white acrylic, speckles: matt black acrylic). A camera (Phantom Miro R311, Vision Research Ltd., UK; resolution 1280 x 800 pixels, sample rate 24 fps; lens, Nikon AF Nikkor 24 – 85 mm) at 500 mm from the test bed and with the field of view perpendicular to the speckled surface was used to film all testing (Fig. 1b). DIC to obtain lateral and axial strain was then carried out using GOM Correlate (2019 Hotfix 7, Rev. 128764, Build 2020-06-18). Poisson's Ratio (v) was obtained by fitting a linear trendline to the lateral vs. axial strain data up to an axial strain of 0.09x (Fig. 2c).

Additional tensile tests (engineering strain 0.4 (28 mm); strain rate 1, 2, 3 s^{-1} (70, 140, 210 mm/s); camera 210 fps) and compression tests (engineering strain 0.4 (4 mm); strain rate 1, 2, 4, 8, 16 s^{-1} (10, 20, 40, 80, 160 mm/s); camera 1600 fps) were carried out at higher strain rates to assess rate dependence. These compression tests were only performed in Z-direction, and each test was repeated three times. Stress, strain, and Young's modulus were obtained using the same method as the quasi-static tests. Viscoelastic material data were obtained through stress relaxation testing. Three cubic samples of each material were compressed to a strain of either 0.2 (2 mm) or 0.4 (4 mm) at a rate of 0.005 s^{-1} (0.05 mm/s). Force was measured while compression was held for 600 s.

Table 2 Material-specific print settings.

Material	Print temp. [°C]	Bed temp. [°C]	Print speed [mm/s]	Flow
Flex Medium	210	30	30	110%
MD Flex	235	60	75	100%
TPU 95A	223	60	25	106%
NinjaFlex	235	50	20	100%

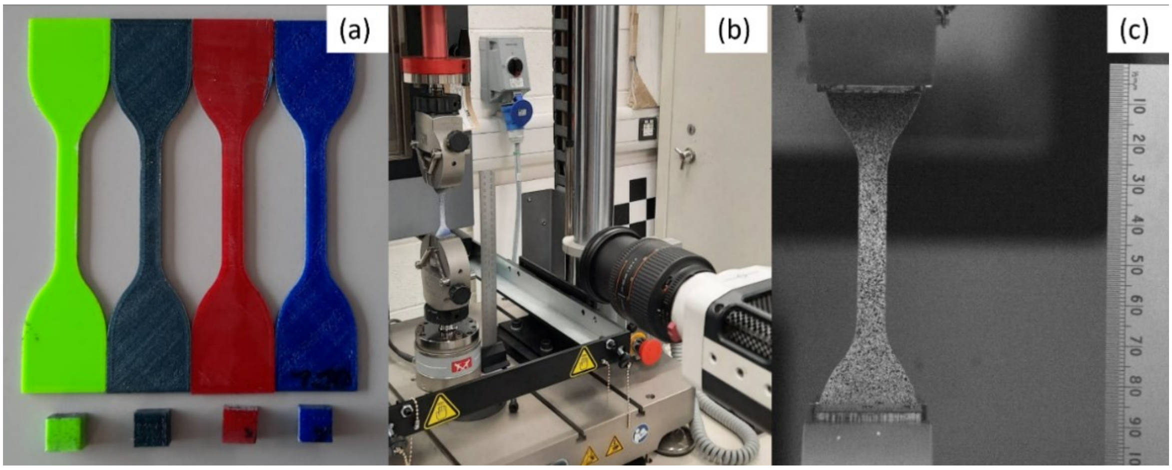

Fig. 1 (a) test samples (from left to right: Flex Medium (neon green), MD Flex (grey blue), TPU 95A (red), Ninjaflex (sapphire blue)); (b) tensile test setup; (c) still from video footage for DIC analysis.

Results

Poisson's ratio (Fig. 2c) ranged between 0.36 and 0.4 (Table 3). Tensile moduli varied up to three times greater than stated on their respective technical data sheets (TDS). For Flex Medium and TPU 95A, compressive modulus did not change depending on the direction relative to layer orientation. For MD Flex and NinjaFlex, lower compression moduli were found when compressed perpendicular to layer orientation (Table 3).

Higher strain rates showed the rate dependence of all TPUs. For both, compression (Fig. 2a) and tensile tests(Fig. 2b), stiffness increased with increasing strain and strain rate (TPU 95A shown exemplary for all materials). During stress relaxation tests, the measured shear modulus decayed to ~75% of its initial magnitude (Fig. 2d).

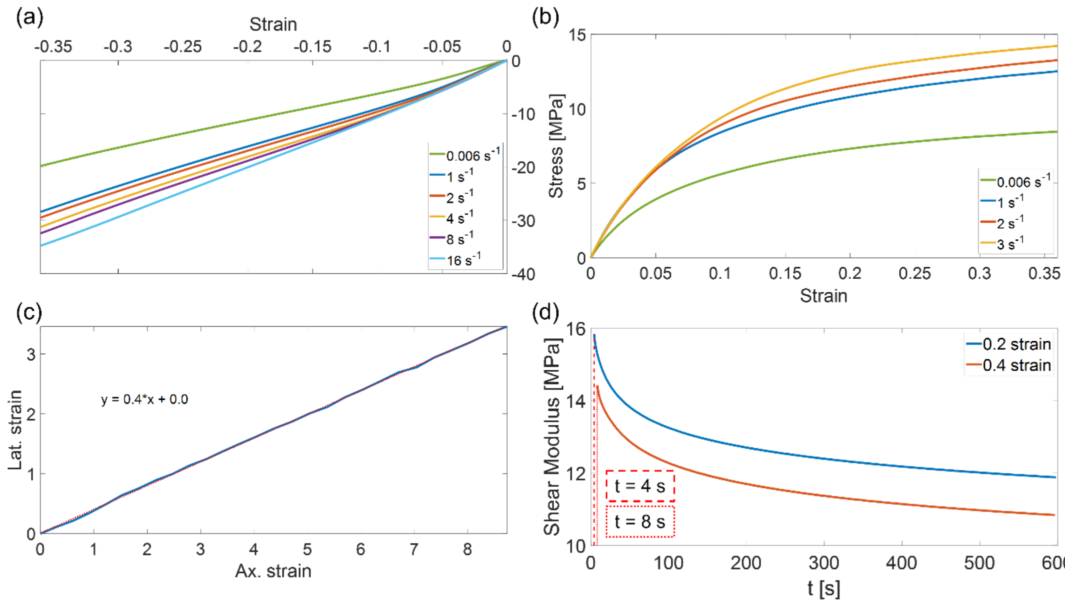

Fig. 2 Test data for TPU 95A; stress vs. strain at different strain rates for (a) compression and (b) tensile testing; (c) lateral vs. axial strain during tensile tests with plotted linear trendline obtained from DIC; (d) stress relaxation force vs. time curve.

Table 3 Poisson's Ratio, Tensile Modulus, deviation from TDS, and directional sensitivity for all four materials obtained from quasi-static testing.

Material	v_{zx}	E_z – Tensile [MPa]	E_z/E_{TDS}	E_z/E_X
Flex Medium	0.38 ± 0.01	147.2 ± 14.3	3.7	0.99
MD Flex	0.37 ± 0.01	130.9 ± 6.3	0.9	0.89
TPU 95A	0.40 ± 0.01	101.2 ± 6.8	3.9	1.00
NinjaFlex	0.36 ± 0.02	24.4 ± 8.9	2.0	0.78

Discussion

The material properties obtained from these prints should enable representation of mechanical behaviour of simulated parts. These properties can be used by other researchers using equivalent printer settings, without the need to do a separate characterisation. Consistency in prints and availability of parameters for simulations can facilitate developments in sports equipment and other fields.

Poisson's Ratios of all materials were similar, and the NinjaFlex v (0.36) was slightly below the value of 0.45 measured previously (Shepherd et al., 2020). Directional sensitivity was observed for two (MD Flex and NinjaFlex) of the four TPUs. Care should be taken when calculating material parameters such as shear modulus from stress relaxation data for a hyperelastic model, as the equation for orthotropic properties differs from an isotropic calculation. Increasing stiffness with increasing strain and strain rate was expected and agrees with literature (Shepherd et al., 2020). Provided results (upon request to lead author or: https://drive.google.com/file/d/1VmJu61ExaTY0pAxJuJaa8PMsJzEKtgxJ/view?usp=sharing) are suitable to obtain coefficients for non-linear hyperelastic models. Similarly, the stress relaxation data can be used to obtain coefficients to model viscoelastic behaviour.

Conflict of interest. We declare no conflicts of interest.

References

International Organization for Standardization. (2017). BS ISO 37:2017 - Rubber, vulcanized or thermoplastic - Determination of tensile stress-strain properties.

Johnston, R., & Kazancı, Z. (2021). Analysis of additively manufactured (3D printed) dual-material auxetic structures under compression. *Additive Manufacturing*, *38*(September 2020), 101783. https://doi.org/10.1016/j.addma.2020.101783

Kajtaz, M., Subic, A., Brandt, M., & Leary, M. (2019). Three-dimensional printing of sports equipment. In *Materials in Sports Equipment*. Elsevier Ltd. https://doi.org/10.1016/B978-0-08-102582-6.00005-8

Shepherd, T., Winwood, K., Venkatraman, P., Alderson, A., & Allen, T. (2020). Validation of a Finite Element Modeling Process for Auxetic Structures under Impact. *Physica Status Solidi (B) Basic Research*, *257*(10), 1–14. https://doi.org/10.1002/pssb.201900197

Zadpoor, A. A. (2016). Mechanical meta-materials. *Materials Horizons*, *3*(5), 371–381. https://doi.org/10.1039/c6mh00065g

https://nbn-resolving.org/urn:nbn:de:bsz:ch1-qucosa2-806704

Entlastung auf dem Kreuzweg – Verbesserung des mechanischen Komforts von Trekkingrucksäcken

Lucas Höschler[1], Frank Ingo Michel[2] & Michael Frisch[3]

[1]Universität Salzburg, FB Sport- und Bewegungswissenschaft, Salzburg, Österreich

[2]VAUDE Sport GmbH & Co. KG, i-team, Tettnang, Deutschland

[3]Universität Bayreuth, Institut für Biomechanik, Bayreuth, Deutschland

Kurzfassung

Um den Diskomfort beim Rucksacktragen zu verringern, wurde ein Trekkingrucksack modifiziert und mithilfe der Druckverteilungsmessung untersucht. Es kam zu einer Reduzierung der Druckbelastungen im Bereich der Kreuzbeingelenke. Die Lastübertragung auf die Beckenflossen wurde verbessert. Der modifizierte Rucksack könnte langfristig der Entstehung von lumbo-sakralen Beschwerden auf Trekkingtouren vorbeugen.

Schlüsselwörter: Rucksack, Druckverteilung, Tragekomfort, Produktentwicklung

Einleitung

Der Tragekomfort ist das entscheidende Kriterium für die Beurteilung von Rucksäcken. Allgemein kann Komfort als Abwesenheit von Diskomfort definiert werden, welcher empirisch bestimmt werden kann (Hertzberg, 1958). Neben psychologischen Ursachen kann Diskomfort durch physikalische Einflüsse wie mechanischen Druck entstehen (Ashkenazy & DeKeyser Ganz, 2019). Zur Bestimmung des Tragekomforts von Rucksäcken wurden in der Vergangenheit standardisierte Befragungen in Verbindung mit Tragetests eingesetzt (Legg et al., 2003). Da die Komfortwahrnehmung individuell sehr unterschiedlich ist und von diversen psychologischen, physiologischen, demografischen und kulturellen Faktoren beeinflusst wird, werden weitere objektive Messmethoden benötigt. Die Messung des Kontaktdrucks zwischen Rucksack und Körper mithilfe mobiler Systeme ermöglicht es, den Tragekomfort von Rucksäcken objektiv zu bestimmen. In vorherigen Studien wurde ein Zusammenhang zwischen Druckparametern und dem subjektiv empfundenen Diskomfort im Schulter- und Beckenbereich nachgewiesen (Martin & Hooper, 2001; Wettenschwiler et al., 2015). Um Verletzungen und Diskomfort im Bereich der Schultern vorzubeugen, werden bei modernen Trekking-Rucksäcken Tragesysteme mit einem ausgeprägten Beckengurt verwendet, welche eine bessere Lastübertragung auf die unteren Extremitäten ermöglichen. Dadurch wird der Tragekomfort verbessert (Lenton et al., 2018) und der Energieverbrauch bei längerer Tragedauer verringert (Pigman et al., 2017). Eine schlechter Lasttransfer auf das Becken kann dagegen zu hohen Belastungen, Beschwerden und Diskomfort im Bereich der Kreuzbeingelenke führen (Bahr, 2019; Goh et al., 1998). Das Ziel dieser Studie war die Entwicklung eines Trekking-Rucksacks, der durch eine Aussparung den lumbo-sakralen Bereich entlastet sowie die Evaluierung des mechanischen Komforts mithilfe von Druckverteilungsmessungen.

Methode

Als Ausgangsmodell für die Entwicklung des Prototyps wurde ein mittelgroßer Trekking-Rucksack (*Asymmetric 42+8*, VAUDE Sport GmbH & Co. KG, Abb. 1a) verwendet. Um eine Entlastung des lumbo-sakralen Bereichs zu erreichen, wurde die Polsterkonfiguration im unteren Rucksackbereich durch eine zentrale, 8 cm breite Aussparung modifiziert. Durch einen größeren Anstellwinkel sollte zudem eine bessere Lastübertragung auf die Beckenflossen erreicht werden (Abb. 1b). Der mechanische Komfort der beiden Rucksäcke (Ausgangsmodell – REF, Prototyp – MOD) wurde in einer Studie mit 17 männlichen Probanden (Alter: 31,7 ± 9,8 Jahre, Größe: 1,80 ± 4,3 m, Gewicht: 74,1 ± 5,0 kg) mithilfe der Druckverteilungsmessung beim Gehen auf dem Laufband bei 4,5 km/h (*Callis ORTHO*, Sprintex Trainingsgeräte GmbH) untersucht. Die individuelle Anpassung der Rucksackeinstellung wurde entsprechend der Herstellerempfehlungen durchgeführt und war identisch zwischen den Rucksäcken. Die Zuladung betrug jeweils 10 kg. Die Probanden trugen einheitliche, enganliegende Kleidung, um Faltenbildungen zu vermeiden. Zur Messung des Kontaktdrucks zwischen Rucksack und Körper an Schulter und Becken wurden zwei flexible Sensormatten verwendet (*Tactilus*, Sensor Products Inc., Messgitter: 32 x 32 und 23 x 19 Sensoren, effektive Messfläche: 2162 und 886 cm²). Die kleinere Matte wurde mittig über dem rechten Schulterdach platziert. Die größere Matte wurde am Rücken unterhalb der Schulterblätter angebracht und deckte den gesamten unteren Rücken, sowie einen Teil der Beckenflossen ab. Die Fixierung der Sensoren erfolgte durch elastische Bänder und Tapestreifen, die außerhalb der Messfläche aufgebracht wurden. Um die Belastungen des Kreuzbeins und den Lasttransfer auf die Beckenflossen zu untersuchen, wurde die Beckenmatte in 3 Segmente unterteilt (Sakrum – orange, Lumbalpolster – rot, Beckenflossen, Abb. 1). In jedem Segment wurden der maximale und durchschnittliche Druck (p_{max}, p_{mean}), sowie die Kontaktfläche (A) gemittelt über 10 Schrittzyklen berechnet. Die Auswertung der Druckdaten wurde in Matlab (*R2020a*, TheMathWorks) durchgeführt.

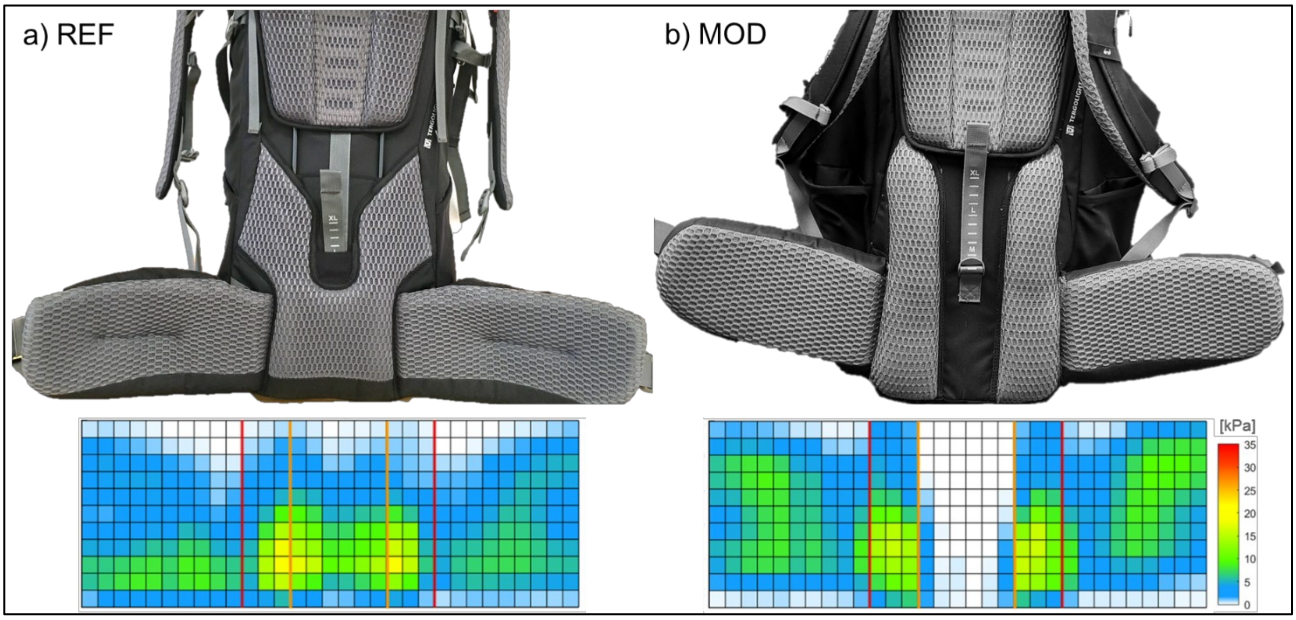

Abb. 1 a) Referenzmodell Asymmetric 42+8 (REF) mit gemittelten Druckbild (Segmente: Sakrum – orange, Lumbalpolster – rot, Beckenflossen); b) Modifizierter Rucksack (MOD) mit gemittelten Druckbild (Segmente: Sakrum – orange, Lumbalpolster – rot, Beckenflossen).

Zur statistischen Analyse von Unterschieden in den Druckparametern zwischen den Rucksackkonditionen wurde der unabhängige T-Test (α = 0,05) in SPSS (*Version 26*, IBM) verwendet.

Ergebnisse

Durch die Aussparung kam es zu einer signifikanten Reduzierung der Kontaktfläche im Sakrum- und Lumbalpolstersegment (Tab. 1). An den Beckenflossen wurde eine signifikante Vergrößerung der Kontaktfläche beim modifizierten Rucksack beobachtet. Die Druckbelastungen im Sakrumsegment (p_{max}, p_{mean}) waren beim MOD geringer, während in den anderen Segmenten kein signifikanter Unterschied gefunden wurde. In den an der Schulter gemessen Parametern bestand kein signifikanter Unterschied zwischen den Rucksäcken (p_{pmax} = 0,77; p_{pmean} = 0,19; p_A = 0,85).

Tab. 1 Druckparameter (maximaler Druck – p_{max}, durchschnittlicher Druck – p_{mean}, Kontaktfläche – A) des Referenzrucksacks (REF) und des modifizierten Modells (MOD) in den Segmenten Sarkum, Lumbalpolster und Beckenflossen. Mittelwerte und Signifikanzen (Sig.) des unabhängigen T-Tests.

	Sakrum			**Lumbalpolster**			**Beckenflossen**		
Parameter	**REF**	**MOD**	***Sig.***	**REF**	**MOD**	***Sig.***	**REF**	**MOD**	***Sig.***
p_{max} [kPa]	22,6	9,1	**< 0,001**	29,7	28,5	0,590	19,0	21,1	0,176
p_{mean} [kPa]	5,6	3,0	**0,017**	6,2	6,9	0,191	4,2	4,6	0,317
A [cm²]	117,4	30,9	**< 0,001**	241,6	169,6	**< 0,001**	421,8	472,3	**0,017**

Diskussion

In dieser Studie wurde ein Trekking-Rucksack entwickelt, der durch eine Aussparung die Belastungen auf das Kreuzbein und die angrenzenden Gelenke reduziert. Durch die Aussparung kam es zu einer nahezu vollständigen Druckentlastung im Sakrumsegment. Druck ist definiert als Kraft pro Fläche. Folglich wäre durch die Reduzierung der Kontaktfläche ein Druckanstieg in den anderen Segmenten zu erwarten gewesen. Trotz der kleineren zur Verfügung stehenden Auflagefläche fand jedoch kein signifikanter Druckanstieg in den anderen Segmenten im Vergleich zum REF Rucksack statt. Allerdings wird anhand der nichtsignifikanten Steigerung des p_{mean} und der vergrößerten Kontaktfläche eine zusätzliche Lastaufnahme an den Beckenflossen entsprechend den Empfehlungen für schwere Trekkingrucksäcke deutlich (Paldauf et al., 2018). Beim Rucksacktragen wird ein durchschnittlicher Druck oberhalb von 20 kPa mit Diskomfort assoziiert (Stevenson et al., 2004). Obwohl die Werte für beide Rucksäcke in allen Segmenten deutlich unterhalb dieser Schwelle lagen, kann durch die verstärkte Lastaufnahme über das unempfindlichere Becken beim MOD eine Reduzierung der Gelenkbelastungen im lumbo-sakralen Bereich (Bahr, 2019; Goh et al., 1998) und eine Steigerung des Tragekomforts (Lenton et al., 2018) vermutet werden.

Bei dem untersuchten Kollektiv handelte es sich um eine sehr homogene Gruppe mit geringer anthropometrischer Variabilität. Zukünftige Studien sollten gezielt den Einfluss anthropometrischer Merkmale auf den Tragekomfort untersuchen, um Rucksackherstellern eine gezieltere, individuellere Produktentwicklung zu ermöglichen. Aufgrund der kurzen Messdauer in dieser Studie können keine Aussagen über den langfristigen Tragekomfort getroffen werden. Die Ergebnisse sprechen jedoch dafür, dass die Modifikationen der Entstehung von belastungsinduzierten Beschwerden auch bei längerer Tragedauer vorbeugen könnten.

Interessenskonflikt Wir erklären keine Interessenskonflikte.

Finanzierung Diese Arbeit erhielt keine finanzielle Förderung.

Literatur

Ashkenazy, S., & DeKeyser Ganz, F. (2019). The Differentiation Between Pain and Discomfort: A Concept Analysis of Discomfort. *Pain management nursing*, *20*(6), 556–562. https://doi.org/10.1016/j.pmn.2019.05.003

Bahr, M. (2019). Das Kreuz mit der Last. *DAV Panorama,* 2019(5), S. 74-76.

Goh, J.-H., Thambyah, A., & Bose, K. (1998). Effects of varying backpack loads on peak forces in the lumbosacral spine during walking. *Clinical Biomechanics*, *13*(1), S26-S31. https://doi.org/10.1016/S0268-0033(97)00071-5

Hertzberg, H. T. E. (1958). Appendix I - Seat Comfort. In R. Hansen & D. Y. Cornog (Hrsg.), *Annotated Bibliography of Applied Physical Anthropology in Human Engineering* (S. 297-300). Defense Technical Information Center.

Legg, S. J., Barr A, A., & Hedderley, D. I. (2003). Subjective perceptual methods for comparing backpacks in the field. *Ergonomics*, *46*(9), 935–955. https://doi.org/10.1080/0014013031000107577

Lenton, G. K., Doyle, T. L. A., Saxby, D. J., Billing, D., Higgs, J., & Lloyd, D. G. (2018). Integrating a hip belt with body armour reduces the magnitude and changes the location of shoulder pressure and perceived discomfort in soldiers. *Ergonomics*, *61*(4), 566–575. https://doi.org/10.1080/00140139.2017.1381278

Martin, J., & Hooper, R. (2001). Military Load Carriage: A Novel Method of Interface Pressure Analysis. In NATO Research and Technology Organization (Vorsitz), *RTO Human Factors and Medicine Panel (HFM) Specialists' Meeting,* Kingston, Canada.

Paldauf, S., Stämpfli, R., Emrich, F., & Michel, F. I. (2018). Load distribution between upper body and pelvis in different load carriage systems. In D. Link, A. Hermann, M. Lames & V. Senner (Hrsg.), *Schriften der Deutschen Vereinigung für Sportwissenschaft: Band 274. Sportinformatik XII: 12. Symposium der dvs-Sektion „Sportinformatik und Sporttechnologie" vom 5.-7. September 2018 in Garching.* Feldhaus, Edition Czwalina.

Pigman, J., Sullivan, W., Leigh, S., & Hosick, P. A. (2017). The Effect of a Backpack Hip Strap on Energy Expenditure While Walking. *Human factors*, *59*(8), 1214–1221. https://doi.org/10.1177/0018720817730179

Stevenson, J. M., Bossi, L. L., Bryant, J. T., Reid, S. A., Pelot, R. P., & Morin, E. L. (2004). A suite of objective biomechanical measurement tools for personal load carriage system assessment. *Ergonomics*, *47*(11), 1160–1179. https://doi.org/10.1080/00140130410001699119

Wettenschwiler, P. D., Lorenzetti, S., Stämpfli, R., Rossi, R. M., Ferguson, S. J., & Annaheim, S. (2015). Mechanical Predictors of Discomfort during Load Carriage. *PloS one*, *10*(11), e0142004. https://doi.org/10.1371/journal.pone.0142004

Postersitzung

https://nbn-resolving.org/urn:nbn:de:bsz:ch1-qucosa2-806704

Evaluierung des mechanischen Komforts von Sitzpolstern in Radhosen – Eine initiale Datenanalyse

Frank I. Michel[1], Sophie Richter[1,2], Alisa Focke[1], Vanessa Crazzolara[1] & Stefan Schwanitz[2]

[1]VAUDE Sport GmbH & Co. KG, ***i***-lab, Obereisenbach, Deutschland

[2]Technische Universität Chemnitz, Professur Sportgerätetechnik, Chemnitz, Deutschland

Kurzfassung

Um den Einfluss des Sitzpolsters in Radhosen auf den mechanischen Komfort besser zu verstehen, wurden der Satteldruck und die Beckenbewegung in Abhängigkeit der Belastungsintensität sowie -dauer beim Radfahren analysiert. Die Ergebnisse der initialen Datenanalyse deuten darauf hin, dass weniger die Stabilitätsparameter, sondern eher die Druckwahrnehmung für die Beurteilung des mechanischen Komforts maßgeblich ist.

Schlüsselwörter: Radhosen, Sitzpolster, Stabilität, Druckverteilung, IMU

Einleitung

Der Radsport ist schon seit einigen Jahren die beliebteste Sportart in Deutschland. Laut Sportsatellitenkonto sind 41 % der deutschen Bevölkerung aktive Radfahrer*innen (BMWi, 2021). Verglichen zum Laufsport, der die zweitbeliebteste Sportart ausmacht, steht das Radfahren im Zusammenhang mit der dafür notwendigen Sportausrüstung bisher weniger im wissenschaftlichen Fokus. Neben dem Fahrrad und dem Sattel trägt die Radhose mit ihrem Sitzpolster maßgeblich zum Sitzkomfort bei. Jedoch lassen sich nur sieben wissenschaftliche Beiträge von lediglich vier Autorengruppen zu den Themengebieten „Sitzpolster“ und „Radhosen“ recherchieren. In den meisten dieser Studien wird versucht, mittels Druckverteilungsmessungen Rückschlüsse auf die Nachgiebigkeitseigenschaften verschieden konstruierter Sitzpolster zu ziehen und Zusammenhänge zur subjektiven Evaluierung des Komforts bzw. Diskomforts zu ermitteln. Obwohl quantitative Unterschiede zwischen Sitzpolstern ermittelt wurden, konnte bisher keine Korrelation im Sinne einer Vorhersage zwischen Druckverteilungsdaten und subjektiver Evaluierung nachgewiesen werden (Marcolin et al., 2015; Wilkinson et al., 2019). Daher ist der Parameter „Stabilität“ zur Interpretation des wahrgenommenen Diskomforts in den Fokus gerückt. Als Indikator für die Stabilität wird der Druckschwerpunkt (Center of Pressure, CoP) mittels Druckverteilung (Larsen et al., 2019) oder die Beckenbewegung mittels 3D-Kinematik quantitativ bestimmt (Marcolin et al., 2015). Innerhalb der subjektiven Evaluierung wird der Parameter Stabilität separat abgefragt. Allerdings konnte auch hier bisher noch kein signifikanter Zusammenhang nachgewiesen werden (Larsen et al., 2019; Marcolin et al., 2015). Das Ziel dieser initialen Datenanalyse, die zu einem größeren Projekt zur Optimierung von Sitz-polstern gehört, besteht in der objektiven und subjektiven Analyse des Parameters Stabilität. Dies erfolgt in Abhängigkeit von der Tretleistung (Belastungsintensität) sowie der Sattelzeit (Belastungsumfang).

Methode

Die initiale Datenanalyse basiert auf sieben Datensätzen. Alle Proband*innen (Geschlecht: 4 ♀, 3 ♂, Alter: ∅ 34,6 ± 9,3 Jahre, Größe: ∅ 173 ± 9,3 cm, Gewicht: ∅ 68,6 ± 10,5 kg), die sich selbst als aktive Radsportler*innen einschätzten, absolvierten zwei Sitzungen. In der ersten Sitzung wurde ein Ausbelastungstest (Rampentest) zur Ermittlung der funktionellen Schwellenleistung (Functional Threshold Power, FTP) durchgeführt, um die Belastungs-intensität (70 % des FTP-Wertes; Trittfrequenz: 80 min^{-1}) für den „Stundentest" zu bestimmen, der in der zweiten Sitzung stattfand (Zwift, 2019). In beiden Sitzungen trugen die Proband*innen ihre eigene Lieblingsradhose. Die Sitzhöhe wurde, analog den Angaben von Holliday (2019), für jede Person ermittelt und am Radergometer eingestellt (Abb. 1a). Als Indikator für die Beckenbewegung wurde in beiden Tests am Sakrum der Person eine Inertialmesseinheit (IMU) (myon aktos mini, menios; Aufnahmefrequenz: 2.000 Hz) befestigt, die die Sakrumwinkel im Raum sowie die Geschwindigkeit (Integral der Beschleunigung) zu definierten Zeitpunkten über 10 s aufzeichnete. Im Stundentest wurde zudem eine Satteldruckmessung (gebioMized®; Aufnahmefrequenz: 200 Hz; 64 resistive Sensoren) durchgeführt. Daraus konnte die Bewegung bzw. Ausdehnung des CoP in anterior-posteriorer (y) sowie in medio-lateraler (x) Richtung, einschließlich des sich daraus ergebenen Flächeninhalts (A=x*y) berechnet werden. Auch im Stundentest wurden zu definierten Zeitpunkten die IMU- sowie die Druckverteilungsdaten über 10 s aufgezeichnet. Zudem beantwortete das Probandenkollektiv zu diesen Zeitpunkten (Tab. 1) standardisierte Fragen zur Stabilität (Gefühl des Rutschens/Wackelns auf dem Sattel) und zur Druckwahrnehmung.

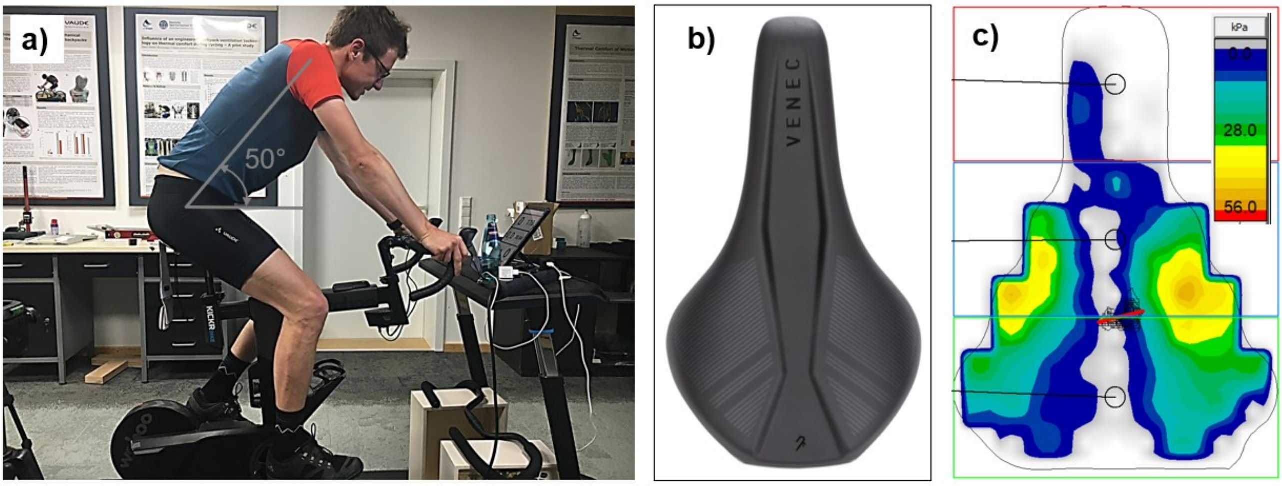

Abb. 1 a) Testsetup: Proband auf wahoo KICKR BIKE mit 50° standardisierter Rumpfneigung in Brakehood-Position; b) Sattel: Cube Natural Fit Venec; c) Exemplarisches Druckverteilungsbild mit Darstellung des Center of Pressure (CoP)

Die Aufbereitung und Auswertung der IMU- und Druckdaten erfolgte in MATLAB® (*R2022a*, MathWorks®). Zur Überprüfung von statistischen Zusammenhängen der ermittelten Parameter im Zeitverlauf wurden in RStudio (Version 1.3.1093) Rangkorrelationskoeffizienten nach Spearman berechnet ($p \leq 0{,}05$).

Ergebnisse

Innerhalb des Rampentests ist eine sehr hohe Korrelation zwischen der seitlichen Kippbewegung des Beckens (Frontalebene) und der Intensität [Watt] zu verzeichnen (Tab. 1). Mit zunehmender Intensität steigt die seitliche Kippbewegung des Beckens. Tendenziell nimmt mit zunehmender Intensität auch die Beckenrotation (Transversalebene) sowie die Sakrum-Geschwindigkeit (Integral der Beschleunigung) zu. Diesbezüglich kann für den Stundentest eine sehr hohe Korrelation zwischen der Sakrum-Geschwindigkeit und der Belastungsdauer analysiert werden. Für die drei Beckenwinkel konnten innerhalb des Stundentests keine signifikanten Korrelationen nachgewiesen werden.

Tab. 1 Mittelwerte (n = 7) der Sakrum-Geschwindigkeit (Integral der Beschleunigung) sowie Sakrum-Winkel als Indikator für die Beckenbewegung in drei Ebenen für den Rampentest und Stundentest (sig. Korrelationen jeweils in *fett* über den entsprechenden Datensatz angegeben: p* ≤ 0,050; p** ≤ 0,010).

	Geschwindigkeit [m/s]	**Frontalebene** [°]	**Transversalebene** [°]	**Sagittalebene** [°]
Rampentest	ρ = 0,9 (p = 0,0833)	**ρ = 1****	ρ = 0,77 (p = 0,103)	ρ = -0,0286 (p = 1)
100 W (n=7)	8,5 ± 2,4	**5,3** ± 2,5	2,8 ± 2,3	2,7 ± 2,4
160 W (n=7)	8,0 ± 2,5	**5,9** ± 2,9	2,5 ± 1,7	2,7 ± 2,8
220 W (n=7)	9,0 ± 2,5	**6,1** ± 2,9	3,4 ± 2,3	2,5 ± 2,8
280 W (n=4)	10,3 ± 2,3	**7,2** ± 3,0	5,6 ± 3,5	2,8 ± 3,2
340 W (n=3)	12,6 ± 4,6	**9,4** ± 6,1	4,3 ± 1,8	3,8 ± 4,2
Stundentest	**ρ = 1***	ρ = 0,1 (p = 0,95)	ρ = 0,7 (p = 0,233)	ρ = -0,1 (p = 0,95)
3 min (n=7)	**7,1** ± 1,3	4,1 ± 2,4	2,8 ± 1,4	1,1 ± 0,5
15 min (n=7)	**7,3** ± 1,2	4,5 ± 2,5	2,9 ± 1,5	1,2 ± 0,6
30 min (n=7)	**7,3** ± 0,7	4,8 ± 2,9	3,2 ± 2,1	1,1 ± 0,7
45 min (n=7)	**7,8** ± 1,2	4,4 ± 2,3	3,5 ± 2,3	1,3 ± 0,6
60 min (n=7)	**7,8** ± 2,2	4,2 ± 2,4	3,1 ± 2,2	0,9 ± 0,2

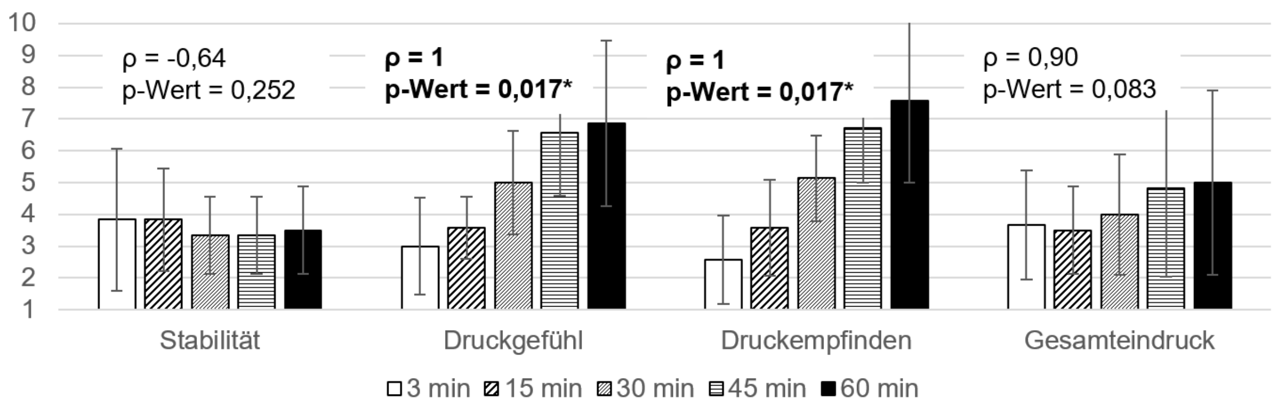

Abb. 2 Mittelwerte (n = 7) zur subjektiven Wahrnehmung (sig. Korrelationen jeweils in *fett* über dem entsprechenden Datensatz angegeben); Stabilität: 1=stabil … 10=wacklig; Druckgefühl: 1=kaum spürbar … 10=stark spürbar; Druckempfinden: 1=kaum unangenehm … 10=sehr unangenehm; Gesamteindruck: 1=sehr gut … 10=sehr schlecht (p* ≤ 0,050; p** ≤ 0,010).

Auch für die drei analysierten CoP-Parameter konnten keine signifikanten Korrelationen in Abhängigkeit von der Belastungsdauer detektiert werden. Dies betrifft ebenso die subjektive Beurteilung der Stabilität (Abb. 2). Die Stabilität wird über die gesamte Belastungsdauer ähnlich wahrgenommen. Demgegenüber wird sowohl das Druckgefühl als auch das Druckempfinden mit zunehmender Belastungsdauer als signifikant spürbarer bzw. unangenehmer eingeschätzt.

Diskussion

Die Ergebnisse der initialen Datenanalyse deuten darauf hin, dass mit zunehmender Belastungsintensität die Beckenbewegung in der Frontalebene zunimmt. Tendenziell ist dies auch für die Beckenrotation sowie für die Sakrum-Geschwindigkeit (Integral der Beschleunigung) zu beobachten. Leider liegen hierzu keine Vergleichsdaten vor. Allerdings wird berichtet, dass sich mit zunehmender Belastungsintensität die CoP-Bewegung vergrößert (Holliday, 2019). In Bezug auf die Belastungsdauer konnte Marcolin et al. (Marcolin et al., 2015) in einem 20-Minuten-Test für eine von drei Sitzpolsterkonditionen eine signifikante Zunahme (∅ 0,7°) der Beckenrotation analysieren. Dieser „Trend" ist bis zu Minute 45 auch im vorliegendem Datensatz zu erkennen. Auch für einen möglichen Zusammenhang zwischen den erhobenen CoP-Parametern und der Belastungsdauer sind keine Vergleichsdaten in der Literatur zu sichten. Jedoch konnten Larsen et al. (Larsen et al., 2019) feststellen, dass mit zunehmender Belastungsdauer der wahrgenommene Diskomfort (Rate of Perceived Discomfort) zugenommen hat. In der vorliegenden Studie nahmen die Proband*innen mit zunehmender Belastungsdauer das Druckempfinden als unangenehmer wahr. Zusammenfassend kann festgestellt werden, dass - basierend auf den vorliegenden Daten – bei einer Belastungsdauer von 60 min in einer moderaten Belastungsintensität (∅ 163 W) und Herzfrequenz (∅ 146 bpm) keine signifikanten Änderungen der Beckenbewegung auftreten und diese auch nicht durch die Personengruppe als solche wahrgenommen werden. Vielmehr deuten die Daten zur subjektiven Evaluierung darauf hin, dass das Druckgefühl auf die Beurteilung des Gesamteindrucks und somit der Wahrnehmung des Diskomforts eine dominantere Rolle spielen könnte. Zukünftig sollte für die Evaluierung von Sitzpolstern sowohl eine variierende Belastungsintensität als auch eine längere Belastungsdauer berücksichtig werden.

Interessenskonflikt Wir erklären keine Interessenskonflikte.

Finanzierung Im Rahmen des A4SEE Fellowship-Programms erhielt Sophie Richter zur Durchführung der Studie finanzielle Unterstützung.

Literatur

BMWi. (2021). *Sportwirtschaft: Fakten & Zahlen - Ausgabe 2021*. Zugriff unter www.bisp.de/SharedDocs/Kurzmeldungen/DE/Nachrichten/2021/SSKSportwirtschaft2021.html

Holliday, W. (2019). Intrinsic factors, performance and dynamic kinematics in optimisation of cycling biomechanics, Dissertation University of Cape town.

Larsen, A., Hansen, E. A., & Madeleine, P. M. (2019). Effects of cycling shorts padding on perceived discomfort and saddle pressure distribution among female cyclists in laboratory conditions. *24th Annual Congress of the European College of Sport Science, ECSS, Prague, 3-6 July 2019*, 66-67.

Marcolin, G., Petrone, N., Reggiani, C., Panizzolo, F. A., & Paoli, A. (2015). Biomechanical comparison of shorts with different pads: An insight into the Perineum Protection Issue. *Medicine, 94*(29), 1-8.

Wilkinson, R. D., Marcus, M., Williams, J., & Carver, T. (2019). Effect of chamois design on rider comfort and saddle pressure during sub-maximal cycling. *Med Sci Sports Exerc*, *51*(6), 52-52.

Zwift. (2019). *Zwift How-To: Using a Ramp Test to Find Your FTP*. Zugriff unter www.zwift.com/news/14263-zwift-how-to-using-a-ramp-test-to-find-your-ftp?__znl=de-de

https://nbn-resolving.org/urn:nbn:de:bsz:ch1-qucosa2-806704

Non-invasive technologies for detecting asymmetric muscle fatigue

Elena Janowicz[1], Carlo Dindorf[1], Eva Bartaguiz[1], Michael Fröhlich[1] and Oliver Ludwig[1]

[1]Technische Universität Kaiserslautern, Department of Sports Science, Kaiserslautern, Germany

Abstract

Early detection of unilateral muscle fatigue and muscular imbalances is important to prevent injury. This study aimed to evaluate the potential of near-infrared thermography (IRT) and raster-stereography (RS) in detecting asymmetries. After unilateral trunk muscle fatigue, IRT detected changes in the skin surface temperature only immediately after exercise, while RS data showed no statistically significant changes.

Keywords: infrared thermography, raster-stereography, muscle asymmetry, muscle fatigue

Introduction

An asymmetrically performed movement can lead to a muscle overload and therefore to injuries. In the long term, this can lead to an imbalance between the muscles and thus to an asymmetrical posture (Bernetti et al., 2020). To prevent this, early detection of asymmetries is important. A common non-invasive method for posture analysis is raster-stereography (RS). This technology detects asymmetries based on the position of anatomical landmarks (Drerup & Hierholzer, 1987). Muscle fatigue may lead to changes in skin surface temperature. Near infrared thermography (IRT) can be used to detect these changes. IRT, along with a scan of anatomic landmarks, might be a promising non-invasive diagnostic tool. Due to the mobility of IRT and the influence of muscle fatigue on the skin surface temperature, it may be possible to develop a feedback system for unilateral fatigue during an activity. Research on the use of IRT in the context of muscle fatigue is so far inconsistent (Al-Mulla et al., 2011). This study was conducted as part of an investigation by Dindorf et al. (2022) and is to the best of our knowledge the only study investigating the thermographic effects of unilateral fatigue in relation to trunk muscles. The aim of this study was to evaluate the potential of IRT and RS in detecting asymmetric muscle fatigue.

Methods

Data were collected from 41 subjects (22 men and 19 women; age: 22.63 ± 3.91 years; height: 173.36 ± 9.95 cm; body-mass-index (BMI): 24.09 ± 2.71 kg*m^{-2}; body fat: 20.92 ± 9.58 %). The study adhered to the criteria of the Declaration of Helsinki and was accepted by the ethics committee of Technische Universität Kaiserslautern (ethics protocol number: 43). The subjects were requested to arrive in a rested state and not to perform any intense activities or take any drugs for 48 h prior to the study. Furthermore, the subjects were asked not to consume large amounts of liquids or food for 2 h prior to the measurement. The intervention took place under controlled environment factors and a controlled room temperature of 20 °C. Fig. 1 depicts the experimental design.

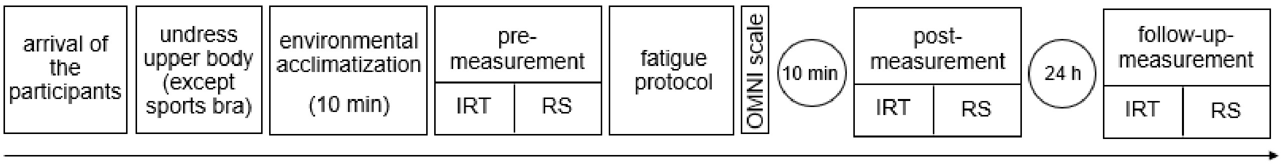

Fig. 1 Experimental design of the present study (IRT = near infrared thermography; RS = raster-stereography)

The fatigue protocol consisted of side bends on a Roman chair on the non-handedness side. The exercise was performed in sets of 20 repetitions to fatigue the lateral trunk flexors unilaterally. Tactile feedback (point of contact with a bar at the endpoint of maximal lateral trunk flexion) was provided to standardise the range of motion. A metronome indicated the movement speed. Sweat was dabbed immediately after it appeared. Termination criteria were defined as (a) inaccurate execution of a movement for more than 4 repetitions of a set, (b) a rated fatigue of more than 7 on the OMNI scale (Robertson, 2004), (c) the inability to perform the full 20 repetitions over 3 sets.

IRT data were determined with the NEC TVS-200 ISS camera (NEC Avionics Infrared Technologies Co., Ltd., Yokohama, Japan) and analysed via the software InfReC Analyzer NS9500 Lite (Nippon Avionics Co., LTD, Yokohama, Japan). To define areas and identify anatomic landmarks for each subject, cork markers were placed on the 12th thoracic vertebra and both posterior superior iliac spines (SIPS). In addition to IRT, RS with a photogrammetric noncontact 3D scanner (Paromed 4D, Neubeuern, Germany) was used. Bony landmarks were marked for measurement using this technique. Only the two posterior upper iliac spines were marked for observing the pelvic position. During the measurement, the subjects stood barefoot at a distance of 2.5 m in front of the scanner in their habitual posture. The locations of all markers were marked on the skin with a waterproof pen to ensure the same position for each measurement.

To analyse the changes in the skin surface temperature and pelvic position for the measurement time points, a repeated-measurement ANOVA was performed. To correct for sphericity violations, Greenhouse-Geisser adjustments were made. Bonferroni correction was performed for post hoc tests. Adjusted p-values were reported and computed with an alpha level of 0.05. For comparison of possible asymmetric differences between the treated side and the contralateral side for the three measurement time points, a dependent t-test for paired samples was calculated. The correlation between skin surface temperature and pelvic position was calculated using the Pearson correlation coefficient. Calculations were performed using SPSS Statistics (version 16, SPSS Inc, Chicago, USA).

Results

After the treatment, the subjects reported a mean score of 8.88 ± 1.01 on the OMNI scale. Fig. 2 shows the exemplary thermographic data of a participant. A comparison of the measurement areas for the measurement times showed the same characteristics for all areas. A statistically significant difference could be found between the three conditions (area a: $F(1.71,54.59) = 25.36$, $p < 0.001$, $n = 33$, $\eta_p^2 = 0.44$; area b: $F(2,64) = 65.10$, $p < 0.001$, $n = 33$, $\eta_p^2 = 0.67$; area c: $F(2,64) = 39.76$, $p < 0.001$, $n = 33$, $\eta_p^2 = 0.55$; area d: $F(2, 64) = 69.49$, $p < 0.001$, $n = 33$, $\eta_p^2 = 0.69$). The skin surface temperature was statistically significantly lower in the post-tests than in the pre- and follow-up tests.

The temperature in the pre- and follow-up tests was not different. The post measurement between the upper areas (*t(34)* = 5.34, $p < 0.001$, $r = 0.68$) and between the lower areas (*t(34)* = 2.92, $p = 0.006$, $r = 0.45$) showed asymmetric side differences. No side asymmetries existed for the pre-test and the follow-up test ($p > 0.05$). A comparison of the upper and lower areas showed no difference ($p > 0.05$). An analysis of the anatomic landmarks via RS showed no statistically significant difference for pelvic inclination in the different measurement times, $F(1.49,55.22) = 0.307$, $p = 0.672$, $n = 38$ (pre: -0.21 ± 2,17°; post: -0.07 ± 2.04°; follow-up: -0.33 ± 2.63°). In addition, the pelvic rotation showed no statistical significance in the different measurement times, $F(2,74) = 0.411$, $p = 0.664$, $n = 38$ (pre: -1.67 ± 2.53°; post: -1.85 ± 2.48°; follow-up: -1.99 ± 2.67°). There was no correlation between the changes in the skin surface temperature and the pelvic position ($p > 0.05$).

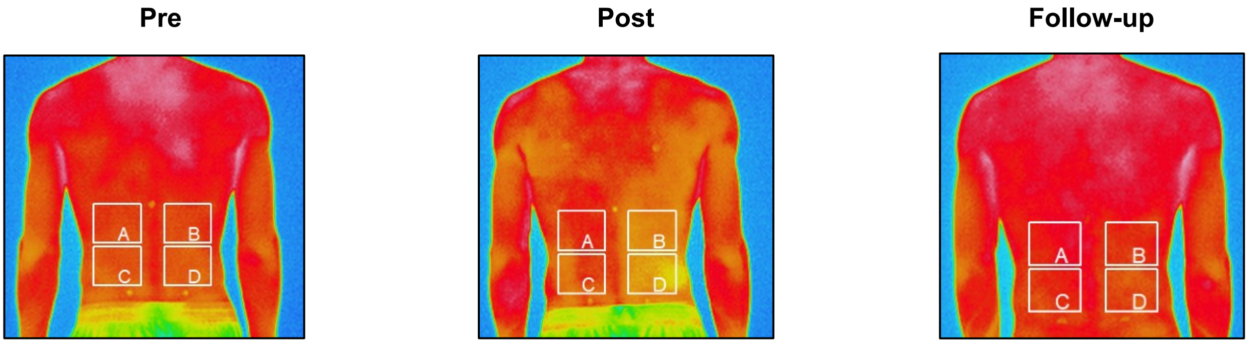

Fig. 2 Exemplary thermographic images of a test person for all three measurement times and visualisation of the measurement areas.

Discussion

The results of the present study show that after unilateral muscle loading, there are thermographic asymmetric changes in skin surface temperature on the treatment side. This is consistent with the muscle fatigue reported by the subjects. The fatigue protocol resulted in a temperature decrease in the skin blood flow of the loaded area immediately after the load (post-test). In the follow-up test (24 h), the temperature increased again and reached a similar level as in the pre-test. This development is consistent with the literature (Fernandes et al., 2016). Compared with the pre-test and the follow-up-test, the post-test showed statistically significant temperature differences from the non-treatment side. The subjects in the study by Stewart et al. (2020) showed a similar effect after fatigue of the knee flexors and extensors. Thus, IRT appears to be a useful technology for detecting asymmetric acute fatigue, since no changes were visible 24 h afterward compared to the pre-test. The RS results showed no systematic effect of unilateral fatigue on pelvic inclination or pelvic rotation. The observed individual differences could be due to different initial muscular states and motor control strategies. In addition, postural stabilisation is achieved through individual activation patterns (Betsch et al., 2011). To the best of our knowledge, there are no studies on RS related to acute unilateral trunk muscle fatigue. RS is not a useful technology to detect acute asymmetric muscle fatigue. Since changes were visible when a single case was observed at a time, RS at the level of individual observation could be a useful tool for detecting postural asymmetries due to the position of bony structures (Drerup & Hierholzer, 1987).

The present study has shown that IRT is suitable for detecting muscular fatigue of trunk muscles after exercise but cannot show the long-term effect. In contrast, acute fatigue does not seem to be visible in the pelvic position considered with RS. However, studies show that continuous unilateral fatigue leads to asymmetries in posture (Bernetti et al., 2020). Therefore, RS seems to provide some necessary information about the long-term effects of asymmetries on posture. For these reasons, IRT should be used in conjunction with RS to detect asymmetries. To apply IRT in wearables, there is a need to further explore the relationship between the progress in changes in the skin surface temperature and muscle fatigue during exercise.

Conflict of interest: The authors declare no conflict of interest.

Funding: This research was funded by Offene Digitalisierungsallianz Pfalz, BMBF [03IHS075B] and Ministerium für Wissenschaft und Gesundheit Rheinland-Pfalz (project: LLL@U.EDU).

References

Al-Mulla, M. R., Sepulveda, F., & Colley, M. (2011). A review of non-invasive techniques to detect and predict localised muscle fatigue. *Sensors (Basel, Switzerland)*, *11*(4), 3545–3594. https://doi.org/10.3390/s110403545

Bernetti, A., Agostini, F., Cacchio, A., Santilli, V., Ruiu, P., Paolucci, T., Paoloni, M., & Mangone, M. (2020). Postural Evaluation in Sports and Sedentary Subjects by Rasterstereographic Back Shape Analysis. *Applied Sciences*, *10*(24), 8838. https://doi.org/10.3390/app10248838

Betsch, M., Schneppendahl, J., Dor, L., Jungbluth, P., Grassmann, J. P., Windolf, J., Thelen, S., Hakimi, M., Rapp, W., & Wild, M. (2011). Influence of foot positions on the spine and pelvis. *Arthritis care & research*, *63*(12), 1758–1765. https://doi.org/10.1002/acr.20601

Dindorf, C., Bartaguiz, E., Janowicz, E., Fröhlich, M., & Ludwig, O. (2022). Effects of Unilateral Muscle Fatigue on Thermographic Skin Surface Temperature of Back and Abdominal Muscles-A Pilot Study. *Sports (Basel, Switzerland)*, *10*(3). https://doi.org/10.3390/sports10030041

Drerup, B., & Hierholzer, E. (1987). Movement of the human pelvis and displacement of related anatomical landmarks on the body surface. *Journal of biomechanics*, *20*(10), 971–977. https://doi.org/10.1016/0021-9290(87)90326-5

Fernandes, A. d. A., Amorim, P. R. D. S., Brito, C. J., Sillero-Quintana, M., & Bouzas Marins, J. C. (2016). Regional Skin Temperature Response to Moderate Aerobic Exercise Measured by Infrared Thermography. *Asian journal of sports medicine*, *7*(1), e29243. https://doi.org/10.5812/asjsm.29243.

Robertson, R. J. (2004). Perceived exertion for practitioners: Rating effort with the OMNI picture system. Human Kinetics.

Stewart, I. B., Moghadam, P., Borg, D. N., Kung, T., Sikka, P., & Minett, G. M. (2020). Thermal Infrared Imaging Can Differentiate Skin Temperature Changes Associated With Intense Single Leg Exercise, But Not With Delayed Onset of Muscle Soreness. *Journal of sports science & medicine*, *19*(3), 469–477.

https://nbn-resolving.org/urn:nbn:de:bsz:ch1-qucosa2-806704

Bestimmung der Skigeschwindigkeit mittels IMU-Daten und maschinellen Lernens

Patrick Carqueville[1], Aljoscha Hermann[1] & Veit Senner[1]

[1]Technische Universität München, Professur für Sportgeräte und -materialien, München, Deutschland

Kurzfassung

Diese Arbeit zeigt den explorativen Ansatz ein künstliches neuronales Netz (kNN) und Daten einer auf dem Ski befindlichen inertialen Messeinheit (IMU) zu verwenden, um auf die Fahrgeschwindigkeit zu schließen. Für das Training des kNN wird dabei die 3D-Geschwindigkeit einer auf dem Ski befindlichen GNSS-Antenne als Zielwert verwendet.

Schlüsselwörter: Skifahren, Geschwindigkeit, Maschinelles Lernen, LSTM, IMU

Abb. 1 Messung im Feld – Systemdarstellung am Beispiel des rechten Skis

Einleitung

Die Geschwindigkeit beim Skifahren ist als Stellgröße für mechatronische Skibindungen ein wichtiger zu ermittelnder Parameter (Hermann & Senner, 2021). Aufgrund möglicher Satellitenabschirmungen sollte die Geschwindigkeitserfassung dabei unabhängig vom Signal des globalen Navigationssatellitensystems (GNSS) erfolgen. Inertiale Messeinheiten (IMUs) sind hierfür geeignete Messsysteme. Jedoch sind diese mit zahlreichen Nachteilen, wie Temperaturabhängigkeit und Signaldrift behaftet. Eine gängige Handhabungsstrategie besteht darin die Sensorwerte basierend auf statischen oder dynamischen Bedingungen oder periodischen Ereignissen zu korrigieren, wie von Fasel (2017) beschrieben. Im Gegensatz zu diesen Strategien soll diese explorative Studie zeigen, inwieweit sich maschinelles Lernen (ML) eignet, um Geschwindigkeiten beim Skifahren anhand von IMU-Daten zu bestimmen. Untergliederte Fragestellungen sind dabei: (i) Inwieweit lässt sich ein trainiertes Model auf neues Terrain übertragen? und (ii) Inwieweit lässt sich ein Model auf ein neues baugleiches System übertragen?

Methode

Feldversuche wurden mit einem paar Ski mit jeweils einer GNSS-Antenne sowie einer IMU durchgeführt. Die IMUs sind mit einem Gyroskop, einem Beschleunigungssensor und einem Temperatursensor bestückt. Die GNSS-Antenne (Typ Series 8 von u-blox Holding AG, Thalwil, Schweiz) nutzt die Daten von GPS- und GLONASS-Satelliten. Die Position der GNSS-Antennen sowie der IMUs sind der Abbildung 1 zu entnehmen. Die Messrate der IMUs beträgt 1000 Hz, die der GNSS-Antennen 25 Hz. IMU-, GNSS- und Datenlogger-Hardware wurden von *2D Meßsysteme GmbH* konfektioniert. An vier Tagen wurden mit vier Probanden mehrere Abfahrten und Liftpassagen (Sessellift und Schlepplift) aufgezeichnet. Drei Tage wurde am Hausberg (Garmisch, Deutschland) gemessen und ein Tag wurde am Ruhestein (Baiersbronn, Deutschland) gemessen. In Summe wurden 5 Stunden 4 Minuten, mit mehr als 2 Stunden reiner Abfahrtszeit, aufgenommen. Die Daten wurden vorverarbeitet, transformiert und in 60 % Trainingsdaten, 16 % Validierungsdaten und 24 % Testdaten aufgeteilt. Die Aufnahmen vom Ruhestein wurden vollständig dem Testdatensatz zugeordnet, um Testdaten eines neuen Skigebiets mit anderen Schneebedingungen zu erhalten. Das verwendete kNN besteht aus zwei *long short-term memory* (LSTM)-Schichten und zwei *Dense*-Schichten mit insgesamt 14.529 trainierbaren Parametern. Abbildung 2 stellt die Netzwerkarchitektur schematisch dar. Das neuronale Netz wurde ausschließlich anhand der Daten des rechten Skis trainiert. Die Beschleunigungsdaten, Gyroskopdaten und Temperaturdaten der IMU des rechten Skis wurden als Modelleingabe und die 3d-GNSS-Geschwindigkeit als Zielgröße verwendet. Das für das rechte Skisystem trainierte neuronale Netz wurde auf die Messdaten des linken Skisystems angewandt.

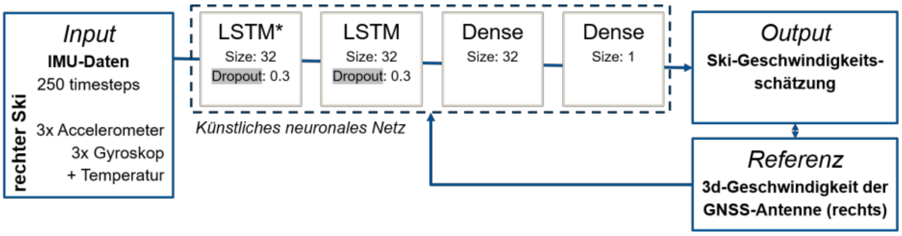

Abb. 2 Netzwerkarchitektur des künstlichen neuronalen Netzes

Ergebnisse

Das GNSS-Referenzsystem empfängt während der Testfahrten Daten von durchschnittlich 15 Satelliten (min. 8 und max. 16). Die 3d-Geschwindigkeitsgenauigkeit, die vom GNSS-System ausgegeben wird, ist minimal 0,14 km/h und im Durchschnitt 0,41 km/h. Abbildung 3 zeigt den Vergleich zwischen der Ausgabegeschwindigkeit *v_kNN* des künstlichen neuronalen Netzes und der 3d-Referenzgeschwindigkeit des GNSS *v_GNSS* für einen Testdatensatz vom Ruhestein des linken Skis. Für diese Testdaten wird ein Pearson-Korrelationskoeffizient von 0,971 und ein mittlerer quadratischer Fehler (MSE) von 3,18 km/h erzielt. Im Mittel sind die ausgegebenen Daten des kNN, bezogen auf die GNSS-Referenzgeschwindigkeit, um +2.52 km/h versetzt. Abbildung 3 (a) zeigt die GNSS-Fahrgeschwindigkeit in Blau sowie die kNN-Vorhersage in Rot. Es ist eine Schleppliftfahrt mit anschließender Abfahrt zu sehen. In Phasen des Stillstands ist ein Versatz zwischen *v_kNN* zu *v_GNSS* ersichtlich. Während der Liftfahrt liegt *v_kNN* ebenfalls zum Großteil über *v_GNSS.* Während der Abfahrt weicht *v_kNN* gleichermaßen in positive und negative Richtung von *v_GNSS* ab. Lediglich gegen Ende der Abfahrt (330-340 s) kommt es zu erhöhten Abweichungen und zu einem deutlichen Unterschätzen der Geschwindigkeit durch das kNN (vgl. umrandete Bereiche in Abb. 3). Abbildung 4 zeigt diesen Ausschnitt weiß umrandet in der Auswertungssoftware mit synchronisiertem Kamerabild. Es ist ersichtlich, dass sich der Proband in diesem Zeitbereich in deutlicher Rücklage befindet. Das Kamerabild aus Abb. 4 ist der Cursorposition aus Abb. 4-links zuzuordnen.

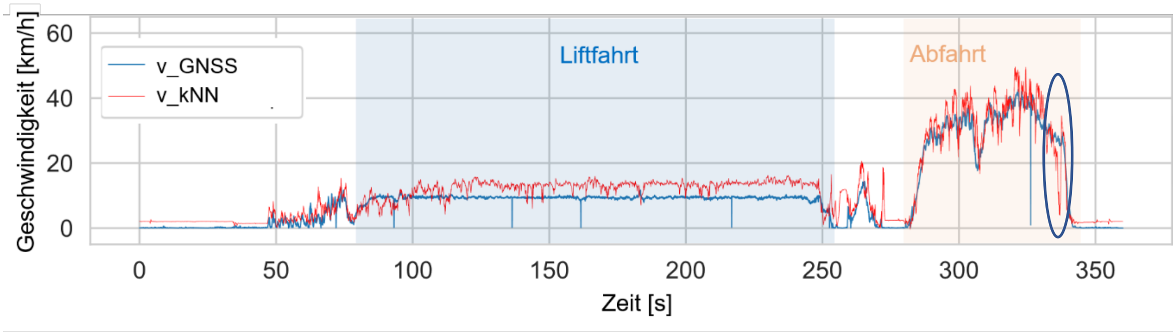

(a)

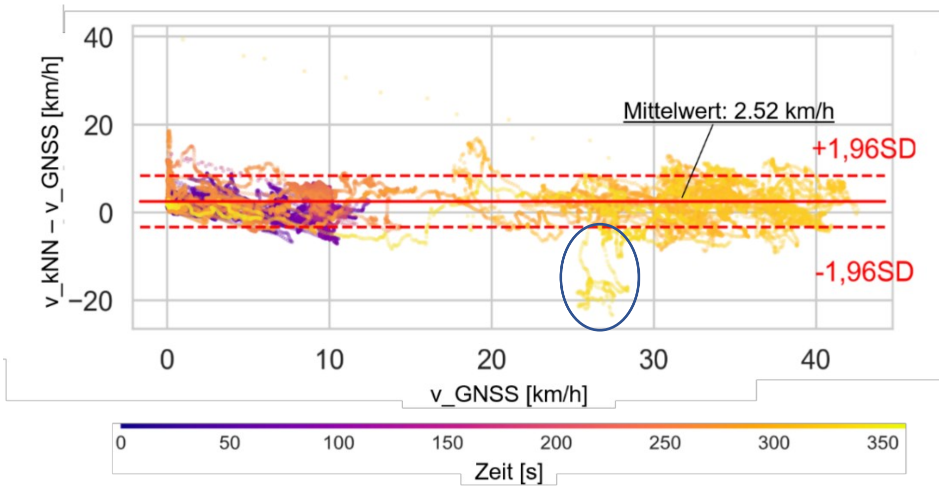

(b)

Abb. 3 Vergleich zwischen der vom künstlichen neuronalen Netz ausgegebenen Geschwindigkeit *v_kNN* und der Referenzgeschwindigkeit des globalen Navigationssattelitensystems *v_GNSS* für einen Testdatensatz für Ruhestein des linken Skisystems (a) Zeitverlauf (b) Bland-Altman-Plot.

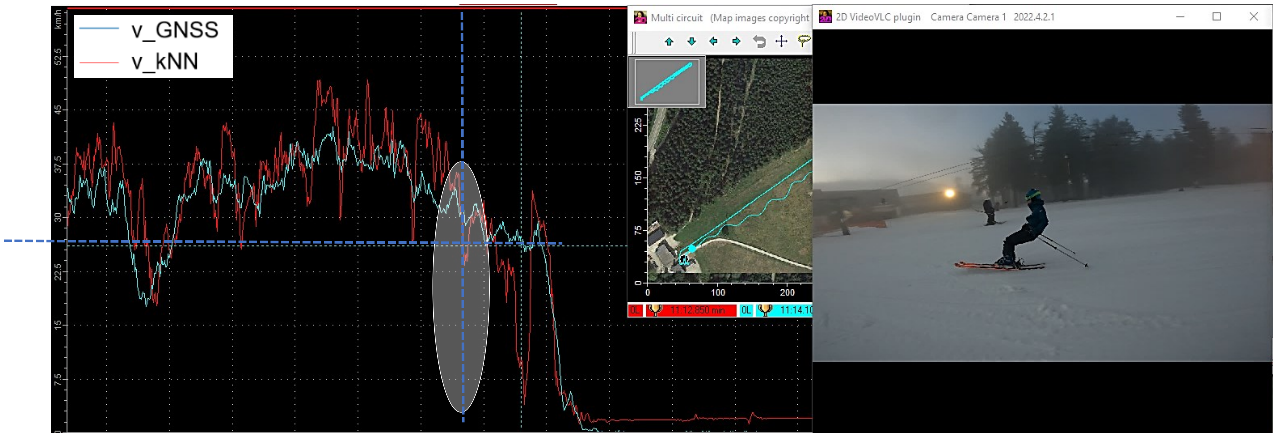

Abb. 4 Darstellung des Testdatenbereichs mit den größten Abweichungen zwischen kNN-Ausgabe und Zielgröße in der Analysesoftware – Fenster von links nach rechts: Zeitverlauf *v_kNN* (rot) und *v_GNSS* (blau); Satellitenbild mit Track und Position, Kamerabild.

Diskussion

Die driftfreie GNSS-unabhängige Geschwindigkeitsbestimmung mittels LSTM-Netzwerks und Dateninput einer auf dem Ski befindlichen IMU, scheint beim Pistenskifahren prinzipiell möglich zu sein. Die Übertragbarkeit des für den rechten Ski trainierten kNNs auf den linken Messski, bei gleichzeitiger Veränderung der Pistenverhältnisse, erzielte gute Ergebnisse. Für eine abschließende Bewertung der Übertragbarkeit auf ein anderes System zu anderen Pistenbedingungen, ist die Anzahl der untersuchten Testfahrten zu gering. Zudem fehlt hierzu die quantifizierte Betrachtung der Pistenverhältnisse. Tendenziell war der Schnee am Ruhestein aufgehäufter und weicher als die Schneebedingungen aus den Trainingsdaten. Trotz Systemwechsel auf den linken Ski besteht ein hoher Pearson-Korrelationskoeffizient von 0,971 und ein geringer MSE von 3,18 km/h zwischen der Ausgabe des ML-Modells *v_kNN* und der GNSS-Referenzgeschwindigkeit *v_GNSS* für die Testdaten des linken Skisystems. Folgende Störeinflüsse könnten hierbei die Übertragbarkeit einschränken: Abweichungen bei der IMU-Montage und herstellungsbedingte Abweichungen von Temperaturabhängigkeit und Sensitivität der IMUs. Diese könnten den durchschnittlich vorhandenen Werteversatz von 2,52 km/h begründen. Deutliche Abweichungen existieren in Phasen hoher Geschwindigkeit. Die Geschwindigkeitsänderungen der kNN-Prognose fallen deutlich höher aus als in Realität. Aufgrund dieser Eigenschaft sowie aufgrund des hohen Rechenaufwands und der Black-Box-Charakteristik von LSTM-Netzwerken erscheint dieser algorithmische Ansatz derzeit als ungeeignet, insbesondere im Hinblick auf die Regelung adaptiver Sicherheitskomponenten. Dennoch zeigt das System einen ersten möglichen Ansatz zur datengetriebenen Detektion abnormaler Fahrzustände, wie Abb. 3 und 4 aufzeigen. Dieser Ansatz soll in künftigen Studien weiter vertieft werden.

Interessenskonflikt Wir erklären keine Interessenskonflikte.

Finanzierung Diese Arbeit wurde mit Mitteln der Bayerischen Forschungsstiftung AZ-1375-19 gefördert.

Literatur

Fasel, B. (2017). Drift reduction for inertial sensor based orientation and position estimation in the presence of high dynamic variability during competitive skiing and daily-life walking. (PhD Thesis). École Polytechnique Fédérale de Lausanne,

Hermann, A., & Senner, V. (2021). Knee injury prevention in alpine skiing. A technological paradigm shift towards a mechatronic ski binding. Journal of Science and Medicine in Sport, 24(10), 1038-1043. doi:10.1016/j.jsams.2020.06.009

https://nbn-resolving.org/urn:nbn:de:bsz:ch1-qucosa2-806704

Practical studies on bike fitting – A biomechanical and physiological analysis under the influence of fatigue

Jonas Dully[1], Eva Bartaguiz[1], Carlo Dindorf[1], Stephan Becker[1] and Michael Fröhlich[1]

[1]Technische Universität Kaiserslautern, 67663 Kaiserslautern, Germany

Abstract

Bike fitting can have a major impact on the performance of cyclists (Bateman, 2014) and can reduce the risk of non-traumatic injuries (Bini et al., 2011). This study shows significant changes in lower body biomechanics of road cyclists during and after fatigue and therefore expands the research from a more practical view. These findings support the expansion of future research using sensor-based analyses of road cycling (e.g., IMUs, oxygen saturation).

Keywords: bike fitting; cycling; movement analysis; fatigue; lower body biomechanics

Introduction

In road cycling it is important to ride as economically as possible because over the course of a cycling stage, any energy saved due to an improved position might help to improve one's overall competition performance (Bateman, 2014) and reduce the risk of non-traumatic injuries (Bini et al., 2011). Regarding the practical application of bike fitting there seem to be no consistent standards on how to perform this (Bini et al., 2014). Occasionally, dynamic bike fitting is performed using submaximal loads perceived as habitual using stationary optical 2D or 3D-systems. Most research has focused on evaluating the efficiency of a seating position at a submaximal load perceived as habitually comfortable (Bini et al. 2014). However, if the relevant angles of the lower body are dependent on different riding intensity levels and the fatigue status, the determination of a position at a fixed submaximal load would underrepresent the real complexity. Cockcroft (2011) proposes that inertial measurement units (IMUs) may have the potential to track the rider's movement in training and competition and may therefore be more realistic than optical 2D/3D methods.

According to the abovementioned aspects, there is a lack of research regarding the influence of a realistic setting in the biomechanics of road cycling. Therefore, this study aimed to determine if different riding intensity levels relative to the individual anaerobic threshold (IAT) result in changes in the biomechanics of the lower body.

Methods

Six well-trained male road cyclists (age: M = 27.17, SD = 3.89 years; height: M = 180.41, SD = 5.31 cm; weight: M = 75.23, SD = 4.91 kg) with M = 8.33 and SD = 4.85 years of (professional) experience in road cycling underwent a dynamic 2D analysis on the bike. Videos were recorded for both sides in the sagittal plane during the test with two iPads (seventh generation, Apple, Cupertino, USA/CA) at 120fps as suggested by Bini et al. (2014). For all the subjects, a knee angle in a 90° position crank position, as well as the knee position in relation to the pedal axis, met the selected reference values (knee angle: 110°-115° in a 90° position; axis of the knee vertically above the pedal axis (Bini et al., 2014). The 90° position was selected for (pre-) evaluation as the forces present in the patellofemoral area are greater than those in the 180° position. The 180° position was additionally used for the following analysis, as it is the most commonly used in bike fitting practices and in other studies (Bini et al., 2011). After the pre-evaluation of the position on the bike, the subjects performed a lactate stepwise incremental test, starting with 100W and an increment of 20W for each time 3min until total exhaustion (Wahl et al., 2017). After reaching exhaustion, the cyclists had a short period of 5min of active regeneration, with low resistance selected as habitually comfortable. After this regeneration the subjects rode an increment of 50W every 3min, starting again with 100W and ending with 250W.

Fig. 1 Measuring procedure and angle definition (metatarsophalangeal joint, the lateral malleolus, the lateral part of the articulatio genus and the trochanter mayor)

For the lower body biomechanics, we focused on the knee and ankle angles, as shown in Fig. 1, because these were observed in most of the previous studies and are of high practical relevance (Swart et al., 2019). The calculations of the joint angles were based on those of Bini et al. (2014). Lactate was measured using a lactate-scout (EKF Diagnostics, Barleben, Germany) and the heart rate with a Polar V800 (Polar Electro, Kempele, Finland) with the matching pulse sensor. The angles were determined using Dartfish ProSuite 8.0 (Dartfish, Freiburg, Switzerland). Three images were selected for each position for each measurement point. The mean values of the three images separately for 90° and 180° positions were used for further calculations. To allow a comparison of the subjects, (a) the power output relative to the individual anaerobic threshold (IAT) was determined. Furthermore, (b) standardized angles were calculated by dividing each angle by the mean angle for the measurements under the IAT (assuming that the angles below the IAT were likely to be relatively similar due to lower fatigue). To answer the research question, the lower body biomechanics of the standardized angles depending on of the relative power output were modelled using linear regression. Outliers were removed if the values reached three times the interquartile range. Calculations were performed using Python (Python Software Foundation, Wilmington, DE, USA) and SPSS Statistics (version 16, SPSS Inc., Chicago, USA).

Results

The test was terminated after total subjective exhaustion (power output: *M* = 373.30, *SD* = 37.70 W; lactate: *M* = 11.58, *SD* = 2.82 mmol/l; heart rate: *M* = 186, *SD* = 16 1/min). The results showed that side asymmetries for the knee and foot relative to the IAT were present. When riding at 80% of the IAT the lowest mean absolute differences for the knee in the 180° position (*M* = 2.98, *SD* = 1.31°) were found. The highest mean absolute side differences were found for the foot in the 90° position (*M* = 5.89, *SD* = 4.85°). Exemplary results for the regression models and visualizations of the changes in knee and foot angles during the progressive intensity increase are presented in Fig 2.

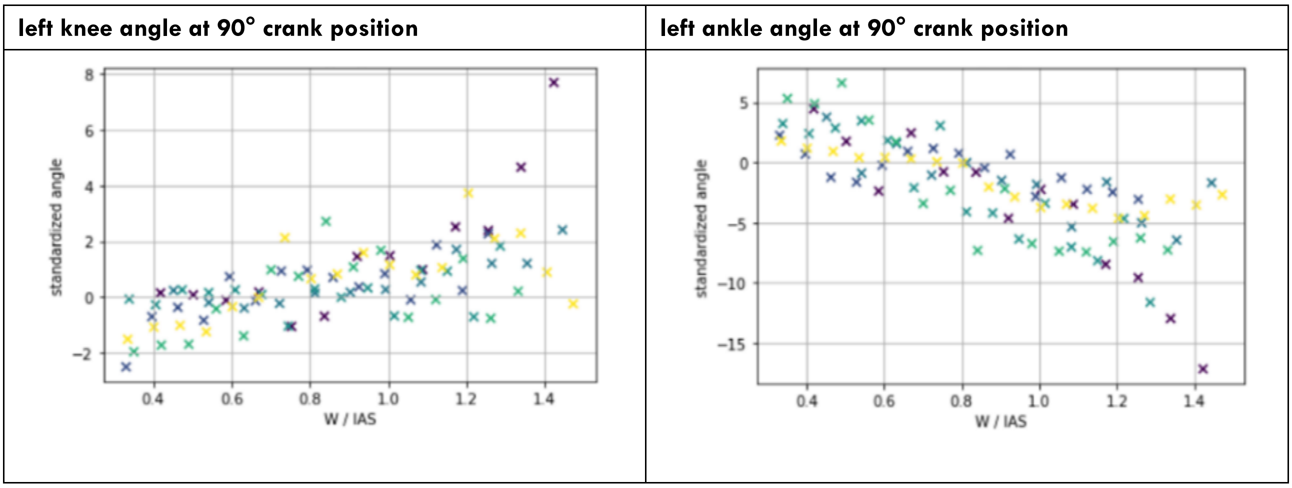

Fig. 2 Changes in the standardized angle (y-axis) relative to each subject's power output in relation to the IAT (x-axis). A value of 0 represents the mean angle of all the measurements (individually per subject) under the IAT. The colour code encodes the individual athletes.

Table 1 Regression models for each angle (L=left; R=right; K=knee; a= ankle)

	90°	180°
LK	*F*(1, 85)=55.47, *p*<.001; R^2=.40; *y*=1.719+2.497*x	*F*(1, 83)=64.70, *p*<.001; R^2=.44; *y*=-2.903+4.383*x
LA	*F*(1, 85)=124.74, *p*<.001; R^2=.59; *y*=6.277-9.504*x	*F*(1, 85)=27.64, *p*<.001; R^2 = .25; *y*=4.078-6.243*x
RK	*F*(1, 84)=74.79, *p*<.001; R^2=.47; *y*=-2.039+3.057*x	*F*(1, 84)=14.85, *p*<.001; R^2=.15; *y*=-2.061+3.059*x
RA	*F*(1, 86)=49.78, *p*<.001; R^2=.37; *y*=6.306-9.135*x	*F*(1, 83)=9.00, *p*=.004; R^2=.0.10; *y*=2.487-3.769*x

The regression models for the respective knee and ankle angles in the different positions showed similar results (Table 1). All the regression models were significant ($p \leq .04$). However, the quality of the fit (R^2) showed that the right knee and left ankle in the 180° position had a noticeably low R^2 ($R^2 < .25$) as compared to the other models ($R^2 \geq .37$), which can all be classified as a strong effect.

Discussion

The current study results showed that with a higher power output relative to the IAT, the joint angles changed significantly. Overall, the knee angles increased while the foot angles decreased. These findings are in accordance with the findings of Swart et al. (2019). Under the IAT, the differences between the respective angles appeared to be almost linear, while with higher levels of fatigue, the differences changed drastically and seemed to be non-linear. This may have been caused by different muscle exhaustion and compensation mechanisms, which seem to be highly individual in the subjects due to their individual physical capacities or additional factors (e.g., pain, limited flexibility, or the presence of side asymmetries). Nevertheless, the individuality of these changes underlines the recommendation for bike fitting conditions to be more realistic.

Taking sensor-based measurements into account could greatly change the field of bike fitting. Optical analysis has significant when measuring the biomechanics of road cycling as the settings in laboratories are not comparable to practical training and competition. Therefore, the use of IMUs to monitor the movement during cycling should be considered as these sensors promise to be valid and to be able to reliably track movements in the field (Teufl et al., 2019). In summary, there is a large quantity of data due to the different technologies available that can be used to describe the biomechanical and physiological states of a cyclist and can therefore help improve bike fitting as well as road cycling practice. Additional research should be carried out combining the different technologies, e.g., power output, pedal forces, near infrared spectroscopy, or sweat measurements, with the suggested use of IMUs to give direct feedback, reduce the risk of non-traumatic injuries, and further optimize the road cycling performance.

Conflict of interest We declare no conflicts of interest.

Funding This work was funded by Offene Digitalisierungsallianz Pfalz, BMBF [03IHS075B].

References

Bateman, J. (2014). Influence of positional biomechanics on gross efficieny within cycling. *Journal of Science & Cycling Book of Abstracts, 3*(2), 4.

Bini, R. R., & Carpes, F. (2014). Joint Kinematics. In R. R. Bini, & F. P. Carpes, *Biomechanics of Cycling* (S. 33-42). Heidelberg: Springer. doi:10.1007/978-3-319-05539-8_3

Bini, R., Hume, P. A., & Croft, J. L. (2011). Effects of bicycle saddle height on knee injury risk and cycling performance. *Spoorts Medicine, 41*(6), 463-476. doi:10.2165/11588740-000000000-00000

Cockcroft, S. J. (2011). An evaluation of inertial motion capture technology for use in the analysis and optimization of road cycling kinematics. Stellenbosch: Stellenbosch University: Faculty of Engineering. doi: 10.1055/a-1738-0252

Swart, J., & Holliday, W. (2019). Cycling Biomechanics Optimization—the (R) Evolution of Bicycle Fitting. *Current Sports Medicine Reports, 18*(12), 490-496. doi:10.1249/JSR.0000000000000665

Teufl, W., Taetz, B., Miezal, M., Lorenz, M., Pietschmann, J., Jöllenbeck, T., Fröhlich, M., & Bleser, G. (2019). Towards an Inertial Sensor-Based Wearable Feedback System for Patients after Total Hip Arthroplasty: Validity and Applicability for Gait Classification with Gait Kinematics-Based Features. *Sensors, 19*(22), 1-20. doi:10.3390/s19225006

Wahl, P., Manunzio, C., Vogt, F., Strütt, S., Volmary, P., Bloch, W., & Mester, J. (2017). Accuracy of a modified lactate minimum test and reverse lactate thershold test to determine maximal lactate steady state. *The Journal of Strength & Conditioning Research, 31*(12), 3489-3496. doi:10.1519/JSC.0000000000001770

https://nbn-resolving.org/urn:nbn:de:bsz:ch1-qucosa2-806704

Analyse von Einflussfaktoren auf die Gurtkräfte am Rucksack

Anika Stöhr[1], Sophie Richter[1,2], Stefan Schwanitz[1] & Frank I. Michel[2]

[1]Technische Universität Chemnitz, Professur Sportgerätetechnik, Chemnitz, Deutschland

[2]VAUDE Sport GmbH & Co. KG, ***i***-lab, Obereisenbach, Deutschland

Kurzfassung

Zur Evaluierung des mechanischen Tragekomforts von Rucksäcken wurden die Einflussfaktoren Geschlecht, Last und Bewegung auf die Gurtkräfte am Rucksack untersucht. Dazu wurde ein individuelles Messsystem entwickelt. Aus der Datenanalyse lässt sich folgern, dass die Gurtkraft nicht vom Geschlecht des Rucksackträgers abhängt. Die Rucksacklast und die Form der Aktivität hingegen sind relevante Indikatoren.

Schlüsselwörter: Gurtkraft, Rucksack, mechanischer Komfort, Geschlecht, Last

Einleitung

Der Rucksack ist als Lastentragesystem ein essenzieller und weit verbreiteter Bestandteil des Alltags und der Freizeitgestaltung. Allerdings ist das Tragen von Lasten generell mit einer hohen Prävalenz von mitunter bleibenden körperlichen Beschwerden durch Diskomfort verknüpft. (Brinjikji et al., 2015) Da Diskomfort ein vorwiegend subjektiv eingeschätztes Phänomen ist, müssen messbare mechanische Parameter abgeleitet werden, die objektive Bewertungen und Vergleiche ermöglichen. In einem Beitrag von Wettenschwiler (Wettenschwiler et al., 2015) konnten für den Rucksack als Lastensystem verschiedene Prädiktoren zur Beurteilung des Diskomforts ermittelt werden. Dazu zählen der Druck an den Auflagestellen sowie die Gurtkräfte.

Der Auflagedruck in verschiedenen Körperregionen wurde im militärischen Kontext bereits häufig untersucht. Die betreffenden Studien haben häufig Limitierungen in ihrer Übertragbarkeit, wie beispielsweise die Beschränkung auf sehr hohe Lasten (Bryant, 2001: 32 kg), limitierte Probandenkollektive (Wettenschwiler, 2015: nur junge Männer) oder die Arbeit an einem Messtorso statt an Probanden (Stevenson, 2004). Für die Analysen des Auflagedrucks wird zumeist mit einer Druckmessmatte gearbeitet.

Da die Gurtkraft zur Beurteilung des Tragekomforts von Rucksäcken bisher nur wenig untersucht wurde, gibt es noch kein bewährtes Vorgehen für die Durchführung und Bewertung von Analysen. Für die Datenerhebung in dieser Studie wurde ein eigens angefertigtes Gurtkraft-Messsystem genutzt. In einer initialen Untersuchung wurde der Einfluss der Faktoren Geschlecht, Rucksackzuladung und Aktivität auf die Gurtkraft betrachtet. Dazu wurden die maßgeblichen Bestandteile des Gurtsystems bestehend aus Beckengurt, Schultergurt rechts und links sowie Brustgurt analysiert. Ziel war es, anhand der erhobenen Probandendaten Abhängigkeiten darzustellen und die gewonnenen Erkenntnisse für die Entwicklung von Rucksäcken nutzbar zu machen.

Methode

Für die Gurtkraftmessung wurden ein Sensorsystem basierend auf Linearpotentiometern (Typ 3046, BOURNS Inc., USA) und eine Übertragungseinheit entwickelt. Die einzelnen Sensoren wurden extern an den vier definierten Gurten befestigt. Das System ist dazu in der Lage, Gurtspannungen direkt am Gurt zu detektieren und diese drahtlos und in Echtzeit auf ein Endgerät zu übersenden (Abtastrate: 4 Hz).

Die Studie wurde mit zehn Personen (Geschlecht: 5♀, 5♂; Alter: ∅ 36 ± 10,1 Jahre; Größe: ∅ 175 ± 7,1 cm; Gewicht: ∅ 69,6 ± 9,2 kg) durchgeführt. Alle Personen sind nach eigenen Angaben sportlich aktiv und nutzen Rucksäcke regelmäßig im Alltag und bei ihren Aktivitäten.

Die Personen trugen in randomisierter Reihenfolge Rucksäcke mit 15kg, 10kg und 5kg Last. Für die Lasten 10 und 15 kg wurde ein Trekkingrucksack (60 l) genutzt. Für 5 kg Last wurde ein Tagesrucksack (20 l) verwendet. Die Personen wurden aufgefordert, die Gurteinstellungen jeweils nach ihren individuellen Präferenzen vorzunehmen. Die Messungen der Gurtkraft erfolgten für jede Testkondition statisch im aufrechten Stand (Abb. 1a, 1b) sowie dynamisch auf dem Laufband (Geschwindigkeit: 4,5 km/h). Mit dem Tagesrucksack wurden zusätzlich Analysen auf einem Ergometer mit 50° standardisierter Rumpfneigung in statischer Brakehood-Position sowie dynamisch (Trittfrequenz: 80 min^{-1}) durchgeführt. Es wurden jeweils Sequenzen über 10 s aufgenommen (Abb. 1c). Mithilfe eines standardisierten Fragebogens wurde vom Probandenkollektiv zusätzlich die subjektive Druckwahrnehmung im statischen Zustand protokolliert.

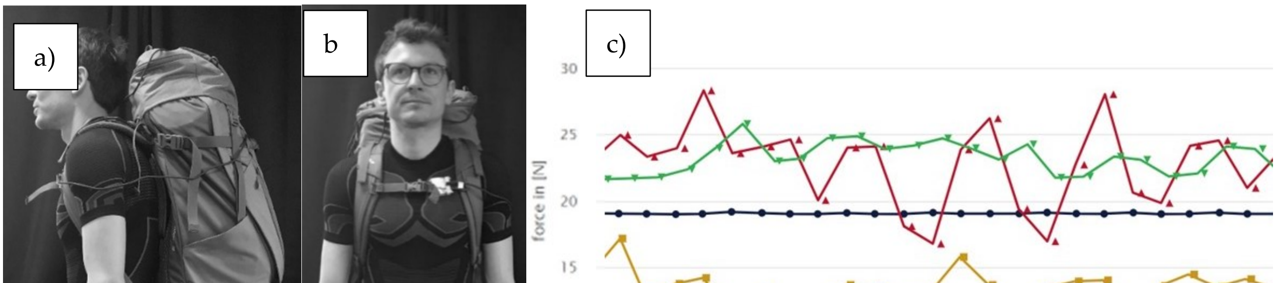

Abb. 2 – a) Seitenansicht instrumentierter Trekkingrucksack (15 kg) im aufrechten Stand; b) Frontalansicht; c) dynamische Anzeige der auftretenden Gurtkräfte beim Fahren auf dem Ergometer (10 s)

Zur Aufbereitung und Auswertung der Daten wurde RStudio (Version 1.3.1093) genutzt. Es wurden Mittelwerte und Standardabweichungen sowie auftretende Gruppierungen betrachtet. Die Datensätze wurden mit nichtparametrischen Testverfahren (Wilcoxon, Kruskal-Wallis) auf signifikante Unterschiede untersucht.

Ergebnisse

Aufgrund einer Fehldimensionierung des Brustgurtsensors wurde auf die Analyse der Brustgurtwerte verzichtet. Die bilateralen Schultergurtsensoren wurden als ein zusammenhängendes System betrachtet und deren Werte in der Analyse aufsummiert.

Im Vergleich der Gurtkräfte von Männern und Frauen konnte bei keiner der Konditionen ein signifikanter Unterschied ermittelt werden. Die Vermutung, dass eine Korrelation zwischen den Brust- und Beckenumfängen der Probanden und den aufgezeichneten Gurtkräften vorliegt, konnte ebenfalls nicht belegt werden. Daher wurden alle weiteren Betrachtungen geschlechtsunabhängig geführt.

Es konnten signifikante Unterschiede in den Gurtkräften von Beckengurt und Schultergurten in Abhängigkeit von der Rucksacklast verzeichnet werden (Abb.2). Je höher die Beladung des Rucksacks ist, desto höher sind die im Gurt detektierten Kräfte. Diese Beobachtungen treffen bei 5 kg, 10 kg und 15 kg Rucksacklast zu.

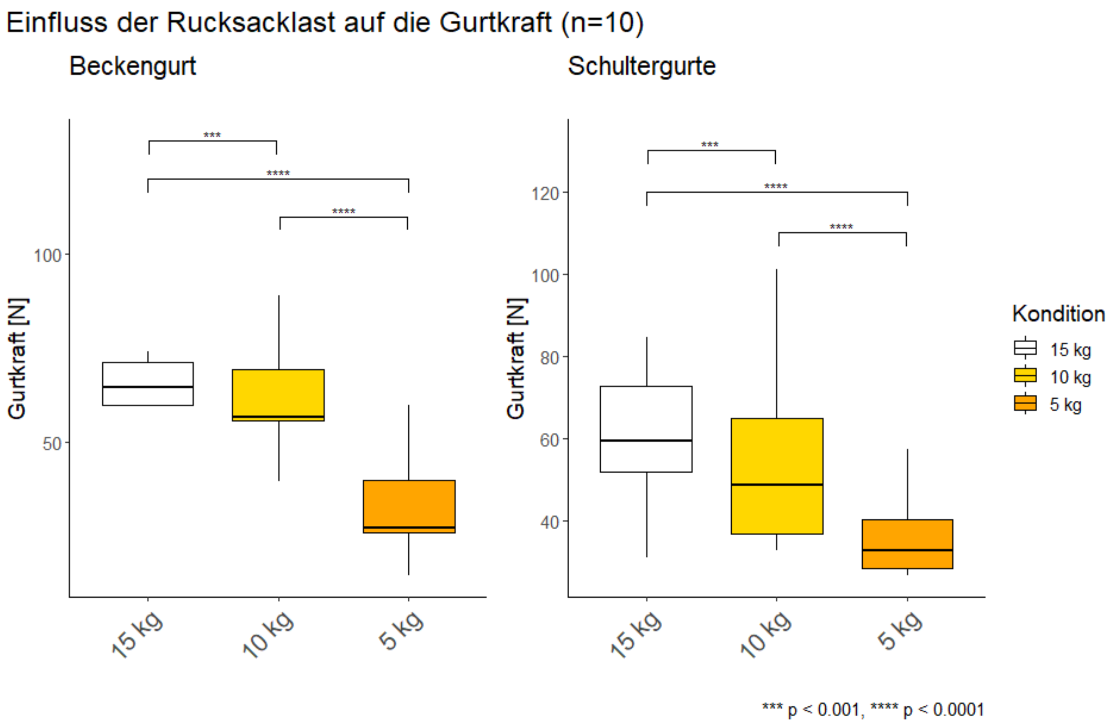

Abb. 3: Unterschiede in der Gurtkraft abhängig von der Rucksacklast (sign. Korrelationen nach Kruskal-Wallis über den jeweiligen Paaren angegeben)

Die Betrachtung von Bewegung als Einflussfaktor lieferte ebenfalls signifikante Resultate. Bei 15 kg sowie 10 kg Rucksacklast lagen im Vergleich die Gurtkräfte an Beckengurt und kumulierten Schultergurten beim Gang auf dem Laufband signifikant höher als in statischer Fahrposition auf dem Fahrrad ($p<0,0001$). Beim Fahren auf dem Ergometer mit 5 kg Rucksacklast traten ebenfalls signifikant höhere Gurtkräfte an allen Gurten auf als im Stand ($p<0,0001$). Das subjektive Feedback der Probanden deckte sich bei allen Durchgängen mit den jeweils objektiv erfassten Gurtkraftwerten.

Diskussion

Das Geschlecht als Einflussfaktor auf die Gurtkraft konnte auf Basis der Datenanalyse ausgeschlossen werden. Leider liegen keine vergleichbaren Erkenntnisse in der Literatur vor, da bisher nur unimodale Studien durchgeführt wurden. Aus der Auswertung der Studienergebnisse lässt sich weiterhin schließen, dass die Gurtkraft von der Zuladung sowie der Aktivität beim Tragen signifikant beeinflusst wird. Diese Ergebnisse sind nur bedingt belastbar, da keine Vergleichsliteratur zur Einordnung vorliegt. Allerdings wurde auch bei Mackie et al. (Mackie et al., 2005) ein grundsätzlicher Einfluss der Rucksacklast auf Schulter- und Beckengurt nachgewiesen. Es muss beachtet werden, dass das Rucksackdesign einen Einfluss auf die Gewichtsverteilung und damit auch auf die Gurtkräfte hat (Mackie et al. 2005). Der in der Studie verwendete Trekkingrucksack ist mit einem Tragesystem versehen, der Tagesrucksack hingegen nicht. Die Wahl der Rucksäcke wurde mit Fokus auf die tatsächliche Anwendung getroffen und ist daher valide. Abschließend kann formuliert werden, dass Gurtkraftsensoren sinnvolle Hilfsmittel zur Kontrolle von Kräften am Rucksack sind. Die Gurtkraft als objektiver Parameter zur vergleichenden Beurteilung vom mechanischen Komfort von Rucksäcken kann die bisher als alleiniges Bewertungsinstrument genutzte Druckkraftmessung ergänzen. Damit besteht eine weitere Option zur neutralen Evaluierung des mechanischen Diskomforts auch an nicht responsiven Messtorsos. Um die in diesem Abstract identifizierten Einflussfaktoren auf die Gurtkraft zu bekräftigen, sind weitere Untersuchungen mit vergleichbarem Studienaufbau nötig.

Interessenskonflikt Wir erklären keine Interessenskonflikte.

Finanzierung Im Rahmen des A4SEE Fellowship-Programms, einer aus EU-Mitteln kofinanzierten Erasmus+ Knowledge Alliance, erhielt Anika Stöhr zur Durchführung der Studie finanzielle Unterstützung.

Literatur

Brinjikji, W., Luetmer, P. H., Comstock, B., Bresnahan, B. W., Chen, L. E., Deyo, R. A., ... & Jarvik, J. G. (2015). Systematic literature review of imaging features of spinal degeneration in asymptomatic populations. *American journal of neuroradiology*, 36(4), 811-816.

Bryant, J. T., Doan, J. B., Stevenson, J. M., Pelot, R. P., & Reid, S. A. (2001). Validation of objective based measures and development of a performance-based ranking method for load carriage systems. Queens Univ Kingston (Ontario) School of Physical and Health Education.

Mackie, H. W., Stevenson, J. M., Reid, S. A., & Legg, S. J. (2005). The effect of simulated school load carriage configurations on shoulder strap tension forces and shoulder interface pressure. *Applied ergonomics*, 36(2), 199-206.

Stevenson, J. M., Bossi, L. L., Bryant, J. T., Reid, S. A., Pelot, R. P., & Morin, E. L. (2004). A suite of objective biomechanical measurement tools for personal load carriage system assessment. *Ergonomics,* 47(11), 1160-1179.

Wettenschwiler, P. D., Lorenzetti, S., Stämpfli, R., Rossi, R. M., Ferguson, S. J., & Annaheim, S. (2015). Mechanical predictors of discomfort during load carriage. *PLoS One*, 10(11), e0142004.

https://nbn-resolving.org/urn:nbn:de:bsz:ch1-qucosa2-806704

Towards Inertial Sensor-Based Position Estimation in Bouldering

Tom Koller[1], Tim Laue[1] & Udo Frese[1]

[1]University of Bremen, Department of Mathematics and Computer Science, Bremen, Germany

Abstract

For some years, inertial sensors have become increasingly popular in various sports applications due to their small size and weight. However – due to the problem of sensor drift – additional sensors are usually required to obtain reliable position estimates. In this paper, we present an approach for position estimation in bouldering that relies solely on inertial sensors and domain knowledge that is modeled as a virtual sensor.

Keywords: Bouldering, Inertial Sensor, Position Estimation, Sensor Fusion

Introduction

Inertial Measurement Units (IMUs) in general integrate sensors for measuring accelerations, rotational velocities, and the magnetic field on three axes. In common sports applications, these measurements are analyzed directly or are used as input for classificators, which recognize different activities or sports-specific motion patterns. In theory, given a known starting position, one could integrate IMU measurements over time and thereby estimate the trajectory of a moving sensor, an approach known as dead reckoning in inertial navigation systems. However, due to accumulating errors, after some time, this process inevitably leads to wrong position estimates. Especially in MEMS-based sensors, which are the ones that are suitable for sports, significant errors might already occur after some seconds. Thus, any IMU-based trajectory estimation is only realizable for short motion sequences, such as weight lifting or the analysis of single stroke motions, e.g. in golf or tennis. Whenever motions are supposed to be tracked over longer time intervals, one has to add additional sensors, defeating the advantages of IMUs regarding size and weight.

In the project *ZaVI* („Zustandsschätzung allein durch Vorwissen und Inertialsensorik“ / „State Estimation Solely based on Prior Knowledge and Inertial Sensing”), we investigated the concept of using prior knowledge about the application domain as an additional input for the estimation process to keep the accumulating errors within bounds. An initial successful sports application of this approach was track cycling, published by Koller et al. (2020). Here, knowledge about the track geometry and the driving behavior of a bicycle allowed to continuously estimate the position of track cyclers over many rounds.

In this paper, we describe the integration of so-called *event-domain knowledge (EDK)* for tracking the positions of the hands of a boulderer along a route. In this context, the EDK consists of known starting holds, a map of the route, and the fact that bouldering consists of a sequence of detectable events, i.e. the gripping of holds. This paper complements a recent publication by Koller et al. (2022) that describes the sensor fusion fundamentals of our approach in detail. In this paper, we focus on the actual sports application and discuss the potential of an inertial sensor-only tracking approach. The approach has been evaluated in a study involving 27 participants. The source code as well as the data gathered during the study has been released as Open Source by Koller (2022), including videos of the trials as well as ground truth data recorded by an external tracking system.

Methods

The implemented approach estimates the position of a single inertial sensor. For the bouldering application, a sensor is attached to the back of each hand of a climber, roughly comparable to the position of a smartwatch or a fitness tracker. They are treated as fully independent of each other. Furthermore, no skeleton model or any other user configuration is used. The two start holds are assumed to be known, as these are usually explicitly marked at a typical bouldering route. However, it is not known, which hand is at which hold. The approach consists of following three components:

The *grip detector* uses the raw inertial sensor data to detect the moments, in which the climber grips a hold. For this purpose, different implementations already exist. In our work, we use the approach by Ladha et al. (2013). The detection of the gripping events allows us to divide the whole climbing process into a sequence of phases of free sensor motion and phases in which the hand (and thus the sensor) is almost fixed at a hold.

The *transition estimation* provides a position estimate given the position of the last hold and the sum of all IMU measurements until the next gripping event is detected. Currently, a least squares optimization over these measurements is performed to determine the transition. However, as described in the Discussion section, faster approaches are generally applicable for this task, too. Compared to existing route classification systems, this approach computes a full trajectory of the sensor between two holds and thus provides more comprehensive motion information for a possible later analysis instead of a mere sequence of holds.

Finally, the grips as well as the transitions are used as an input for a *particle filter* that incorporates the event-domain knowledge for the sensor position estimation. The particle filter approach has been chosen as it suits best to a domain, in which discrete gripping events and multimodalities such as sets of probable holds (on a bouldering route, the climber is free to decide about the sequence of the used holds) need to be modeled. We use a standard particle filter implementation. To improve precision, a particle filter smoother, as described by Doucet and Johansen (2011), is used. A detailed formal description of our approach is given in Koller et al. (2022). The event-domain knowledge consists of the detected gripping events and a previously created map of the bouldering route. In the map, the actual shape of a hold is not modeled, but just its position on the wall. However, in general, the used approach would allow an integration of such shapes, which would be a necessity for routes incorporating huge macros, for instance. This would require a different distance measure, based on dynamically generated contact points. In the current version, this has not yet been realized to keep the generation of map data manageable and the gripping distribution simple. Whenever a gripping event is detected, the most likely hold is determined and each sample's weight is set accordingly. Touching or holding the wall is possible, too. This is handled by using a uniform distribution with a constant likelihood.

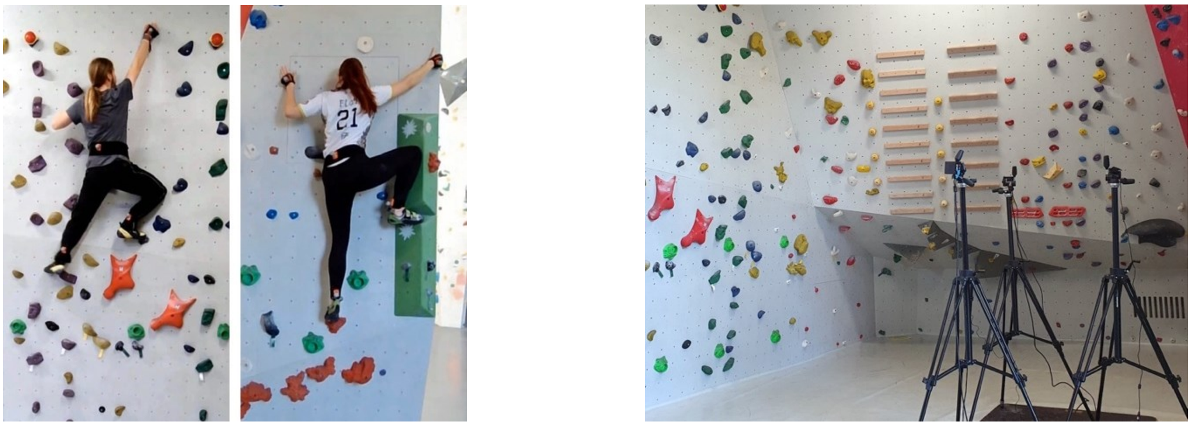

(a) (b)

Fig. 1 (a) Two of the routes used for the evaluation, the climbers wear gloves with attached sensors. Additional sensors were attached to the tailbone and the heels, but not used for the work presented in this paper; (b) The setup for obtaining ground truth data and video recordings.

Results

For the evaluation of our approach, a study with 27 participants (6 female, 21 male) was conducted at the DAV-Kletterzentrum Bremen, a professional climbing venue. The participants, who all had at least some experience regarding bouldering, climbed 12 different routes, some of them are depicted in Fig. 1a. Some routes were climbed multiple times, resulting in a total 775 valid trials of the left hand and 769 of the right hand. The routes were of different difficulty (within amateur level) but all located on normal vertical walls, i.e. without any major overhangs and complex volumes, which would, however, not oppose our approach in general, as long as the geometry is known. Furthermore, the routes, except for one, did not require any dynamic moves such as jumps.

The approach does not rely on any specific inertial sensor. For our experiments, we used XSens MTw Awinda sensors, which are robust and reliable and which allow a wireless data transfer. For obtaining ground truth information, an ART TrackPack system with two cameras was used (see Fig. 1b). The system requires markers that we attached to the sensors. The ART provides millimeter precision ground truth data, but is subject to occlusions by body parts. The experimental results were obtained offline on recorded datasets, which contain inertial sensor data, synchronized with ground truth and videos.

The data of 4 participants has been used for the development and tuning of the approach, the data of the other 23 was used for evaluation. Over these datasets, the median position error of a sensor, compared to the ground truth information, was 0.132 m. When not using the particle filter smoother but a standard particle filter, the error was 0.145 m. In contrast, when not using the map part of the event-domain, the error almost doubles to 0.266 m. However, in some experiments, outliers occurred, leading to errors of multiple meters. Typical causes were outlier measurements, caused by abrupt motions at holds, exceeding the sensor's range and thereby affecting the transition estimator, as well as grips to the wall near a hold, causing the particle filter to shift the overall estimate towards the hold. In such situations, the approach might lose track of the sensor and generate huge estimation errors.

Discussion

Overall, we demonstrated that it is possible to conduct position estimation of a climber's hand in a bouldering scenario by using an inertial sensor only. The median error that was achieved in our experiments is significantly below the distance between two holds on a typical bouldering route, making an actual application appear realistic. However, of course, routes still exist that do not meet this condition. Furthermore, it is shown that the incorporation of event-domain knowledge leads to a significant decrease of the error. In comparison to existing approaches for route classification, our approach provides position information for any point of time of the activity, enabling a later analysis of the climber's motion, if desired. Nevertheless, the described outlier cases still require solutions such as sensors with a wider measurement range or a model that differentiates more reliably between gripping a wall or a hold. Using IMUs for this kind of sports application bears several advantages over other sensors such as cameras, for instance lower costs, less space and time for setup, and no problems regarding occlusions. In addition to the proof of concept of inertial sensor-only position estimation in bouldering, our work results in a rich dataset that is available as Open Source and provides other researchers opportunities for their work. The presented results are based on an offline approach that incorporates computationally expensive approaches. For an online application on a wearable device, one has to consider some adaptions. The results indicate that replacing the particle smoother by a standard particle filter, which can be assumed to run in realtime on a wearable device, only leads to a small loss in precision. Furthermore, the least squares approach in the transition estimation also needs to be replaced, for instance by a Kalman filter. However, a comparison of precision regarding this component remains future work.

Conflict of interest We declare no conflicts of interest.

Funding This work was funded by the DFG as project *ZaVI* under the grant number FR 2620/3-1.

References

Doucet, A., Johansen, A. M. (2011). Tutorial on Particle Filtering and Smoothing: Fifteen Years Later. In *The Oxford Handbook of Nonlinear Filtering* (pp. 656-704). Oxford University Press.

Koller, T., Frese, U. (2020). State Observability through Prior Knowledge: Analysis of the Height Map Prior for Track Cycling. *Sensors 20*(9).

Koller, T., Laue, T., Frese, U. (2022). Event-Domain Knowledge in Inertial Sensor Based State Estimation of Human Motion. In *Proceedings of the 25th International Conference on Information Fusion. FUSION 2022.*

Koller, T. (2022). ZaVI Datasets. http://www.informatik.uni-bremen.de/zavi-datasets/info.html.

Ladha, C., Hammerla, N. Y., Olivier, P., Plötz, T. (2013). ClimbAX: Skill Assessment for Climbing Enthusiasts. In *Proceedings of the 2013 ACM International Joint Conference on Pervasive and Ubiquitous Computing* (pp. 235–244). Association for Computing Machinery.

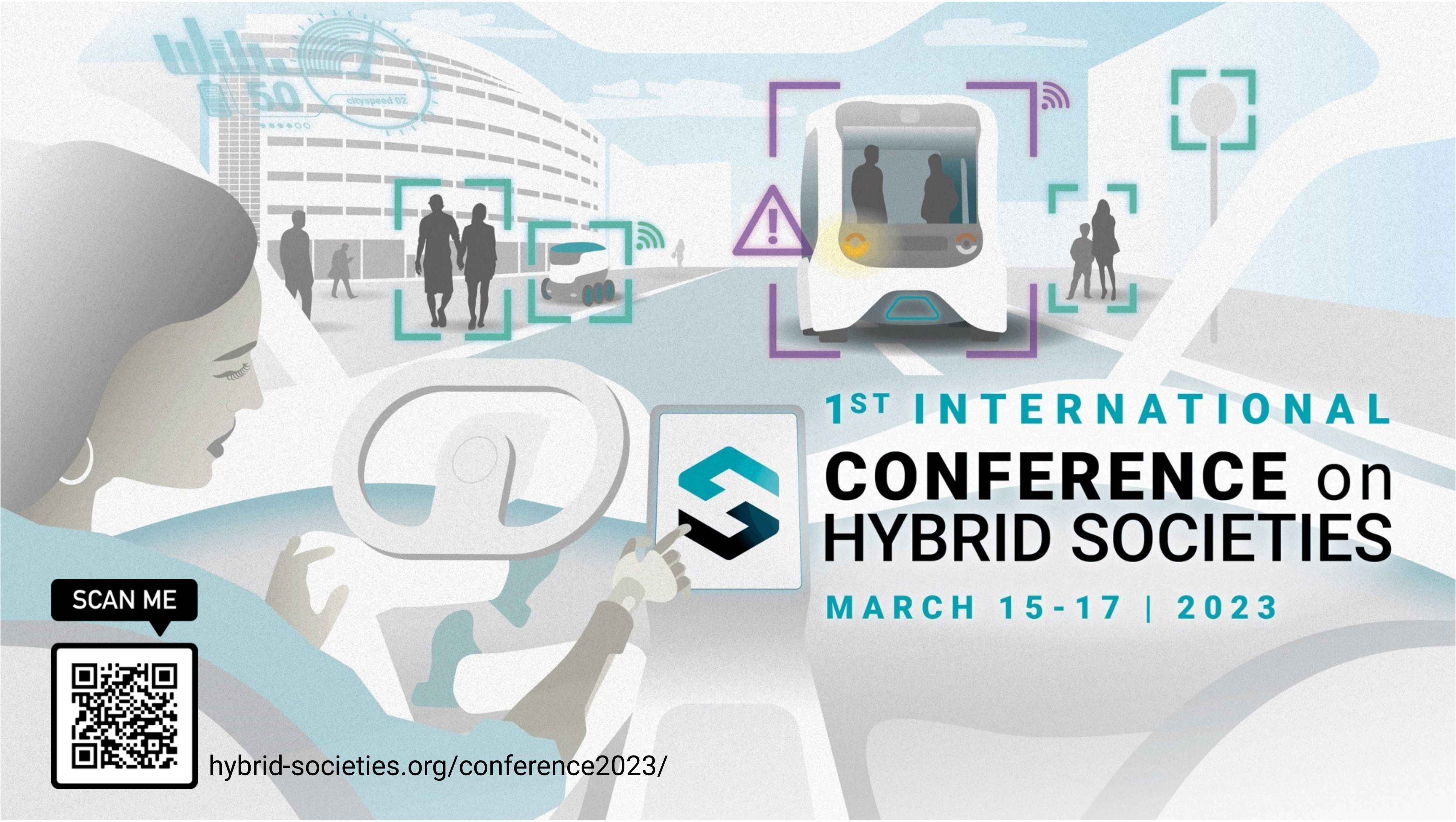
50
cityspeed 02
1ST INTERNATIONAL
CONFERENCE on
HYBRID SOCIETIES
MARCH 15-17 | 2023
SCAN ME
hybrid-societies.org/conference2023/

SPORTGERÄTETECHNIK

Fakultät für Maschinenbau
Institut für Strukturleichtbau
Professur Sportgerätetechnik
www.tu-chemnitz.de/mb/sgt

TECHNISCHE UNIVERSITÄT
CHEMNITZ

Technische Universität Chemnitz
09107 Chemnitz
www.tu-chemnitz.de